8-1-2014

EFFECTS OF ADDITION OF SMALL PERCENTAGES OF FLY ASH ON LIQUEFACTION CHARACTERISTICS OF SAND

Rakam Lama Tamang
Southern Illinois University Carbondale, rakamlama@siu.edu

EFFECTS OF ADDITION OF SMALL PERCENTAGES OF FLY ASH ON LIQUEFACTION CHARACTERISTICS OF SAND

by

Rakam Lama Tamang

B.E., Institute of Engineering, Pulchowk Campus, Nepal, 2010

A Thesis
Submitted in Partial Fulfillment of the Requirements
for the Master of Science in Civil Engineering

Department of Civil and Environmental Engineering
in the Graduate School
Southern Illinois University Carbondale

August 2014

THESIS APPROVAL

EFFECTS OF ADDITION OF SMALL PERCENTAGES OF FLY ASH ON LIQUEFACTION CHARACTERISTICS OF SAND

by

Rakam Lama Tamang

A Thesis Submitted in Partial Fulfillment of the Requirements for the
Degree of Master of Science in the field of
Civil Engineering

Approved by:

Dr. Vijay Puri, Chair

Dr. Sanjeev Kumar

Dr. Prabir Kolay

Graduate School
Southern Illinois University Carbondale
June 17, 2014

AN ABSTRACT OF THE THESIS OF

Rakam Lama Tamang, for the Master of Science degree in Civil Engineering, presented on 06/17/2014, at Southern Illinois University Carbondale.

TITLE: EFFECTS OF ADDITION OF SMALL PERCENTAGES OF FLY ASH ON LIQUEFACTION CHARACTERISTICS OF SAND

MAJOR PROFESSOR: Dr. Vijay Puri

Severe damages to physical infrastructures as well as lifeline facilities have been observed during past earthquakes. Saturated sands as well as sands containing fines liquefied. The effect of fines on liquefaction resistance of sand is not fully understood till today. The basis of comparison and types of fines are reported as important factors affecting effects of fines on liquefaction. The fly ash is non-plastic and finer. Hence, study of liquefaction behavior of sand-fly ash mixtures may be helpful for the understanding of effects of fines on liquefaction resistance. The objective of this study were (1) to investigate effects of addition of fly ash on pore water pressure generation and deformation characteristics of sand, (2) to study effects of confining pressure on liquefaction resistance of sand-fly ash mixtures, and (3) to study Youngs modulus and damping ratio of sand-fly ash mixtures.

Stress controlled cyclic triaxial tests were performed on clean sand, fly ash and sand-fly ash mixtures containing 10, 20 % of fly ash. For the evaluation of effects of confining pressure in liquefaction resistance, three series of tests were conducted at 5, 10 and 15 psi initial effective confining pressures. The reversible shear stress was applied systematically by varying CSR (Cyclic Stress Ratio) from 0.1 to 0.5. But, the tests were conducted only in 5 psi effective confining pressure in case of pure fly ash.

The results obtained from the tests were used to compare the effects on liquefaction resistance in terms of pore water pressure build up, deformation behavior and effective confining pressure. Based on the results, it was observed that, the liquefaction resistance decreases with an increase in cyclic shear stresses at a given initial confining pressure. Liquefaction resistance also decreases with an increase in confining pressure for any CSR values. Further, the effects of fly ash content on liquefaction resistance was found to depend upon the confining pressure. For all effective confining pressure, liquefaction resistance decreased with an addition of 10 % fly ash. However, when the fly ash content was increased to 20 %, the liquefaction resistance increased. Moreover, the liquefaction resistance of sand containing 20 % fly ash was higher than clean sand at 5 psi effective confining pressure. On the other hand, it was lower than clean sand for the effective confining pressure 10 and 15 psi. The brittleness of the sample was found to increase with an addition of fly ash. Youngs modulus and damping ratio were also determined. The Youngs modulus was found to decrease with an increase in axial strain for clean sand, and for sand containing 10 and 20 % fly ash. It was also noted that, Youngs modulus increases with an increase in confining pressure. The damping ratio increases with an increase in axial strain. No distinct variation of damping ratio with confining pressure was observed.

ACKNOWLEDGEMENTS

I would like to express my deepest appreciation to my advisor Dr. Vijay Puri for his continuous support, guidance, valuable suggestions, time and encouragement for research. Without his support, the thesis would not have been possible. Further, I would like to thank my committee member Dr. Sanjeev Kumar and Dr. Prabir Kolay for their direction and advice during research work.

I owe deepest gratitude to our Research Supervisor, Mr. John Hester for the technical assistance in lab and management of testing materials. I would also like to express my deepest gratitude to entire faculty, for helping me to develop my background in the civil engineering.

Furthermore, I would like to acknowledge the staff and colleagues at the Southern Illinois University's Civil and Environmental Engineering Department for their cooperation and help during research.

Last but not least, I would like to thank my parents, Mr. Santa Bir Tamang and Mrs. Jog Maya Tamang for their support, encouragement for the study and long distance love.

LIST OF TABLES

LIST OF FIGURES

CHAPTER 1

INTRODUCTION

Earthquakes are frequent in tectonically active zones and significant damage to most infrastructures as well as life line facilities has been observed during major earthquakes. Most of the damages during earthquake in sandy and silty type of soil are due to liquefaction. Liquefaction occurs during earthquake in saturated sandy soil which results in loss of soil strength and bearing capacity due to increase in pore water pressure. The liquefaction damages during Nigata, Japan earthquake (1964) and Anchorage Alaska earthquake (1964), drew attention of the engineering community for a better understanding of liquefaction mechanism. The initial laboratory studies during 1960-80 were focused in clean sand. After that, several field studies have been performed for the evaluation of liquefaction in terms of Standard Penetration Test (SPT), Cone Penetration Test (CPT). Several case studies reported that, sands containing fines can also liquefy as observed in Central Chile earthquake (1985), (De Alba et al., 1988), Saguenay earthquake (1988) (Tuttle et al., 1988), Superstition hills earthquake, California (1987), (Holzer et al., 1989).

Research on sand with fines was mainly started after 1960. Initially, the fines were supposed to increase liquefaction resistance (Seed et al, 1985). Subsequent laboratory investigations indicated controversial results. Most researches conducted at constant global void ratio indicate that the liquefaction resistance decreases initially up to threshold fine content and then increases on increasing fine content. On the other hand at constant relative density, most of the researchers indicate that the liquefaction resistance increases with an increase in fine contents and then decreases (Polito and Martin, 2001; Sadek and Saleh, 2007). However, even for the same relative

density, Singh (1996); Schmidt (2008) observed decrease in liquefaction resistance with increase in fine content. For constant sand skeleton void ratio, there is no significant effect of fine content at loosest state (Kuerbis et al., 1987). Further, Thevanayagam et al. (2000) observed increase in liquefaction resistance with an addition of fine contents at constant intergranular void ratio. Plastic and non-plastic fines have been used for the evaluation of effects of fines. The suitable parameter for comparison which simulates real field condition and role of fines are still unclear. Most of researches have compared the effect of on same confining pressure which does not simulate the different depths. The naturally occurring sand contains various types of fines, so it is crucial to understand effects of the various types of fines at different depth on liquefaction potential of sand.

1.1 Scope of research

This thesis presents the results from laboratory tests on mixtures with various percentages of fly ash in sand. The results from the cyclic triaxial test are evaluated in terms of deformation and pore pressure generation characteristics on application of cyclic loads.

Ottawa 20-30 ASTM C 778 sand was used in this research. The samples were prepared at a constant relative density of 50 %, using method of under compaction suggested by Ladd (1978). The stress controlled cyclic triaxial tests were performed on clean sand. In order to compare, the effect of fly ash on liquefaction potential of sand, cyclic triaxial tests were conducted on the mixtures of sand with 10 and 20 % fly ash. Some tests on pure fly ash were conducted for the comparison of liquefaction resistance of sand and fly ash. Further, for the investigation of the effect of confining pressure, tests were conducted at three different confining pressure of 5, 10 and 15 psi with different cyclic stress ratios varying from 0.1 to 0.5. The pore pressure and deformation were measured during the cyclic phase.

1.2 Organization of thesis

This thesis consists of five chapters. Chapter 1 describes the introduction of the topics, problem statement, and scope of research and organization of the thesis. The subsequent topics are summarized below.

Chapter 2 presents a brief review of relevant background information and relevant research work on liquefaction. The pore water pressure generation mechanism during liquefaction is discussed at the beginning and previous studies on clean sand are presented. Then, the microstructure of sand and fine mixtures, effects of non-plastic and plastic fines on liquefaction potential are discussed, which includes the critical review of the cyclic triaxial results of laboratory studies performed by several researchers.

Chapter 3 presents the methodology of the research work. It includes the brief introduction of cyclic triaxial test, simulation of earthquake condition in cyclic triaxial test. Then, sample preparation technique, details of testing program, set up for geo comp cyclic triaxial equipment are discussed. Materials used for this research are also discussed.

Chapter 4 presents results obtained from cyclic triaxial tests on clean sand, pure fly ash, and sand-fly ash mixtures containing 10 and 20 % fly ash. Index properties of the tested materials are presented at the beginning. Then, typical test results and effect of confining pressure on pore water pressure build up and deformation are discussed. The effect of addition of fly ash in liquefaction potential is interpreted in terms of pore pressure generation and deformation characteristics. Finally, results on Youngs modulus and damping properties are presented.

Chapter 5 presents the conclusions of this research work. It highlights the effect of confining pressure on liquefaction characteristics of clean sand and sand containing 10 and 20 % fly ash,

effects of addition of fly ash to clean sand on liquefaction characteristics. Finally, suggestions for future research works are given.

CHAPTER 2

LITERATURE REVIEW

2.1. Introduction

The liquefaction studies on clean sands and sands containing plastic and non-plastic fines are presented here. These are based on the results of other investigators.

2.2. Liquefaction

When cyclic load is applied to saturated sands under the undrained condition, the pore water pressure increases. If the cyclic load is sufficient to develop pore water pressure equal to the effective overburden pressure, then the effective stress will become zero and the soil loses its strength. This condition is called initial liquefaction (Seed, 1979). Further, during liquefaction, deformation occurs at low residual stress due to buildup and maintenance of pore water pressures. On further loading after initial liquefaction, if the soil stabilizes and pore water pressure drops due to dilation or remaining resistance, it is called cyclic mobility (Seed, 1979). The liquefaction is found to be disastrous. Damages to physical infrastructures such as bridges, dams, retaining walls, roads, and buildings have been observed during past earthquakes. Casagrande (1936) explained the liquefaction in terms of critical void ratio. The void ratio, at which the volume does not change in shear loading is known as a critical void ratio. If the initial void ratio of sand is greater than the critical void ratio, then sand tends to contract on shear loading. Due to contraction, positive pore water pressure develops. The sand may liquefy depending upon the magnitude of cyclic loading. Further, it dilates if the initial void ratio is less than the critical void ratio. As a result, pore water pressure decreases and sand gains strength and stability. However, Casagrande (1938) noticed that the critical void ratio is not constant; it

depends upon the confining pressure. The critical void ratio decreases on increasing confining pressure. Moreover, the volume change in static loading is different from cyclic loading (Casagrande, 1936). So, liquefaction phenomenon cannot be explained in terms of critical void ratio.

For a proper explanation of liquefaction phenomenon, Prakash and Mathur (1965) conducted tests on shaking table. In addition, Seed and Lee (1966) used the cyclic triaxial test for the simulation of earthquake loading and conducted tests on clean saturated sand.

2.2.1. Pore water pressure generation during liquefaction

During an earthquake, the shear waves propagate upwards and cyclic shear stress is induced in the ground that may compact cohesionless soil. The stresses from soil transfers to water because of compaction. The soil tends to rebound to maintain the constant volume. The pore water pressure increases due to transfer of stresses as well as the rebound of soil. In Figure 2-1, if cyclic load is applied at A, for the drained condition, there will be decrease in voids due to expulsion of water. Most of the earthquakes are short term, so there is less chance of drainage. As a result, the volume of soil remains constant, which results increase in pore water pressure. Due to increase in pore water pressure, effective stress decreases. Depending upon the magnitude of cyclic loading and types of soil, the pore water pressure goes on increasing. If the cyclic load is sufficient to cause initial liquefaction, the effective overburden pressure drops to zero which is represented by point C.

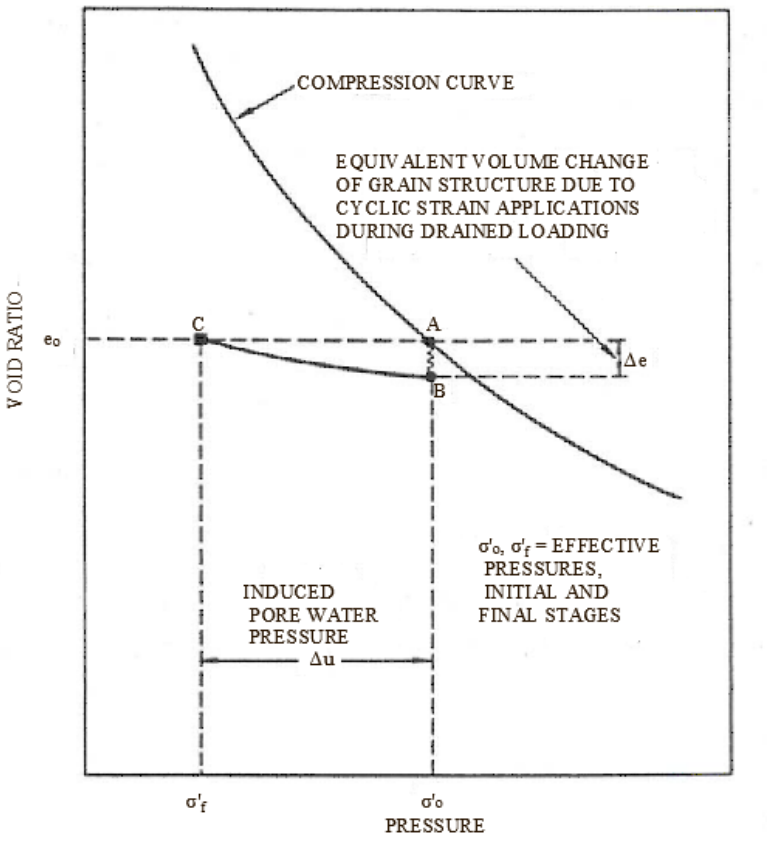

Figure 2-1 Schematic illustration of pore water pressure generation during cyclic loading (Seed, 1979).

The rate of the pore water pressure generation depends upon the type of sand, relative density, grain size, etc. Based on the cyclic triaxial tests performed on clean sand by Lee and Albasia (1974), Seed et al. (1976) presented (Figure 2-2), which illustrates the relationship between pore pressure ratio and cyclic ratio for clean sands. Cyclic ratio is the ratio of the number of cycles (N) to number of cycles required for initial liquefaction (N_l). Moreover, they proposed simplified procedure along with an empirical equation for the determination of pore water pressure during earthquake loading in the field for saturated sandy sites.

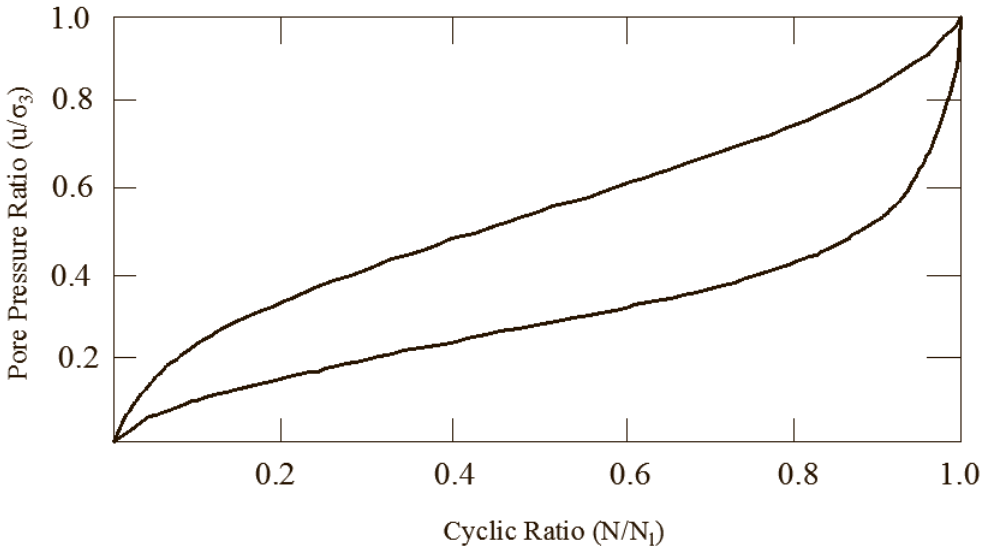

Figure 2-2 Rate of pore pressure build up in cyclic triaxial test (Seed et al., 1976).

2.2.2. Factors affecting liquefaction

The liquefaction potential of the sand depends upon the relative density, grain size, previous strain history, confining pressure, soil fabrics, lateral earth pressure and over consolidation ratio, etc. To study effect of sample preparation on liquefaction resistance of sands, Mullis et al. (1977) performed cyclic triaxial tests on samples prepared at a constant relative density by eight different methods namely (1) high frequency vibration on moist samples, (2) moist tamping, (3) moist rodding, (4) low frequency vibration on dry samples, (5) high frequency vibration on dry samples, (6) pluviated-water, (7) pluviated-air, and (8) dry rodding. The results are summarized in terms of the Cyclic Stress Ratio and number of cycles. They reported that the sample prepared by applying high frequency vibrations on moist sample had the highest liquefaction resistance. A variation up to 200 % in liquefaction resistance was observed as shown in Figure 2-3. The samples prepared by dry method had lower resistance than moist methods. Furthermore, cyclic resistance depended upon the frequency of vibration. The difference in cyclic resistance is due to variation of fabrics of samples when using different methods. Similar results were obtained by

DeGregorio (1990). They conducted consolidated undrained test on Ottawa sand samples, which were prepared using dry pluviation, moist tamping, and moist vibration methods. The peak and steady state strength were increased in the order of dry pluviation, moist tamping, and moist vibration, respectively. Moreover, the dry pluviation method exhibited higher pore water pressure response.

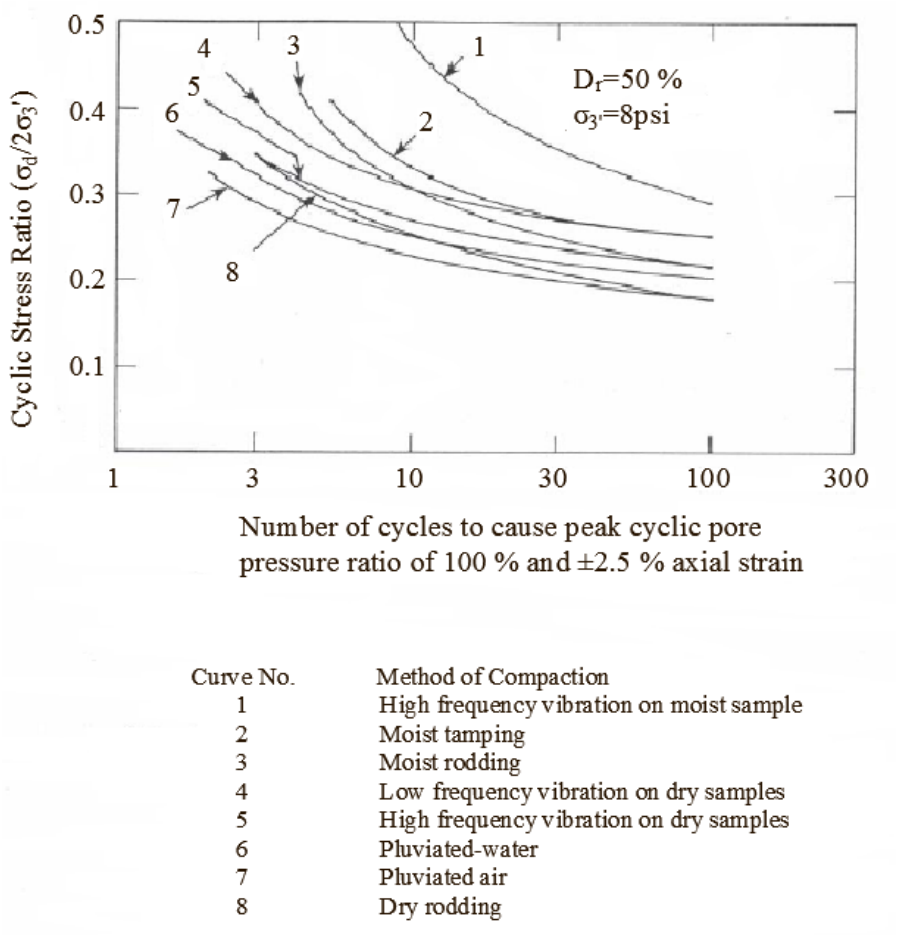

Figure 2-3 Effect of specimen preparation method on cyclic strength (Mulilis et al., 1977).

Strain history has a significant effect on the cyclic resistance of sands. Seed et al. (1977) conducted shake table tests and simulated series of earthquakes having different magnitude. They reported that previous strain history increases the liquefaction resistance of sand. The strain due to foreshock increases the confining pressure, which further increases the coefficient of earth

pressure at rest (K_O). As a result, the liquefaction resistance increases. The increase in CSR due to pre straining is around 150 % that is shown in Figure 2-4. It depends upon the magnitude of foreshock.

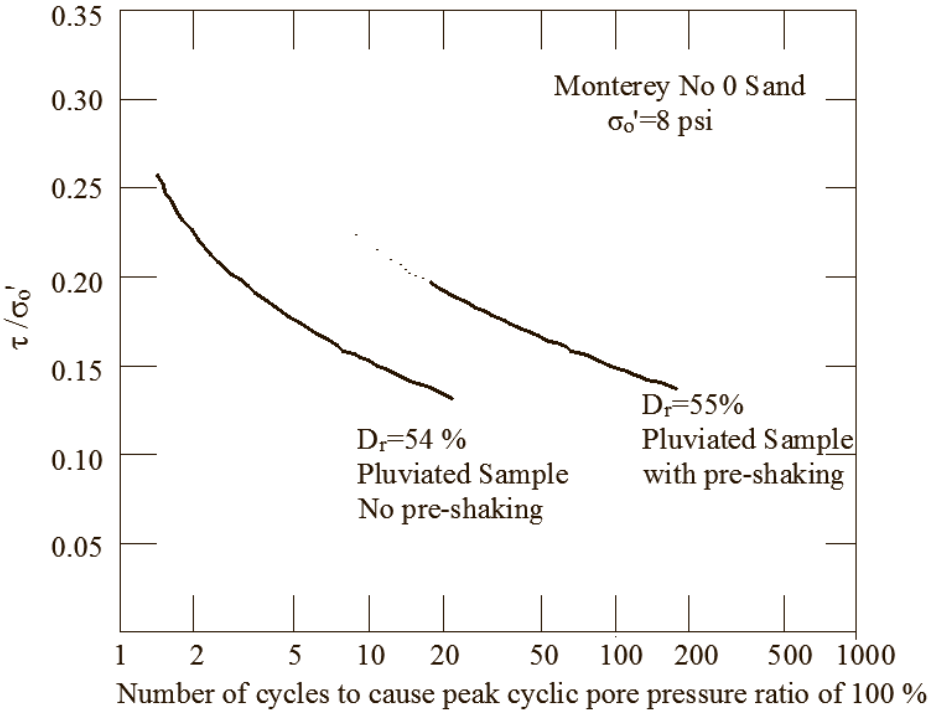

Figure 2-4 Effect of seismic history on cyclic strength of sands (Seed et al., 1977).

The lateral earth pressure coefficient and over consolidation ratio also affect the cyclic resistance. In order to evaluate the effects of these parameters, Seed and Peacock (1971) conducted cyclic shear tests on saturated sand varying the OCR (Over Consolidation Ratio) from 1 to 8. They reported that as OCR increases, K_O also increases as a result, liquefaction resistance also increases. Ishibashi and Sherif (1974) obtained similar type of results in their lab experiments. Furthermore, Finn et al (1971), Seed and Peacock (1971), and Castro (1975) analytically supported the above results.

Moreover, the Cyclic Stress Ratio depends upon the packing and grain size of soil. Based on the simple shear tests conducted on Monterey sand, De Alba et al. (1976) reported that the liquefaction resistance increases with relative density. Seed and Lee (1966) observed that, for the same cyclic shear stress applied, the number of cycles required to cause liquefaction increases with an increase in confining pressure. Further, Castro and Poulos (1977), reported similar results, i.e. as the confining pressure increases, the cyclic load required to cause liquefaction increases.

Mori et al. (1978) investigated the effect of sample disturbance on the cyclic strength of sand. They reported that the cyclic resistance increases due to prior strain history, but that would be lost during sampling and transportation. They collected undisturbed samples having over consolidation ratio of 8, from a depth of 80 ft. and conducted cyclic triaxial tests after consolidating the samples with confining pressures similar to those existing in-situ. In order to investigate the effect of prior strain, they conducted another series of tests. Samples were consolidated at pre consolidation pressure during the consolidation phase. After that, confining pressure was decreased slowly to the in-situ field confining pressure, which was used in previous series of tests. The results show that the samples that have been consolidated to preconsolidation pressure show higher strength than the samples consolidated to present overburden pressure as shown in Figure 2-5.

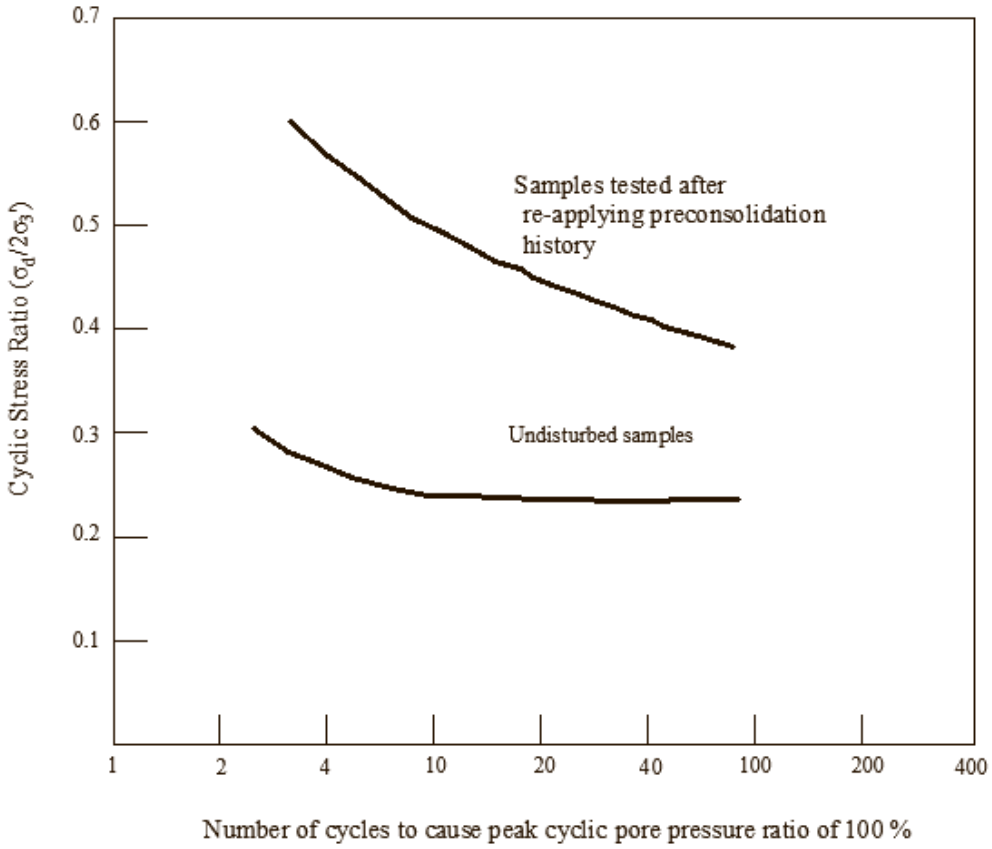

Figure 2-5 Effect of pre-consolidation on cyclic loading characteristics of undisturbed samples (Mori et al., 1978).

Liquefaction potential can be evaluated by cyclic stress and cyclic strain approach. Seed and Idriss (1971) proposed simplified approach for the evaluation of liquefaction potential. The liquefaction potential was evaluated by comparing shear stress required to cause liquefaction and shear stress induced by the earthquake. The peak ground acceleration can be estimated from site response analysis and the shear stress induced at different depth in the ground can be determined using the unit weight of the soil layer, depth, and maximum acceleration. The shear stresses induced by the earthquake are not uniform, for the simplification of the problem, it can be converted to average shear stress induced corresponding to 65 % of maximum shear stress (Seed et al., 1975). Several researchers have performed the cyclic triaxial tests on sands with different mean particle size (D_{50}) at 50 % relative density. The cyclic stress ratio required to cause

liquefaction of clean sand in ten cycles with corresponding D_{50} can be determined from the Figure 2-6 (Seed and Idriss, 1971). The graph of shear stress induced by earthquake and shear stress required to cause liquefaction can be plotted with respect to depth as shown in Figure 2-7. If shear stress induced due to earthquake is more than the shear stress required to cause liquefaction, then soil at that depth will liquefy.

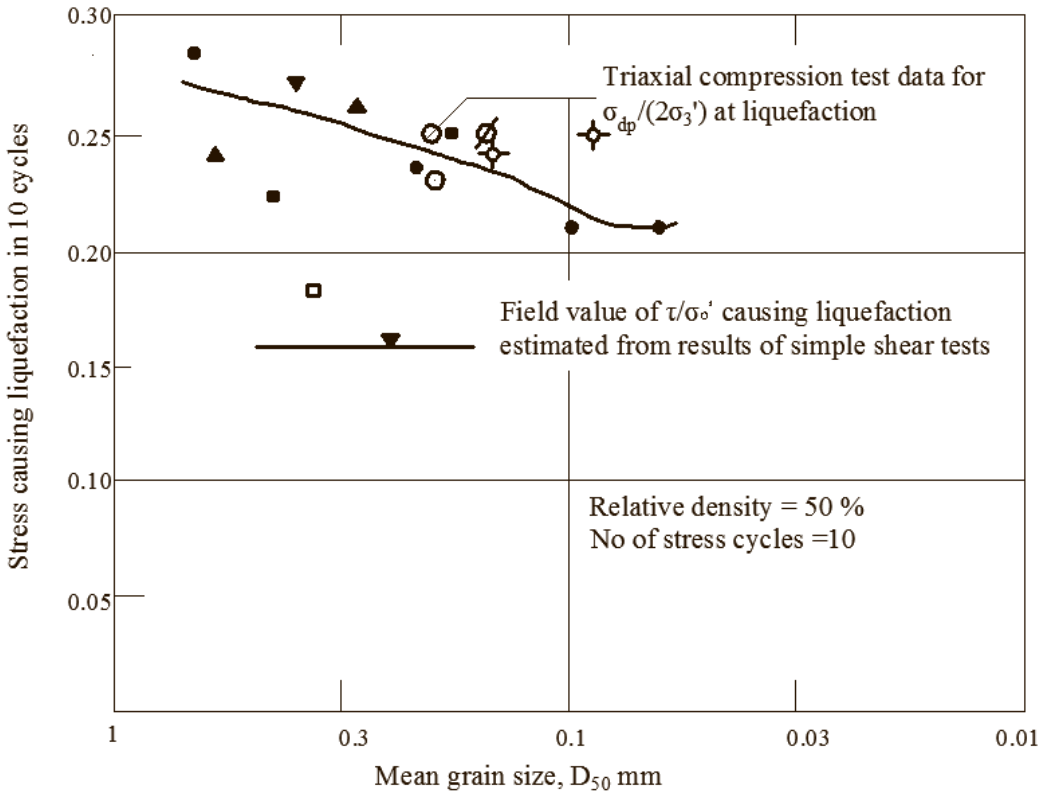

Figure 2-6 Stress ratio causing liquefaction in 10 cycles (Seed and Idriss, 1971).

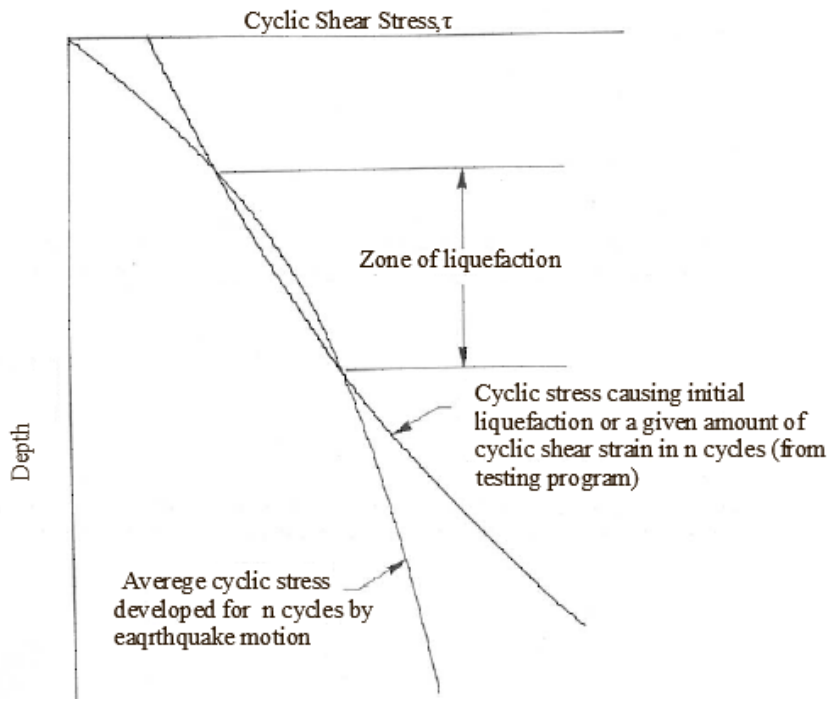

Figure 2-7 Cyclic stress approach for the evaluation of liquefaction potential (Seed and Idriss. 1971).

In addition to the use of Figure 2-6 for the determination of Cyclic Stress Ratio causing liquefaction, several other laboratory and field methods are also available. Cyclic triaxial test, cyclic simple shear test, SPT, CPT, and shear wave velocity can be used for the evaluation of liquefaction potential.

Cyclic triaxial test was developed by Seed and Lee (1966) and used for the study of liquefaction characteristics of sand. After that, it has been used for liquefaction studies, although it has certain limitations. It cannot produce correct initial condition for normally consolidated sands, K_O=1. Further, it has several other limitations (1) stress concentration at the base and the cap of sample, (2) rotation of major principle plane by 90 degrees during two halves of cycle, (3) invalidation of the test due to the development of necking in the specimen, (4) variation of intermediate principal stress during two halves of loading cycle, (5) difficulty to maintain Cyclic Stress Ratio above 0.6, and (6) Cyclic Stress Ratio in this test is the ratio of shear stress to confining pressure

so it does not give the actual field CSR, and should be converted to actual field condition. Finn et al. (1971), Seed and Peacock (1971), Castro (1975) have recommended the conversion factor for the conversion of CSR from cyclic triaxial to actual field for different Ko conditions.

Peacock and Seed (1968) used cyclic simple shear test for liquefaction studies. The CSR required for causing liquefaction can be determined from the cyclic shear test. However, the cyclic simple shear test has certain demerits such as (1) difficulty in preparing representative samples, (2) the development of uniform shear stress and shear strain, and (3) avoidance of stress concentration. The stress concentration can be reduced using large diameter samples and lower height and conducting large-scale simple shear test (De Alba et al, 1976). Cyclic torsional test (Ishihara and Li, 1972), (Ishibashi and Sherif, 1974) avoids stress concentration. Further, the shaking during an earthquake is multidirectional and so the unidirectional shaking in the lab does not truly simulate the field condition. In addition, shear stress required to cause liquefaction in two directional shaking is 10-20 % lesser than one directional shaking (Pyke et al., 1975).

Besides laboratory experiments, field test such as SPT can be used for the liquefaction potential evaluation. Japanese engineer Kishida (1966), Koizumi (1966) and Oshaki (1966) used SPT-blow count to differentiate the liquefiable and non-liquefiable soil during Nigata earthquake based upon SPT blow count and overburden pressure. The plots, they have presented are useful only for the same magnitude earthquake and water table condition. Seed and Peacock (1971) provided the correlation between CSR and relative density. Based on field observations of sites which did or did not liquefy, Seed et al. (1983) presented a plot, which is shown in Figure 2-8 between (τ/σ_o') and $(N_1)_{60}$. From this graph, the CSR required to cause liquefaction in the field corresponding to $(N_1)_{60}$ can be obtained. It can be noted $(N_1)_{60}$ is the blow count corrected for effective overburden stress.

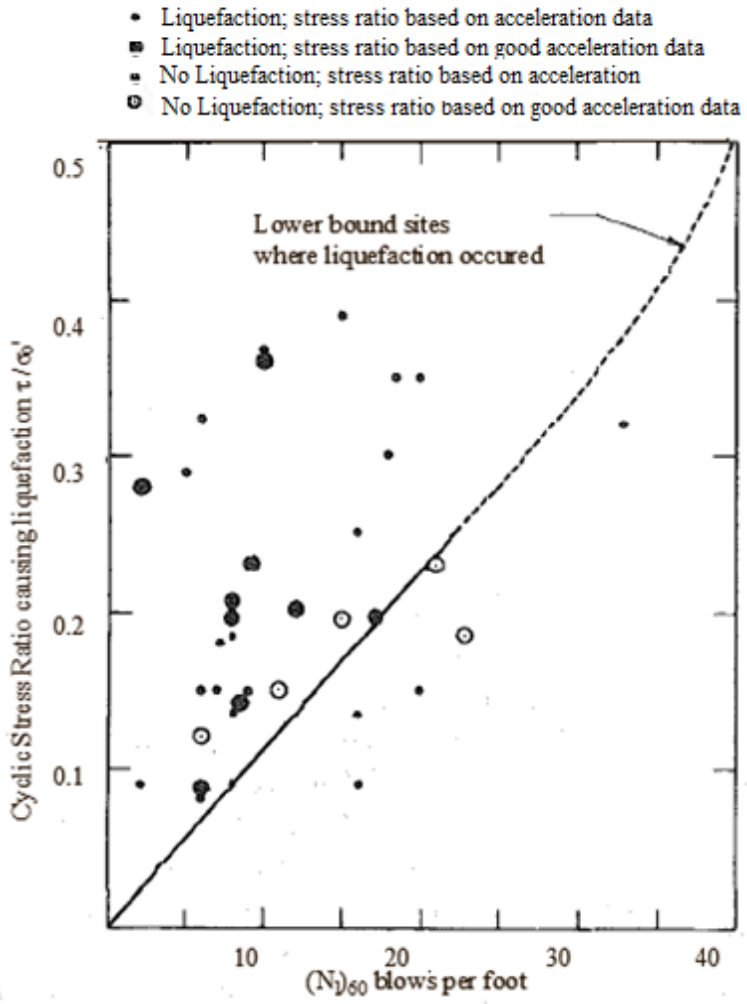

Figure 2-8 Correlation between CSR causing liquefaction and SPT $(N_1)_{60}$ values, (Seed et al., 1983).

2.3. Effects of fines on microstructure of sands

The structure of the sand changes on addition of fine particles. The addition of fine particles creates metastable structure. The deformation behavior of the mixture depends on the packing of the particles, whether it is loose or densely packed. In the mixture of coarse and fine-grained material, the packing depends upon the relative size and proportion of the particles. On adding fine particles in coarse particles, initially, the fine particles fill the voids in between the coarse particles. On further increasing the amount of fines, the fine particles replace the coarse particles

(Cubrinovski and Ishihara, 2002). Lade et al. (1998) reported that, the fine particles can be confined in the void space of coarse particles, if the ratio of diameter of coarse to fine particle is greater than 6.5. Moreover, minimum void ratio increases with an increase in ratio of diameter of coarse to fine particle. Laboratory studies on the mixture of gap graded Cambria sand and Nevada fines, have shown that, the e_{max} and e_{min} decrease with increase in fine content up to 20 % and for 20-40 %, it is nearly constant, after 40 %, it increases as shown in Figure 2-9 (Lade et al., 1998). The minimum void ratio decreases with an increase in fine content, for all mixtures and the amount of decrease depends upon the size of coarse and fine particles. The decrease in minimum void ratio continues with increase in D_{50} / d_{50} (where, D_{50}=Mean grain size of coarse material and d_{50} = mean grain size of the fine material). Further, maximum void ratio also follows a similar pattern (Cubrinovski and Ishihara, 2002). Based on the experiments performed on 300 samples, they proposed relationship between maximum and minimum void ratio for different percentages of non-plastic fines and void ratio range, which is shown in Figure 2-10. Besides percentage of fine content, grain size and angularity also affects the internal structure of sands.

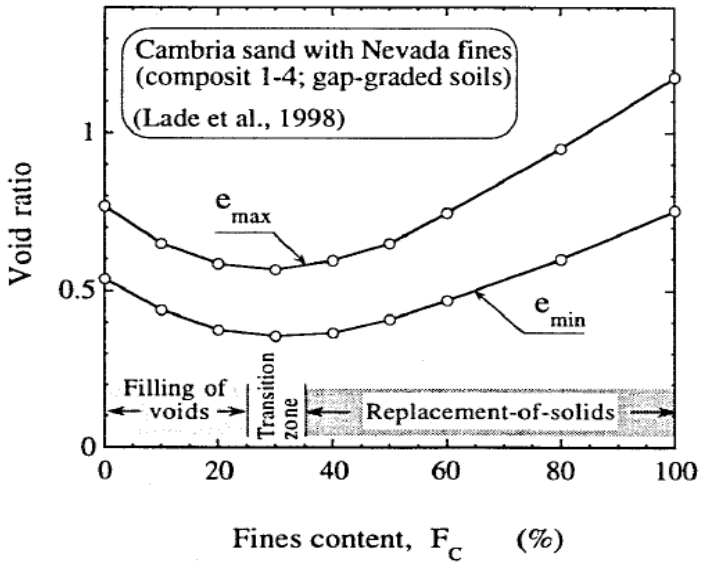

Figure 2-9 Variation of e_{max} and e_{min} with fine content for mixture of Cambria sand and Nevada fines (Lade et al., 1998).

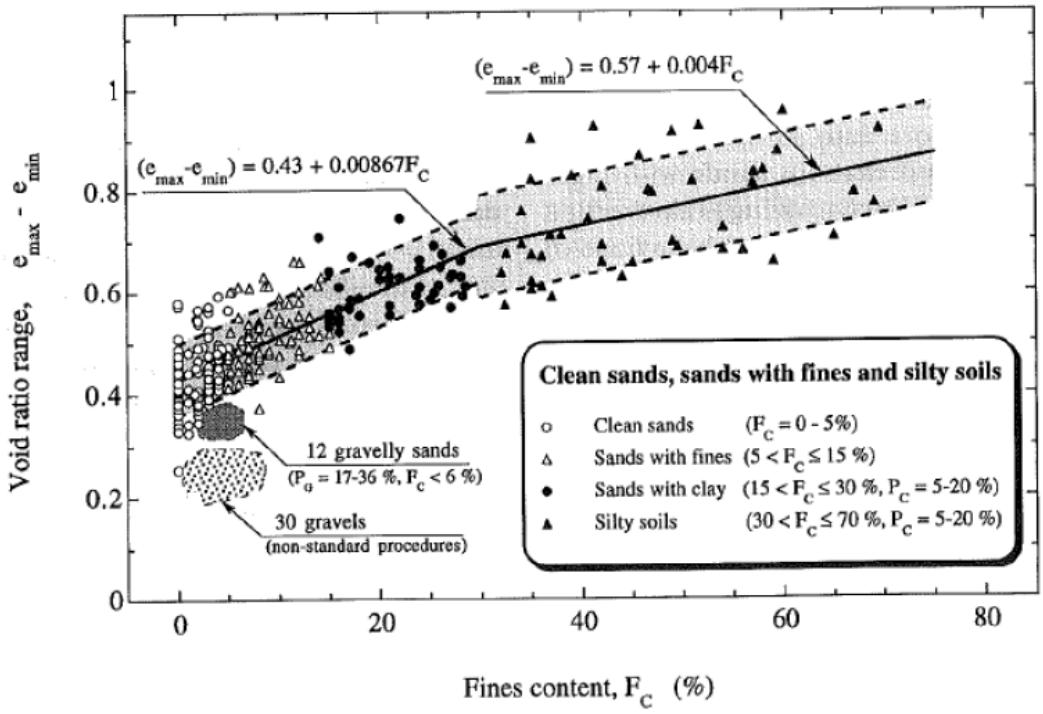

Figure 2-10 Variation in the void ratio range, ($e_{max} - e_{min}$), with fines content (Cubrinovski and Ishihara, 2002).

Thevanayagam (1998), Thevanayagam et al. (2000) and Thevanayagam (2007) classified the granular mixes of fine and coarse grained material as shown in Figure 2-11. They described the participation of coarse and fine particles in force chain depending upon the percentage of fines. For fine particles less than threshold fine content, granular mixes are classified into three different categories. The threshold fine content depends upon the shape and size of particles and it ranges from (25 to 45 %) for most sands (Polito and Martin, 2001). If the ratio of D_{50} / d_{50} of the particle is greater than 6.5, i.e. fines are finer than coarse particles, the fine particles confine in the matrix of coarse particles and fine particles can move during the cyclic load application (case i). On repeating the layer of fine particles, the fine particle may not be confined in the voids of sand, which results case ii. On further increasing the fine particles, it may not confine into the voids of sand and some fine particle may separate the coarse particles and act as separating layer. Fine particles can participate in force chain in case ii and iii, where as there is no role of fines in force chain in case i.

When the fine particles exceed the threshold fine content, then; the fine particles have a vital role in force chain. If fines are less than limiting fine content, it results case iv-1. Particles are fully dispersed and coarse particles act as reinforcing element. On increasing fines above the limiting fine content, coarse particles are partially dispersed and do not have a significant effect on force chain (case iv-2).

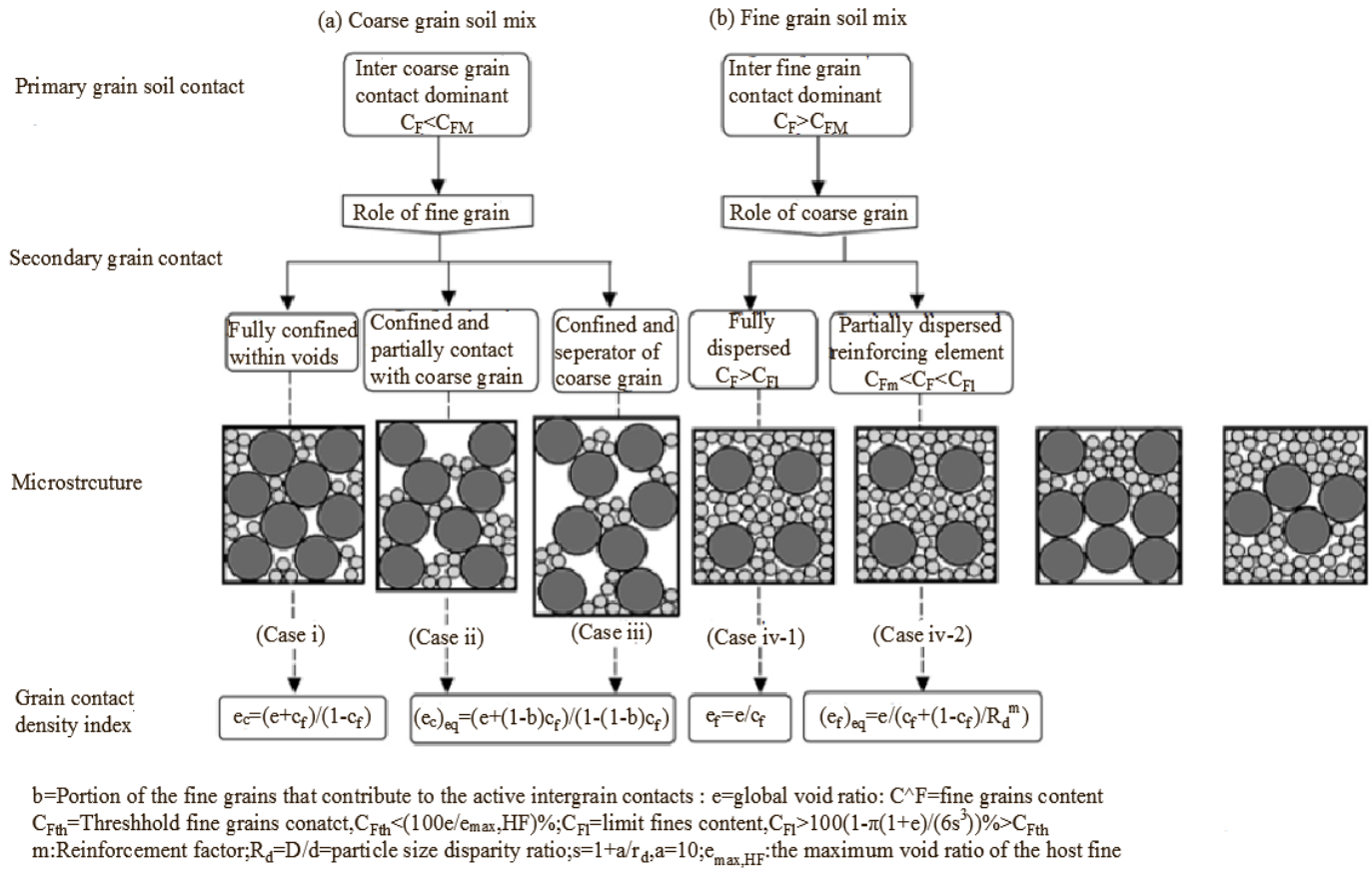

Figure 2-11 Classification of intergranular sands and fines mixtures (Thevanayagam, 2007).

2.4. Effects of fines on liquefaction potential of sands

The sands containing fines were supposed to have higher liquefaction resistance than clean sands, which is supported by several field investigations. However, results of subsequent laboratory experiments do not indicate a clear conclusion. Review of past literature indicates that, the effect of fines differs with the basis of comparison. The comparison can be made in terms of : (a) Global void ratio, (b) Skeletal void ratio, and (c) Relative density. Further, even for same basis of comparison, the effects are different. Several plastic and non-plastic fines have been used in laboratory investigations.

Dezfulian (1984) conducted cyclic triaxial tests on undisturbed soil consisting of silty clayey, clayey silt, silty sand with mean diameter varying from 0.002 to 0.2 mm (average 0.07 mm) and fines varying from 7 to 100 percent. Liquefaction resistance was compared based on number of cycles required for 5 % double amplitude strain. It was observed that, there was an increase in liquefaction resistance with increase in silt contents. No information was given about plasticity index, and diameter of silt particle present in the sand.

2.4.1. Field investigation

Based on the field data from Japan, Tatsuoka et al. (1980) compared the liquefaction potential of silty clay and clean sands. They concluded that, silty sands are less susceptible to liquefaction than clean sands when it is compared based on SPT N value. Further, they suggested that, CSR for silty sand could be determined using SPT-CSR curve for clean sands by adding 7 to the N value of silty sands. The similar effect of the fine was observed by Zhou (1981). He collected the field data during Tangshan earthquake (China) for the determination of CSR required to cause liquefaction. Then, he recommended to increase the SPT N value depending upon the fine contents. For 30 % fine contents, it was around 6, which is similar to Japanese studies. Then, Seed et al., (1985) collected more field data containing fines and plotted CSR versus $(N_1)_{60}$ value plots for soil which did or did not liquefy in the field. They specified the boundary line separating the condition causing the liquefaction and non-liquefaction as shown in Figure 2-12. It shows that, for same $(N_1)_{60}$ value, the liquefaction resistance increases with fine contents, which is consistent with the observation of Tokimatsu and Yoshimi (1981).

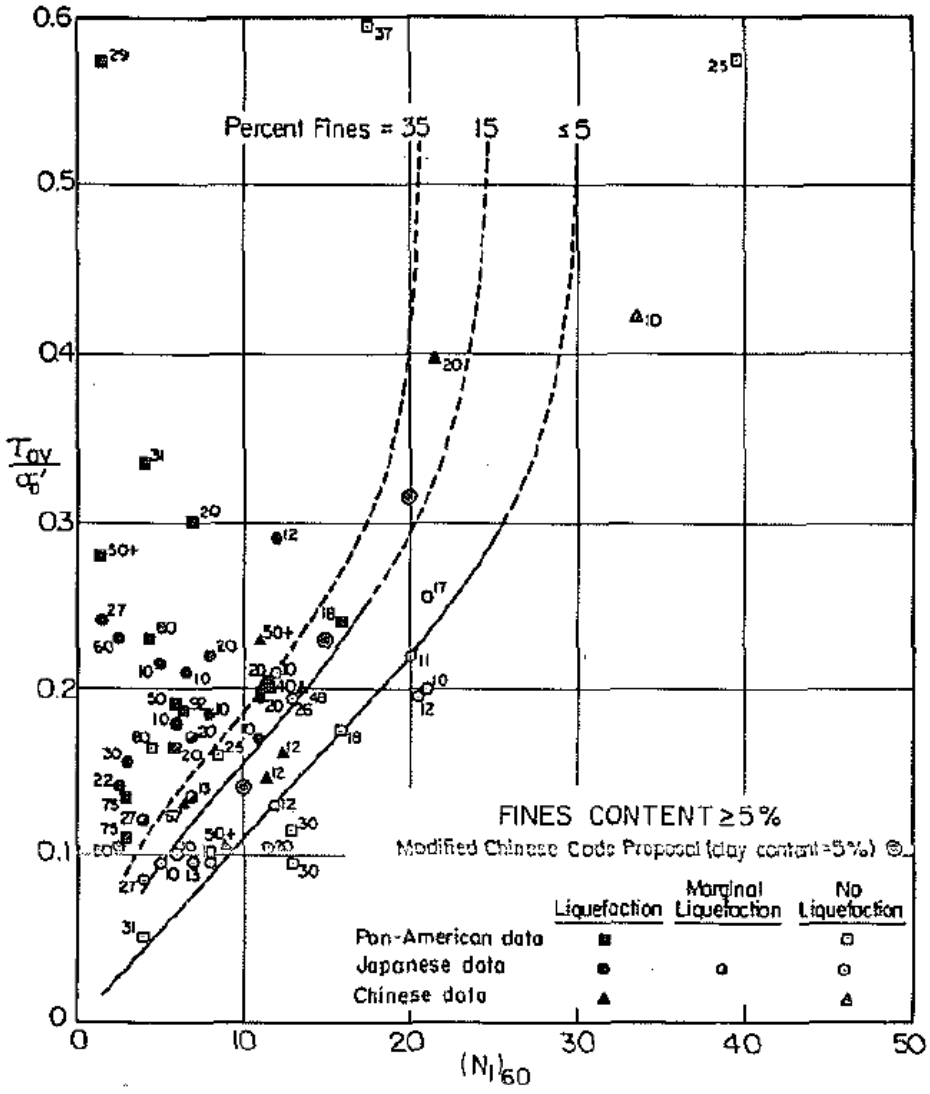

Figure 2-12 Relationship between stress ratio causing liquefaction and $(N_1)_{60}$ values for silty sands for M=7.5 earthquakes (Seed et al., 1985).

2.4.2. Laboratory investigations of effects of fines

The results of cyclic triaxial tests performed by various researchers are presented in this section. It includes the evaluation of effects of fines at (1) constant global void ratio, (2) constant skeletal void ratio, and (3) constant relative density. Then, the effects of plasticity of fines on liquefaction resistance are presented.

2.4.2.1. Constant global void ratio

Several researchers have been evaluating the effects of fine content, by preparing the sample at constant global void ratio for each silt content. Chang et al. (1982) conducted the cyclic triaxial tests on the mixtures of sand and silt, which contained silts up to 100 %. At a constant global void ratio, they reported that the liquefaction resistance decreases on adding 10 % silt in clean sand. On further addition of silt, the liquefaction resistance was seen to increase. The silt they have mixed with clean sand had higher liquefaction resistance than clean sand as well as sand-silt mixture. Further, they observed that, the liquefaction resistance increases with mean grain diameter, i.e. the sands have higher liquefaction resistance than fines. The summary of the test results is shown in Figure 2-13.

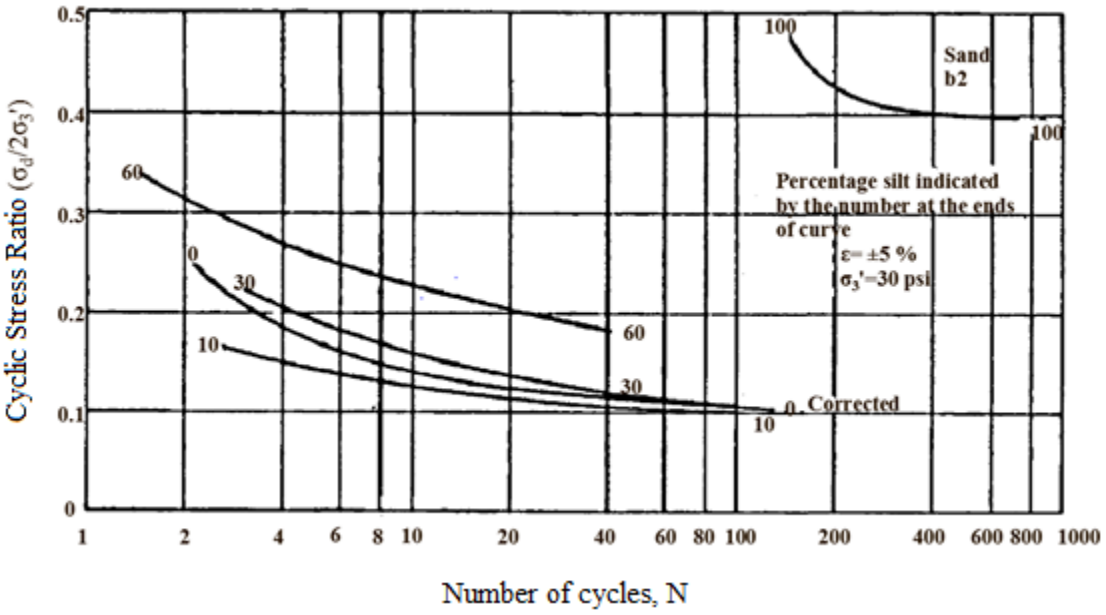

Figure 2-13 Effect of silt content on cyclic shear resistance (Chang et al., 1982).

Koester (1994) reported that, the liquefaction resistance decreases on the addition of fines up to 24 to 30%. Then it increases with further increase in percentage of fine content. The variation of cyclic resistance with various percentages of fines content is shown in Figure 2-14.

The results were based on cyclic triaxial tests performed on the mixture of sand, silt and plastic clay at a constant global void ratio of 0.558 and plasticity index of 4.

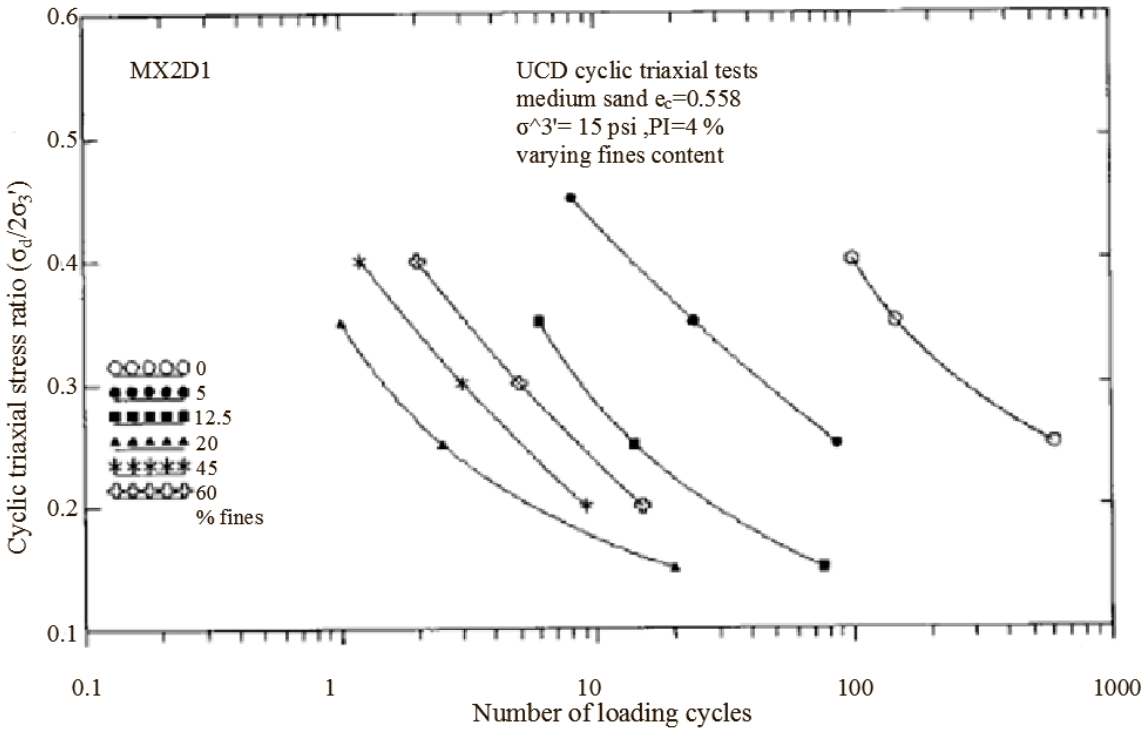

Figure 2-14 Cyclic triaxial strength curves for medium sand mixtures (Koester, 1994).

Further, Thevanayagam et al. (2000) also investigated the effects of fines at constant global void ratio. The mean grain size of the sand and fines were 0.024 mm and 0.007 mm, respectively and ratio of the mean grain diameter of sand to mean grain diameter of fines was 3.42. They observed that the liquefaction resistance decreases on adding fines up to threshold fine content. Further addition of fines above threshold fine content, increases the liquefaction resistance. The variation of Cyclic Stress Ratio with fines is shown in Figure 2-15.

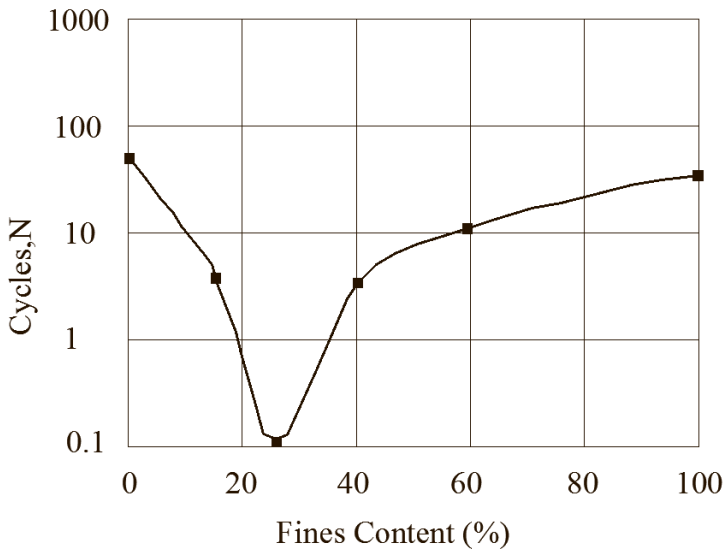

Figure 2-15 Effect of fine content on liquefaction resistance at constant void ratio (Thevanayagam et al., 2000).

Similar results were obtained by Polito and Martin (2001). They conducted cyclic triaxial tests on two types of sands adding non-plastic silts ranging from 4 to 75%. They used Monterey sand and Yatesvile sand as a coarse material, having mean grain diameters of 0.43 mm and 0.18 mm, respectively. As fines, silt obtained from the fine grained portion of Yatesvile sand having a mean grain diameter 0.03 mm was used. The ratio of the mean grain diameter of Monterey sand and Yatesvile sand to fines were 14.33 and 6, respectively. At a constant global void ratio, they obtained similar results on both types of sand. The liquefaction resistance decreases up to limiting silt content, after that, it increases with an increase in silt content. Figure 2-16 shows the variation of liquefaction resistance with silt content for Monterey sand.

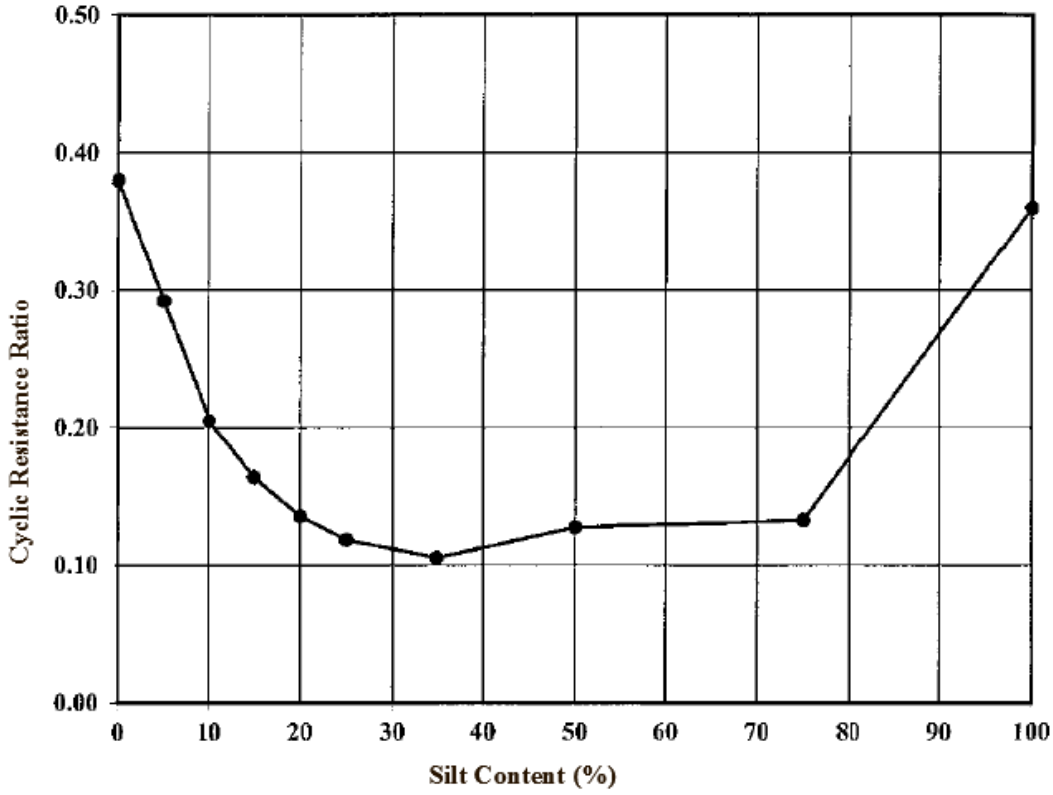

Figure 2-16 Cyclic resistance of Monterey sand at constant void ratio with variation in silt content (Polito and Martin, 2001).

Further, Xenaki and Athanasopoulos et al. (2003) and Athanasopoulos and Xenaki (2008) conducted cyclic triaxial tests on the mixture of sand containing six different percentages of non-plastic fines at constant global void ratio. The mean grain diameter (D_{50}) for sand and (d_{50}) for fines were .12 mm and .02 mm, respectively. The ratio of the mean grain diameter ratio for sand to fine was 6. They observed that, the liquefaction resistance decreased on increase in the fines content up to threshold limit of 44 %, after that the trend was reversed with an increase in fines. The effect of fines on cyclic stress ratio causing liquefaction is shown in Figure 2-17. Further, they interpreted the result in terms of intergranular void ratio and interfine void ratio based on the conceptual framework of Thevanayagam (2000). They concluded that for the same intergranular void ratio, the liquefaction resistance of sand increases with an increase in the fines

content, which is similar to the observation of Seed et al. (1985). For fines above the threshold fine content, they analyzed the result in terms of the interfine void ratio. For the constant interfine void ratio, the liquefaction resistance was decreased on increasing fines content. However, they did not have sufficient data for the analysis of the result in terms of the intergranular void ratio and interfine void ratio.

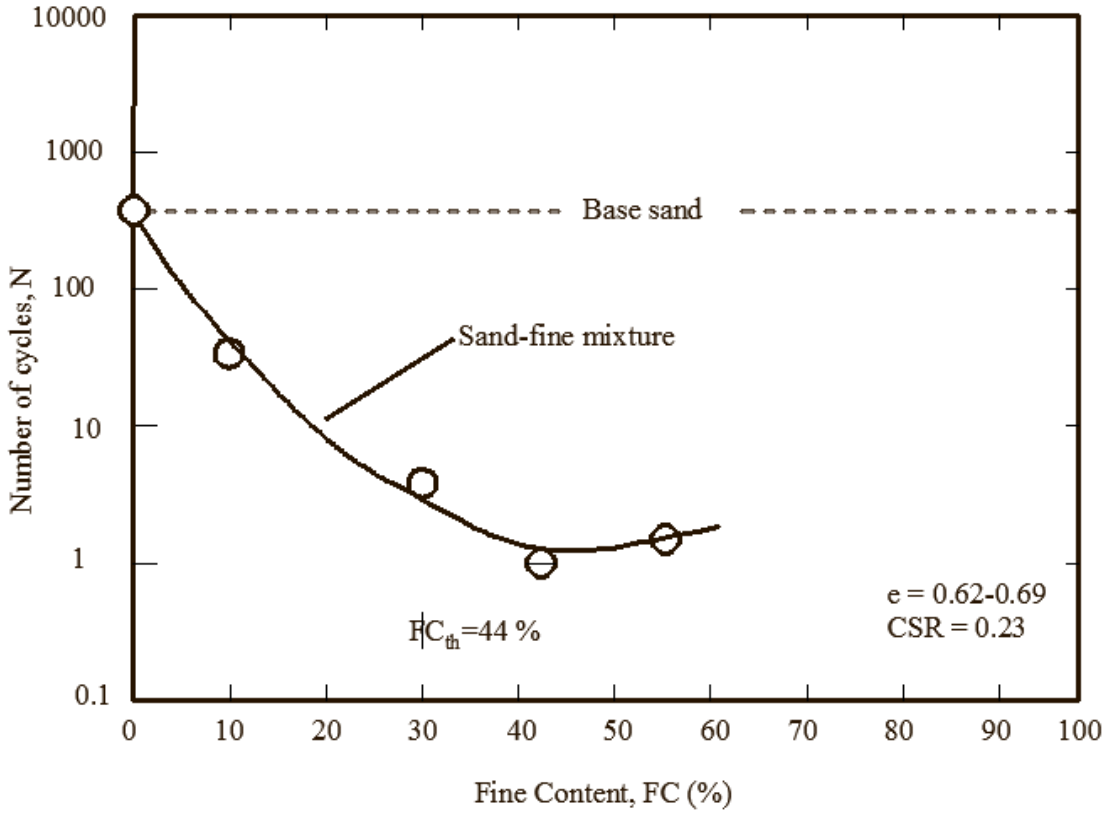

Figure 2-17 Effects of fines content on the liquefaction resistance of sand-non plastic fines mixtures for constant global void ratio (Xenaki and Athanasopoulos, 2003).

Sitharam et al. (2013) conducted cyclic triaxial tests on the mixture of clean sand obtained from Ahmedabad, after removal of fines and non-plastic quarry dust. The mean grain diameter (D_{50}) of tested sand and quarry dust was 0.375 mm and 0.037 mm, respectively. The ratio of the mean grain size of sand to quarry dust was 10.13 and limiting silt content was 21%. For a constant

global void ratio, the liquefaction resistance decreases with increase in fine content up to limiting silt content and trend reverses on increasing above, as shown in Figure 2-18.

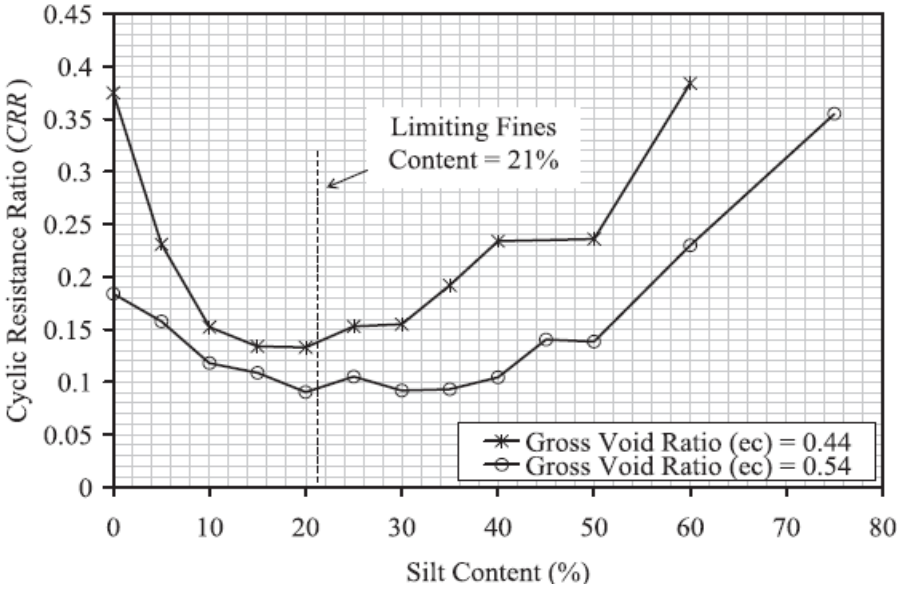

Figure 2-18 Variation of cyclic resistance of sandy soils with silt content tested at constant post consolidation average gross void ratio (Sitharam et al., 2013).

Above review indicates that, most of the researchers are getting a similar type of results on comparing liquefaction resistance at constant global void ratio. Liquefaction resistance has been seen to decrease up to a certain fines content and then increases as the fines content increases.

2.4.2.2. Constant sand skeletal void ratio

Some of the research on effect of fines on liquefaction of sands was conducted at constant skeletal void ratio. The skeletal void ratio was defined by Kuerbis and Vaid (1988) as the void ratio of the sand-fine mixture, which is calculated by considering the fines as void. Sand skeleton void ratio ($e_{skeleton}$)is expressed as,

$$e_{skeleton} = \frac{V_T G_S \rho_{w-(M-M_{silt})}}{M - M_{silt}}$$

Where, V_T = Total volume of the specimen, G_s = Specific gravity of sand, ρ_w= density of water, M = total mass of the specimen, M_{silt}= mass of the silt.

Kuerbis and Vaid (1988) studied the effect of fines in stress controlled cyclic triaxial test device on Brinda tailing sand and Kamloops silt as fines. Samples were prepared by slurry deposition method developed by Kuerbis (1987). At constant skeletal void ratio, they observed that, silty sand in the loosest state has similar liquefaction resistance regardless of fine content, even though there was large variation in void ratio. Further, for same sand skeletal void ratio, there was a reduction in liquefaction resistance with an increase in silt content. On the other hand, liquefaction resistance increases on decreasing void ratio, which is shown in Figure 2-19.

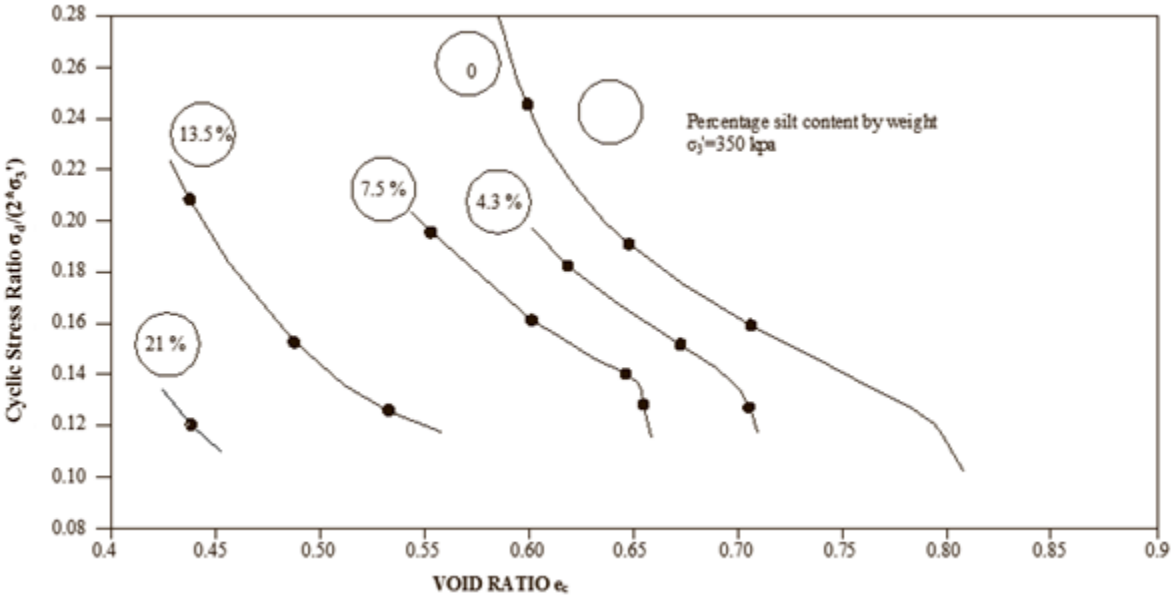

Figure 2-19 Variation of silty 20/200 sand cyclic strength with silt content and skeletal void ratio (Kuerbis and Vaid, 1988).

Further, Polito and Martin (2001) observed different behavior on Monterey sand and Yatesvile sand. Below limiting silt content, the cyclic resistance was constant for Monterey sand. On the other hand, it increased with an increase in silt contents. In addition, they observed a strong

correlation for Monterey sand with skeletal void ratio. The cyclic resistance was found to decrease on increasing skeletal void ratio for both, above and below limiting silt content. However, they found scattered result for Monterey sand. The cyclic resistance decreased with an increase in silt content up to 50 %.

Thevanayagam (1998) replaced the term sand skeleton void ratio by the intergranular void ratio for the mixture having silt content below the limiting fine content. Thevanayagam et al. (2000) explained their result in terms of the intergranular void ratio for the fines below threshold fine content. According to them, the liquefaction resistance increases with an increase in silt content at constant intergranular void ratio. On the other hand, for the fines above threshold fine content, liquefaction resistance decreases with increase in fine content at constant interfine void ratio.

2.4.2.3. Constant relative density

Kuerbis and Vaid (1988) conducted tests at constant relative density. The silt content was varied up to 21 %. They reported that, the liquefaction resistance decreases on an increase in the silt content. They also compared the result in terms of constant skeleton relative density and found that the liquefaction resistance increases with the addition of silt.

Singh (1996) performed cyclic triaxial tests on reconstituted samples of Flint shot no. #4 sand (mean grain diameter 0.3 mm), containing 10, 20, and 30 % silt which was retained on no. 200. The liquefaction resistance of sand-silt mixture decreased on addition of 10 and 20 % silt whereas; it was slightly increased on addition of 30 % silt. However, it was lower than that of clean sand. Further, he reported that, the clean silt has lower liquefaction resistance and the sand containing 10, 20 and 30 % silt has lower liquefaction resistance than clean silt. The variation of liquefaction resistance with different sand and silt contents is shown in Figure 2-20. In this tests, there was variation in back pressure applied for different sand, silt combinations. The back

pressure applied for saturation of 20 and 30 % sand-silt mixtures was lower than that for clean sand whereas, for clean silt it was higher. The liquefaction resistance increases with increase in back pressure (Xia and Hu, 1991). Xia and Hu observed that on increasing back pressure from 0 to 382.4 kPa, the cyclic stress ratio required for liquefaction at same number of cycles, was increased by two times. In case of Singh‘s experiment, there was a difference of 200 kPa in back pressure in between clean silt and clean sand. If Singh (1996) had conducted the tests with same back pressure, the silt might have significantly lower liquefaction resistance than clean sand whereas there might be an increase in the liquefaction resistance in sand containing 30 % silt than for 20 % silt.

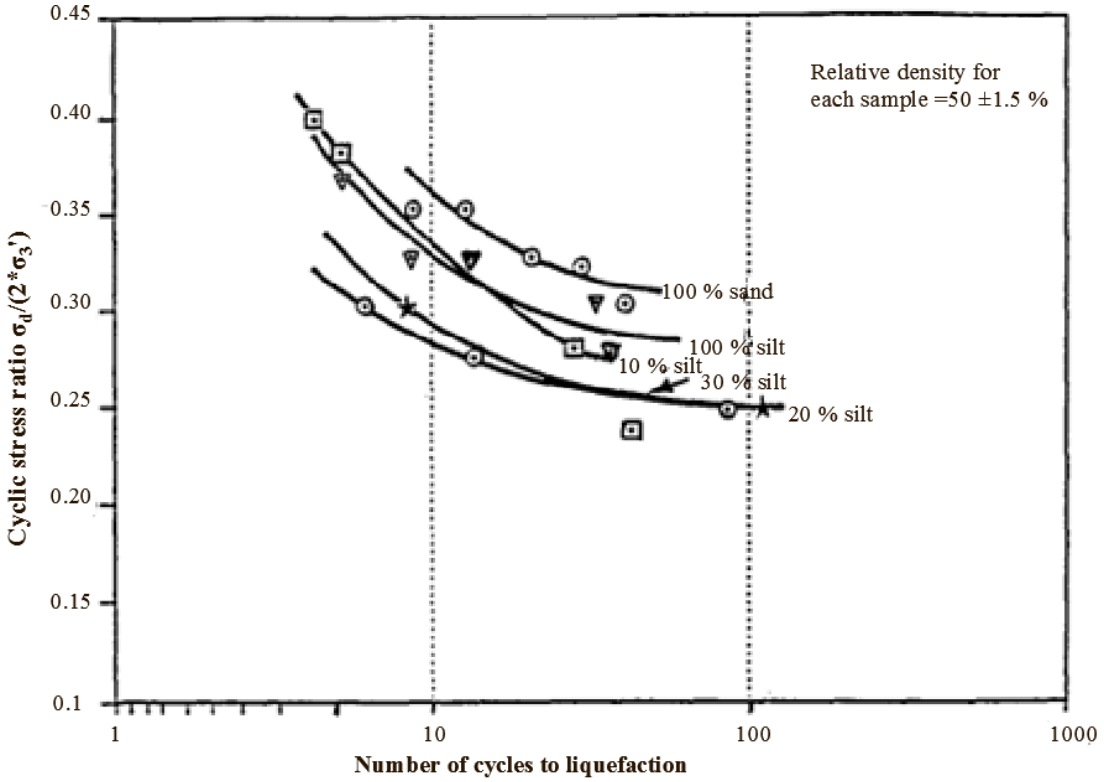

Figure 2-20 Relationship between cyclic stress ratio and number of cycles to initial liquefaction for reconstituted samples of sand containing different percentage of silt (Singh, 1996).

In order to investigate the effects of fines at constant relative density, Amini and Qui (2000) conducted cyclic triaxial tests on the mixture of Ottawa (20-30) sand and low plastic silt of PI=3.

They have used moist tamping and wet Pluviation method, simulating the homogeneous and layered condition, respectively. No information was provided regarding the particle size of silt and limiting silt content. They observed that the liquefaction resistance increases with addition of silt up to 50 %, at constant relative density as shown in Figure 2-21. On increasing the effective confining pressure, the liquefaction resistance was reduced. Further, they did not observe variation in liquefaction resistance for the uniform and layered soil.

In addition to the sand skeleton void ratio and global void ratio, Polito and Martin (2001) also compared the effects of fines at constant relative density**.** They observed that, for silt contents less than the limiting silt content, the cyclic resistance increases with an increase in relative density. They got a similar trend for silt contents above the limiting silt content; however, the cyclic resistance was lower than that of sand, silt mixture below limiting silt content. Further, the rate of increase in cyclic resistance with relative density was slower. For the samples prepared at constant relative density, they observed almost constant cyclic resistance up to limiting silt content and decrease in cyclic resistance on increasing above limiting silt content as shown in Figure 2-22.

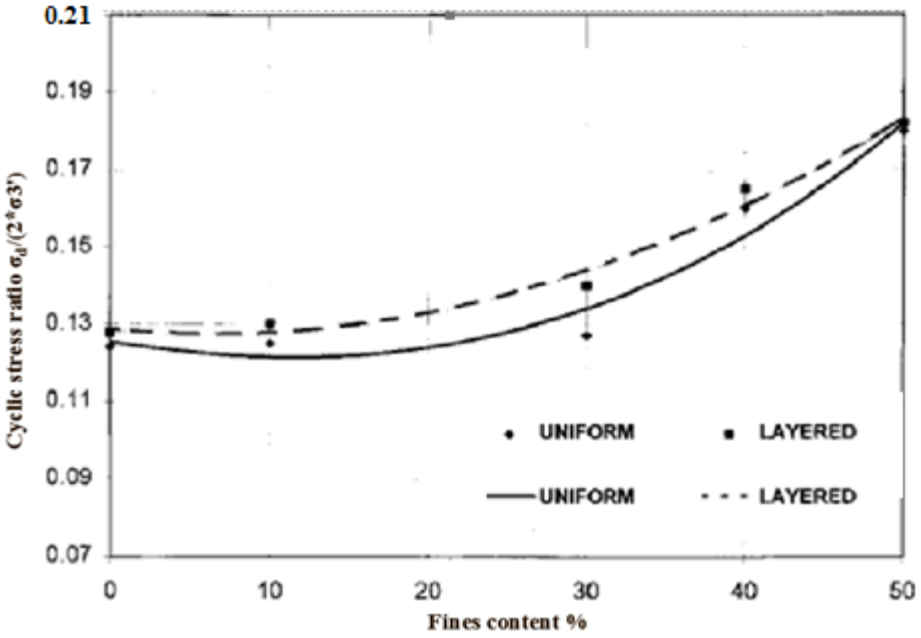

Figure 2-21 Comparison of liquefaction behavior of layered and uniform soil as function of silt content for stress ratio to cause liquefaction at 10 cycles (Amini and Qui, 2000).

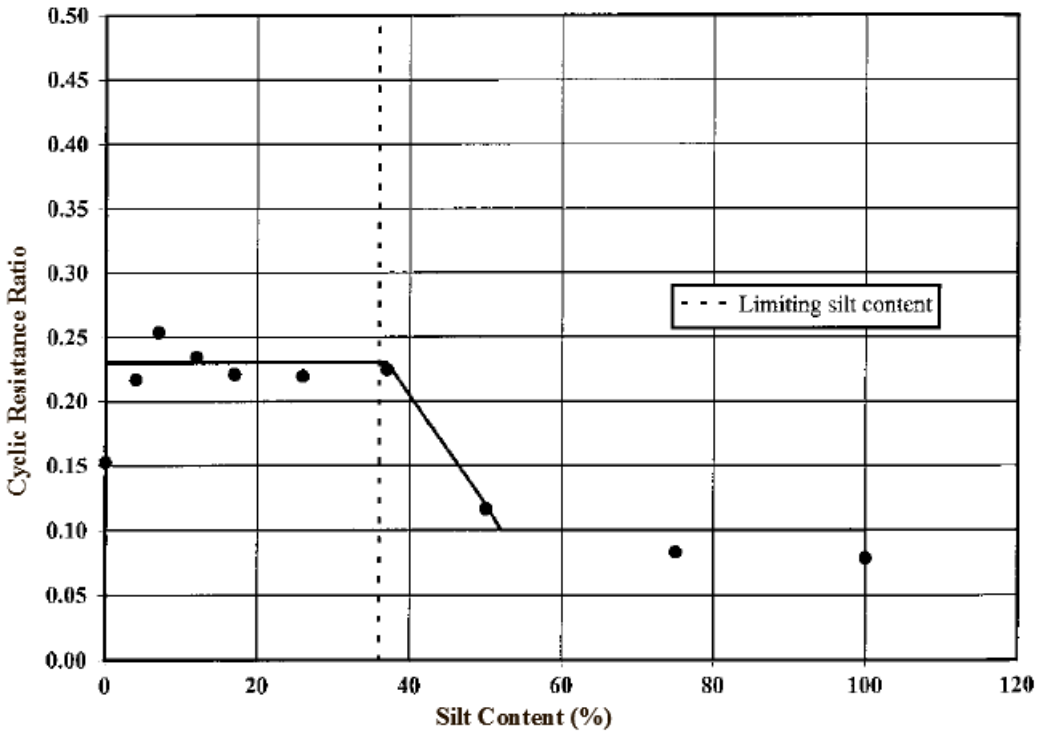

Figure 2-22 Variation of cyclic resistance with silt content for Yatesvile sand specimen at 30 % relative density (Polito and Martin, 2001).

Sadek and Saleh (2007) also used relative density as a basis of comparison. They conducted cyclic triaxial tests on Ottawa sand having mean grain size of 0.31 mm, containing non plastic fines obtained from rock quarries, with mean grain diameter 0.02 mm. The ratio of the mean grain size of sand to fine is 15.5. At constant relative density of 50, 60, 70, and 80 %, on adding non-plastic fines (rock flour from quarries), the liquefaction resistance was increased up to 10 % fines, and then it was reduced on further increasing fine contents. The variation of cyclic resistance with various percentages of silt is shown in Figure 2-23.

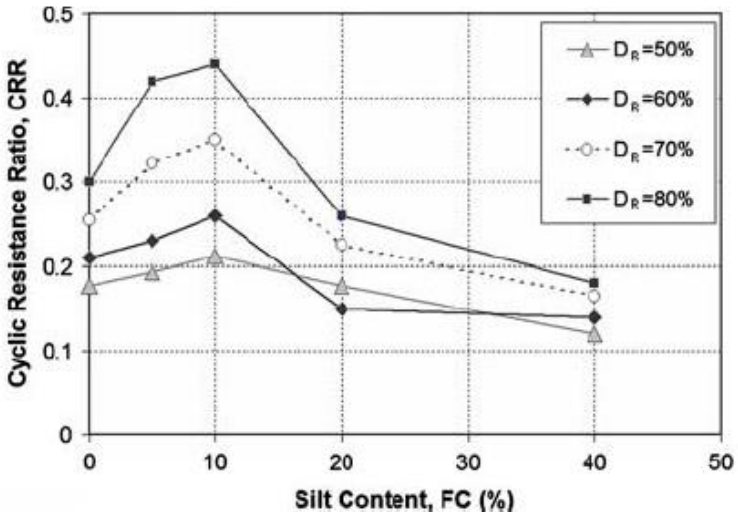

Figure 2-23 CSR versus fine content (Sadek and Saleh, 2007).

Cubrinovski and Rees (2008) conducted undrained triaxial and cyclic triaxial tests on the mixture of sand and non-plastic fines. The information of particle sizes on sand and fines are not available. On similar relative density, they reported that, the liquefaction resistance decreases with increase in fines content up to 30 %. However, if state concept is used as a basis of comparison, they reported, liquefaction resistance increases with addition of fines.

Further, Schmidt (2008) evaluated the effect of mica content on cyclic resistance of poorly graded sand. He conducted the cyclic triaxial tests on sand containing 2, 5, and 10 % mica. He reported that at constant relative density, the liquefaction resistance decreases on increasing mica content.

In addition to evaluation of fine content, based on global void ratio, skeletal void ratio, and relative density, a different parameter namely constant dry density was used by Wang and Wang (2010) studied the effect at constant dry density. They added non-plastic fines up to 45 % in sand. Based on cyclic triaxial tests, they observed that, the liquefaction resistance decreases up to limiting fine content 30 % (Figure 2-24). After that, it increases with an addition of silt contents. This is similar to observation made by Polito and martin (2001).

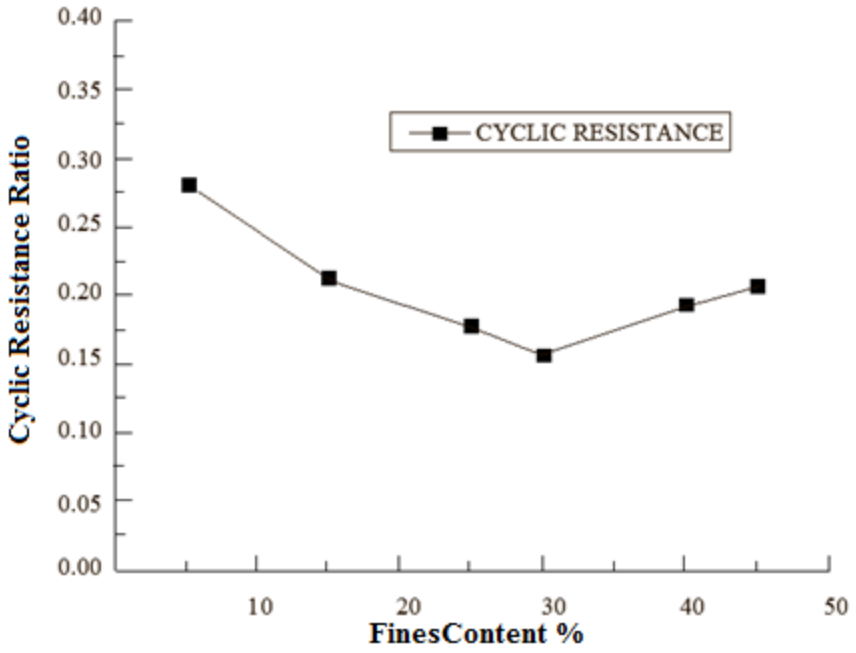

Figure 2-24 Variation in liquefaction resistance with fine content for initial liquefaction at 20 cycles (Wang and Wang, 2010).

2.4.2.4. Effects of plasticity of fines

Initially, clays were believed to be non-liquefiable. However, clay, sands, and silts containing fines are found to have liquefied during several earthquakes. During Mino-Owari, Tohnakai and Fukui earthquake, coarse grained soil (50 % particles less than 2 mm) were found to have liquefied (Kishida, 1969). The plasticity index of the fines was found to affect the stress-strain behavior of the soil. Boulanger and Idriss (2006) reported that the fine-grained soil shows clay like stress-strain behavior for $PI \geq 7$.

Based on the cyclic triaxial tests conducted on tailings material from Chile and Japan with artificially ground quartz powder, Ishihara et al. (1980) observed that cyclic resistance depends upon the plasticity index. The tailings material having PI = 15 to 20 have higher liquefaction resistance than non-plastic tailings sand.

Puri (1984) conducted the cyclic triaxial tests on silt-clay mixture. The plasticity index of the silt was altered adding clay fines. The tests were conducted at PI = 10,15, and 20. The liquefaction resistance was found to increase with an increase in plasticity index. Further, Prakash and Puri (2010) presented the results of Puri (1984) and Sandoval (1989). They reported that, at the same void ratio, the liquefaction resistance decreases for $PI \leq 4$, and after that, it increases as PI increases (Figure 2-25).

For the evaluation of variation of the liquefaction resistance of sand with plasticity index, Law and Ling (1992) conducted cyclic triaxial tests on samples with different composition of sand, silt, and clay. The new Liskeard clay was used which had PI=50. They observed that, liquefaction resistance was found to increase on increasing the clay content at constant void ratio. On the other hand, liquefaction resistance decreased on increasing the non-plastic fines at constant void ratio.

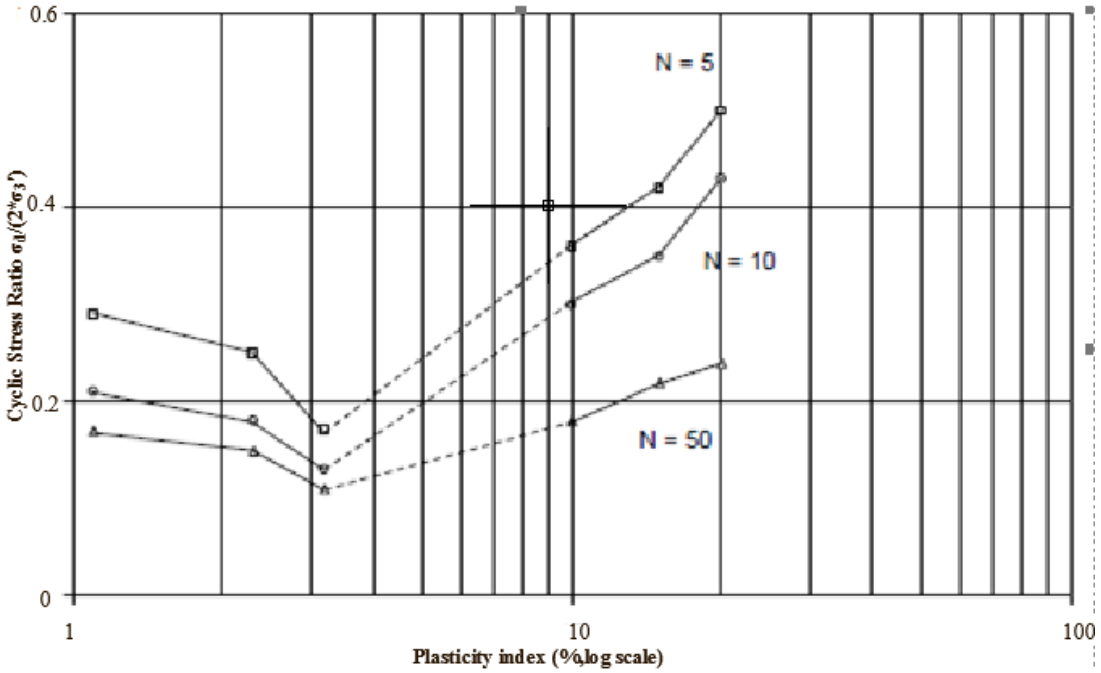

Figure 2-25 Cyclic stress ratio versus plasticity for silt clay mixture (Prakash and Puri, 2010).

Sadek and Saleh (2007) conducted cyclic triaxial tests on sand-fines mixtures using 10 % fines and varied the clay fraction within the fines to change the PI of the samples. They observed that the liquefaction resistance was decreased with an increase in PI up to certain PI value and after that, it increased, as shown in Figure 2-26. Similar result was obtained in a recent study conducted by Park and Kim (2013) on sand containing 10 % fines consisting of silt, kaolinite, and bentonite. Liquefaction resistance was seen to decrease with an increase in PI. They compared the liquefaction resistance at constant global void ratio and the added fines had PI ranging from 8 to 377. The variation of cyclic resistance with PI is shown in Figure 2-27.

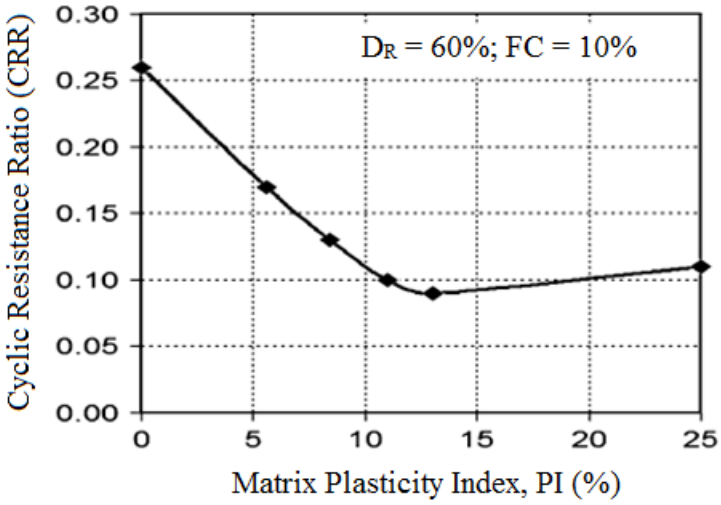

Figure 2-26 Variation of cyclic resistance with PI (Sadek and Saleh, 2007).

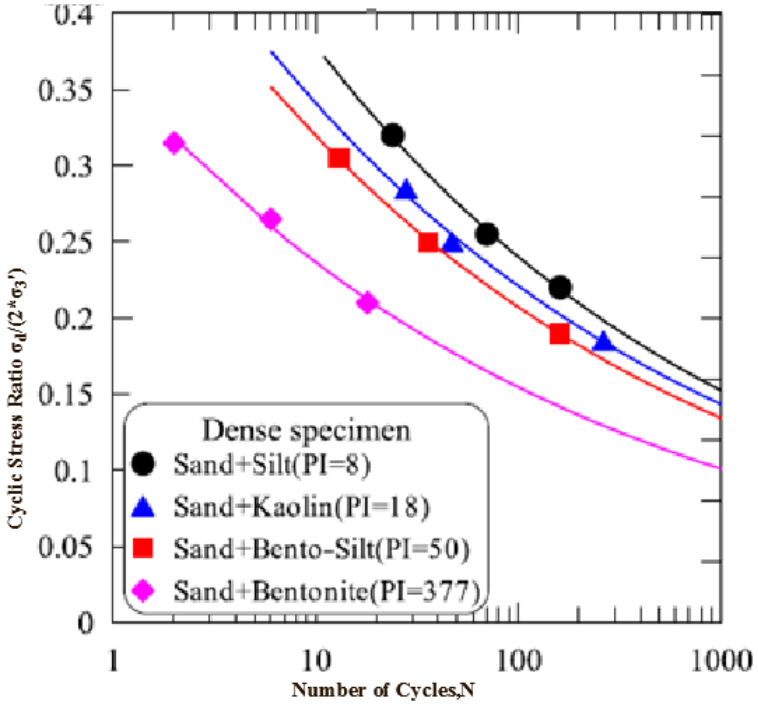

Figure 2-27 Variation of liquefaction resistance with PI (Park and Kim, 2013).

2.5. Summary

During an earthquake, the soil is subjected to cyclic shear stress, which increases the pore water pressures in the soil. Depending upon the magnitude of earthquake and type of soils, the excess pressure may increase up to the effective overburden pressure. If excess pressure equals to overburden pressure, the soil liquefies. Stress and strain approaches are available for the evaluation of liquefaction.

The microstructures of the sand changes on mixing the fines. It can be classified into several classes depending upon the amount of fines, limiting silt content. The role of fines in force chain differs with the amount of fines.

Several researchers have evaluated effects of fines in the field as well as in the laboratory. The reviews of literature indicates that, there is a lot of variation in results obtained on liquefaction resistance depending upon the basis of comparison. The most common basis of comparisons are (1) the standard penetration value, (2) the global void ratio, (3) the skeletal void ratio, and (4) the relative density.

The researches using same standard penetration value $(N_1)_{60}$ as the basis of compariosn reported that liquefaction resistance increases with addition of fines. However, researches using same global void ratio as the criteria observed that the liquefaction resistance decreases initially with an addition of fines, after that it increases. The results using the same skeletal void ratio as the criteria present controversial data. Some of researchers reported that, the liquefaction resistance remains constant on same skeletal void ratio. On the other hand, few researchers observed that, it decreases with addition of fines. Finally, researches using same relative density as the basis of comparison indicated that, the liquefaction resistance initially increases and after that it decreases on addition of fines.

From the review of literature, it can be concluded that, the main reason for variation in the effects of fines is the basis of comparison. Nevertheless, the variation can be observed on same basis of comparison. The variation might be because of testing procedure, particle sizes, liquefaction resistance of added fines and plasticity of fines. Less literature is available for comparison at same relative density and does not indicate clear conclusion. For the investigation of effects of addition of fly ash, relative density might be appropriate parameter.

CHAPTER 3

METHODOLOGY

3.1. Introduction

This chapter describes testing methodology and materials used in this research. The materials used in this research are presented in the beginning, and include index properties of sand, fly ash and sand-fly ash mixtures. Then, the cyclic triaxial test and its use in the simulation of earthquake loading are discussed. The testing procedures such as sample preparation, initialization, saturation, consolidation, cyclic shear phase and data obtained during the tests are given.

3.2. Materials

Clean sand, pure fly ash and sand-fly ash mixtures containing 10 and 20 % fly ash were tested on cyclic triaxial equipment. The properties of clean sand, fly ash and it's mixture are given below.

3.2.1. Sand

The Ottawa (20-30) sand corresponding to ASTM C 778 was used in this research. It is a natural silica sand, which is commercially supplied by Humboldt. In order to find out the grain size properties, sieve analysis was performed according to ASTM D 422. The grain size distribution of sand is shown in Figure 3-1. The sand was classified as Poorly Graded Sand (SP) as the Unified System. The specific gravity of the sand was determined from Quanta chrome gas pycnometer, in accordance with ASTM D5550-06. The maximum and minimum void ratios were determined according to ASTM D4254 and ASTM D 4253, respectively. ASTM method 1 a was used for the determination of maximum and minimum void ratios.

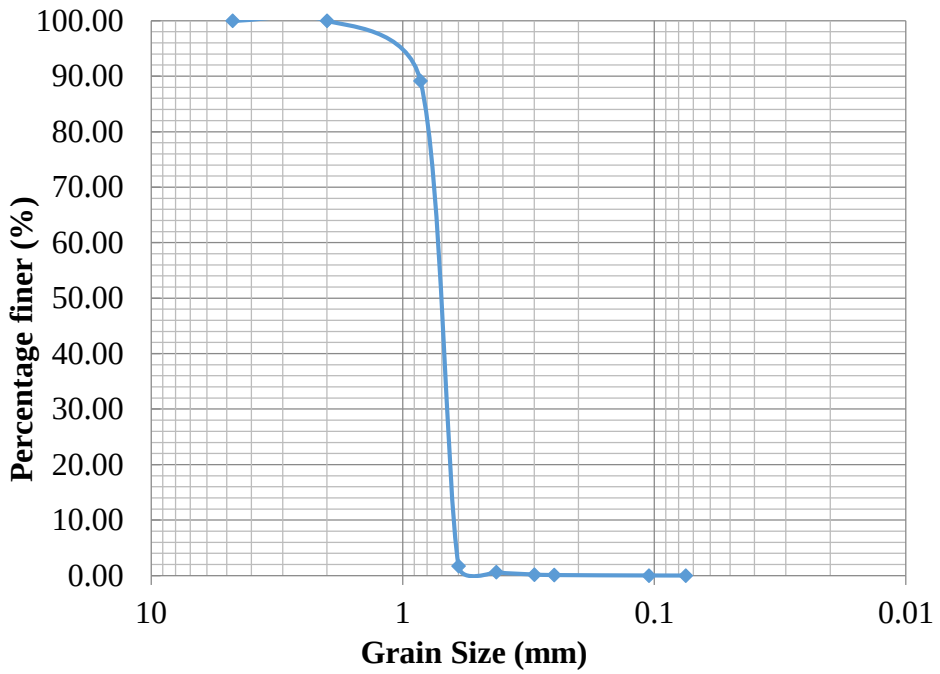

Figure 3-1 Grain size distribution of Ottawa (20-30) sand.

3.2.2. Fly ash

The fly ash used in these tests was obtained from Springfield city utility power plant which use coal. During coal combustion the fly ash is produced as a by-product. For the particle size analysis, hydrometer test was conducted according to ASTM D 422. The particle size distribution curve for the Fly ash is shown in Figure 3-2.

ASTM D 4253 and D 4254 are applicable for the determination of maximum and minimum void ratios of soils containing fines (finer than .075 mm) up to 15 %. For higher fine contents, the ASTM procedure gives inconsistent results. However, there is no other method which is applicable to all ranges of fine particles. So, this method was used for the determination of maximum and minimum void ratio for sand and also for sand- fly ash mixture. The test was repeated three times and the average values were obtained.

During minimum void ratio determination, the fly ash particles flow out on vibrating the mold. The loss of sample on vibrating 2.68 kg fly ash, was around 1.2 kg. In order to prevent the loss of the sample during vibration, the plastic and filter paper having the same diameter as the surcharge weight were taken. The Silicon grease was applied to the plastic and filter papers. Then it was kept at the top of the sample in the mold. After that, the surcharge weight was placed and vibrated. This process prevented the loss of the sample during vibration.

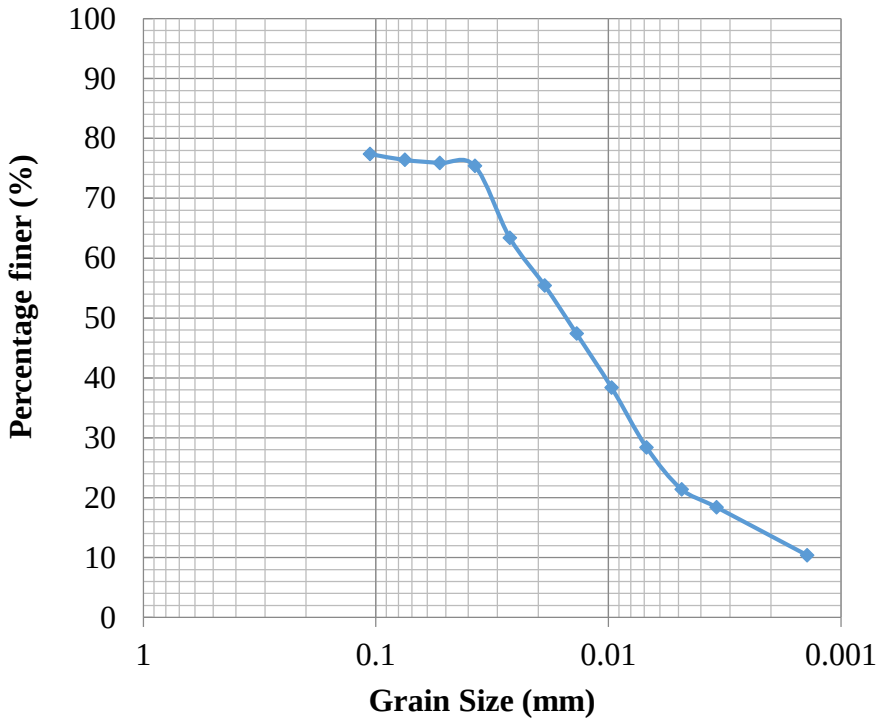

Figure 3-2 Grain size distribution curve for fly ash.

The chemical composition of fly ash is shown in Table 3-3. The principal componenets of fly ash are Silica, Ferric oxide, Alumina, Lime, etc. Silica content is maximum in the fly ash, which is 55 %, whereas Chlorine is least 0.02 %. The sum of silica , alumina and ferric oxide is 85.55 %, which is greater than 70 %. The loss on ignition (LOI) is 1.72 %, which is less than 6 %.

Hence, according to chemical composition criteria of ASTM C618-12a, the fly ash can be classified as type F.

Table 3-1 Chemical composition of fly ash (Mohanty, 2014).

Compositions	**Percentage (%)**
SiO_2	55.01
Fe_2O_3	16.33
Al_2O_3	14.46
CaO	5.95
Na_2O	1.89
LOI	1.72
K_2O	1.66
Cl	0.02
S	1.28
TiO_2	0.82
MnO_2	0.06
MgO	0.68
P_2O_5	0.08
BaO	0.04
Total	100.00

3.2.3. Mixture of sand and fly ash

The mixtures of sand-fly ash were prepared by adding 10 and 20 % fly ash to clean sand. The specific gravity of the mixtures was determined by using the gas pycnometer. Similar to clean sand and fly ash, the maximum and minimum void ratios were determined in accordance with ASTM D4254 and ASTM D 4253, respectively.

3.3. Test procedure

3.3.1. Cyclic triaxial test

Seed and Lee (1966) used cyclic triaxial test for liquefaction studies on clean saturated sand. Now, it is a commonly used lab equipment for liquefaction studies. A cylindrical samples of soil enclosed in a rubber membrane is used in the test. After, Seed and Lee (1966), cyclic triaxial equipment have been modified several times. Improvements in back pressure saturation and cyclic load applications technique have been made.

3.3.2. Simulation of earthquake condition in cyclic triaxial test

For level ground, the soil at any depth is subjected to overburden pressure (σ_o) and lateral earth pressure ($K_o\sigma_o$) as shown in Figure 3-3. During earthquake, shear waves propagate upwards from underlying rocks through the soil mass. As shear wave propagates, the soil mass gets deformed due to the development of shear stress (τ_{hv}). The direction of shear stress reverses many times during the earthquake, which produces the cyclic effect as shown in Figure 3-3.

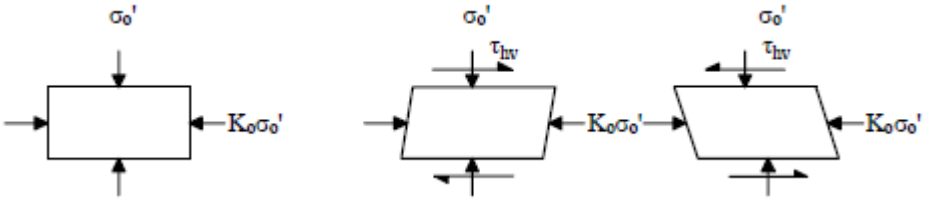

Figure 3-3 Conceptual field loading condition (Seed and Lee, 1966).

The earthquake loading condition can be simulated correctly in a cyclic simple shear test, however the sample preparation is difficult. Further, due to stress concentration effect at the edge of the sample, it shows lower liquefaction potential (Seed and Peacock, 1971). Due to the

widespread availability and simplicity of the test procedure, cyclic triaxial test is commonly used for studying liquefaction of soils.

In cyclic triaxial test, the sample is consolidated with an effective confining pressure corresponding to the field overburden pressure. During consolidation, there is no application of shear stress which represents level ground conditions. The stress condition during the consolidation phase is shown in case (a), of Figure 3-4. Then, during the first half cycle of cyclic phase, deviator stress (σ_{dp}) is applied in the downward direction as in case (c). That will produce shear stress ($\sigma_{dp/2}$) on a 45º plane. On changing the direction of deviator stress upwards during the next half cycle as shown in case e (Figure 3-4), the direction of shear stress induced also changes. The shear stress induced at 45º plane is analogous to the shear stress induced during earthquake. The application of downward and upward deviator stress can be continued to desired number of cycles which simulates the required earthquake.

However, above loading condition does not satisfy the constant mean extreme principal stress condition throughout the cycle. In order to achieve that condition, all around confining pressure should be decreased by ($\sigma_{dp/2}$) during downward application of load, which results in case (b) (Figure 3-4). Whereas, it should be increased by ($\sigma_{dp/2}$) during upward application of load, which results in the loading condition shown in case (d) of Figure 3-4. The decrease in confining pressure in case (b) results in a decrease in pore water pressure by ($\sigma_{dp/2}$). On the other hand, the increase in confining pressure in case (d) results in an increase in pore water pressure by ($\sigma_{dp/2}$). The effective stress at the desired condition does not change. Furthermore, deformation of the sample depends upon the effective stress, so no correction is necessary for deformation. Therefore desired stress condition as shown in case (a) and (d), can be obtained by subtracting and adding to the pore water pressure a correction equal to ($\sigma_{dp/2}$) during downward and upward

application of deviator stress respectively. Geo comp cyclic triaxial equipment which was used in this research, automatically corrects the pore water pressure.

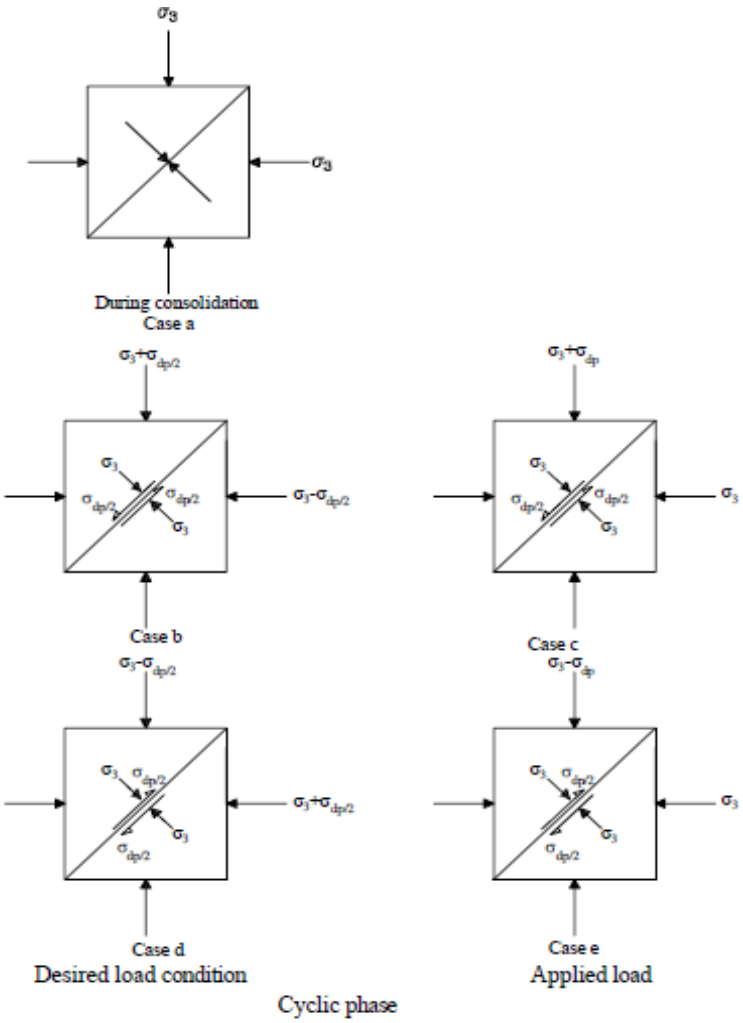

Figure 3-4 Loading condition in cyclic triaxial test (Seed and Lee, 1966).

3.3.3. Testing equipment

The cyclic triaxial equipment manufactured by Geo Comp is used in this research. It's fully automated equipment which consists of (a) Load trac-II load frame, (b) Linear Electro – Mechanical Actuator (LEMA), (c) external displacement sensor, (d) Cyclic triaxial chamber, (e)

Water trap chamber and pressure regulator, and (g) external pressure sensors for sample and cell. The cyclic triaxial set up in the Geo tech lab of SIUC is shown in Figure 3-5.

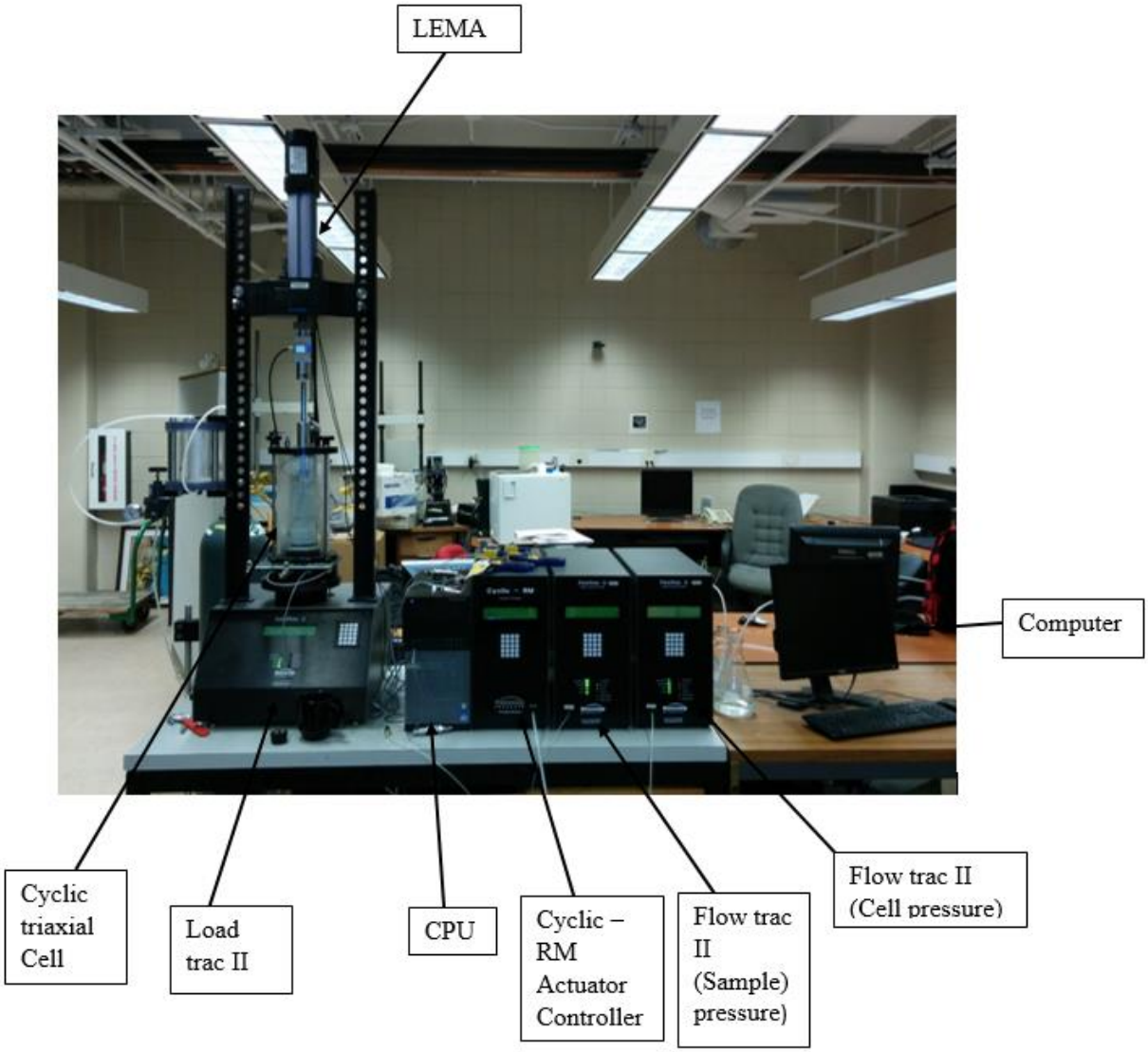

Figure 3-5 Cyclic triaxial set up at geotechnical lab, SIUC.

Load trac –II frame consists of embedded control system and component generating the force on the soil sample. It is responsible for the application of load to the sample. It also measures the load applied to the specimen and the resulting deformation. It is capable of applying static load

up to 20,000 lbs and measurement of displacement up to 3 inches. It has provision for manual as well as automatic operation.

Cyclic load is applied from the Linear Electromechanical Actuator (LEMA) which has a capacity of 1000 lbs. LEMA is a self-contained unit which can apply precise cyclic load to the specimen with high resolution feedback system. It can apply the load at frequency 0 to 10 Hz. The displacement is measured with an external independent sensor during the cyclic phase, and has a travel of 2 inches. During saturation and consolidation phases, internal sensor in load trac ii continuously measures the displacement and records in computer.

Cyclic triaxial chamber consists of chamber, load cell, piston coupling and modified base for cyclic testing. There are cell and sample flow pumps, to control the flow and pressure of the cell and sample, respectively. Flow pumps consist of high speed precision micro stepper which regulates the pressure and volume of the flow. Further, micro stepper is controlled by a microprocessor, which is responsible for driving the piston in and out of flow pump. The pressure transducer present at the end of the flow pump measures the pressure and provides the feedback to control the board and maintains required pressure. The flow pump diagram is shown in Figure 3-6. The flow trac has 250 ml volume capacity.

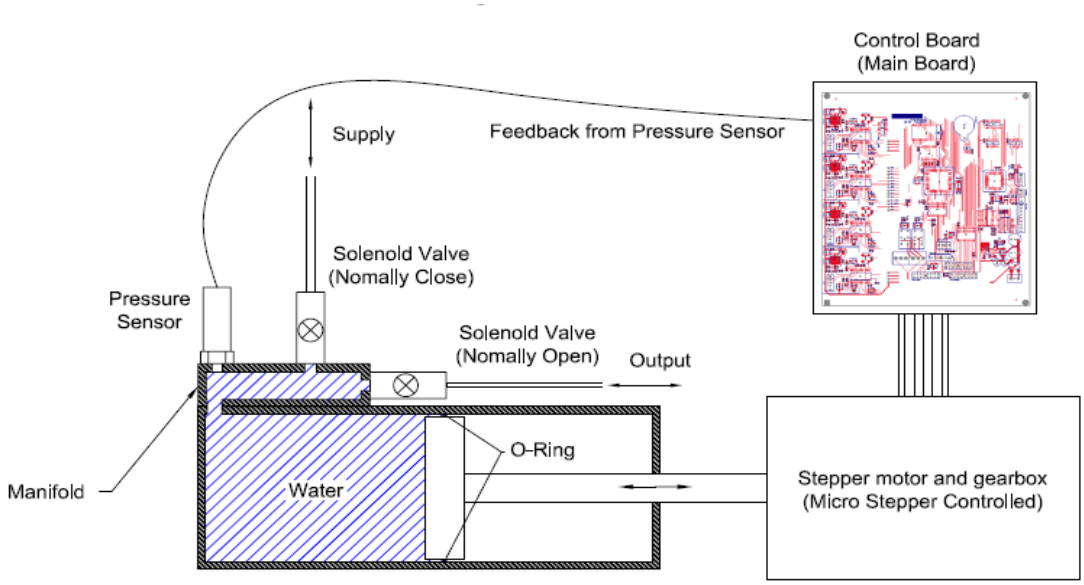

Figure 3-6 Flow pump diagram (Geo comp, 2013).

The cell and sample pressure are measured from both external pressure sensors as well as internal flow pump pressure sensor. Both have the capacity of measuring 200 psi. After consolidation, air pocket should be formed in the cell for the application of cyclic load. This can be achieved by emptying the cell by certain amounts. During emptying of cells, water trap chamber/regulator is responsible for maintaining constant cell pressure.

Cyclic triaxial software is used for controlling and monitoring the tests. After completion of each step, the software automatically changes to next step. However, at the beginning of the cyclic phase, pressure in the water trap chamber should be maintained manually. It is capable of recording complete set of data for each phase and it automatically generates the report at the end of the test. The report consists of plots of the load - number of cycles, shear stress- number of cycles, axial strain-number of cycles, cell pressure-number of cycles, excess pressure-number of cycles, peak to peak deviator stress-number of cycles, and peak to peak axial strain-number of

cycles. Additionally, it computes the damping ratio, Youngs modulus and also plots the damping ratio and Youngs modulus against the axial strain and the number of cycles.

3.3.4. Sample preparation

There are several methods of sample preparation, for liquefaction studies in cyclic triaxial test. Dry pluviation, water sedimentation, moist under compaction, and slurry deposition are common methods. The fabrics of soil formed depends upon the method of sample preparation. The sample preparation technique is chosen depending upon the types of soils in the field. The sample was prepared using the method of under compaction suggested by Ladd (1978) in this research.

3.3.5. Sample preparation using of the method of under compaction

3.3.5.1. Concept of method of under compaction

In the method of under compaction, the sand is compacted in layers. The height of compacted layer is decreased from bottom to top systematically. Each layer is compacted to lower density than desired. The density of the bottom layer is lowest, whereas top layer is highest. So, the energy required to compact subsequent top layers goes on increasing. On compacting subsequent top layers, the bottom layers also get compacted. Therefore, all layers get uniform compaction, which produces a uniform density throughout the sample. This method prevents the problem of segregation of particles. It is also an easier method of sample preparation and samples of a wide range of relative density can be prepared. Further, it gives the optimum cyclic strength at a given relative density.

3.3.5.2. Calculation of weight of sample

All samples were prepared at a relative density of 50 %. The length and diameter of the samples were 5.7 inches and 2.85 inches, respectively. Based on the maximum and minimum void ratio obtained for various fly ash contents, void ratio for each combination was calculated. The dry and wet unit weights were calculated using the void ratio, water content, specific gravity and degree of saturation. For clean sand and sand containing 10 % fly ash, the sample was prepared at 30 % degree of saturation. Whereas for fly ash and sand containing 20 % fly ash, the sample was prepared at 40 % degree of saturation. The degree of saturation was selected in such a way that, the fly ash and sand can be mixed properly.

For the first layer, 8 % under compaction was considered, it goes on decreasing on subsequent top layers and reduces to zero at the top layer. The percent under compaction was calculated using the formula provided by Ladd (1978). On the basis of percent under compaction, the height of each of the six layers was calculated. The mixed sand and fly ash mixture was divided into equal six parts. The sample calculation for clean sand at a 50 % relative density is described below.

For clean sand, the percent undercompaction is calculated from the equation (3.1). The percent undercompaction was 8, 6.4, 4.8, 3.2, 1.6, 0 for each layer respectively from bottom to top.

Percent under compaction for n layer

$$U_n = U_{ni} - \left(\frac{U_{ni}-U_{nt}}{n_t-1}\right) * (n-1) \quad \text{.....(3.1)}$$

Where, U_{ni} = Percent under compaction for first layer, n_t=total number of layer, n=number of layer being considered.

Then, compacted height of each layer was calculated using equation (3.2). For the first bottom layer, the compacted height was 1.03, whereas for other layers it was 0.934.

$$h_n = \frac{h_t}{n_t}(n-1) + \left(1 + \frac{U_n}{100}\right) \quad \text{.....(3.2)}$$

Where, (h_n) = height of specimen at the top of n_{th} layer and h_t=total height of sample.

The void ratio of the sample for a 50 % relative density was calculated from equation (3.3). The maximum and minimum void ratio of clean sand are 0.71 and 0.51, respectively. The void ratio for 50 % relative density was found to be 0.61.

$$Relative\ Density = \frac{e_{max} - e}{e_{max} - e_{min}} \quad \text{.....(3.3)}$$

Where, e_{max}, e_{min} = maximum and minimum void ratio, respectively

Using the void ratio and specific gravity, the dry unit weight of the sand for a relative density of 50 % was calculated using equation (3.4). The specific gravity of clean sand is 2.67 and dry unit weight was obtained as 16.27 kN/m^3. The dry weight of required sand sample was calculated by multiplying the dry unit weight and volume of the sample. The dry weight of the sample was calculated as 988.19 gm. After that, the water content of the soil was calculated with the help of equation (3.5). For the 30 % degree of saturation, water content was found as 6.85 %. Then, total wet weight of sample was calculated multiplying the dry weight by (1+ w) and it was 1056 gm. The wet weight of each layer was found to be 175.98 gm.

$$Dry\ Unit\ Weight\ (\gamma_d) = \frac{G_s \gamma_w}{1+e} \quad \text{..... (3.4)}$$

Where, G_s= specific gravity

$$Water\ content\ (w) = \frac{S_r e}{G_s} \quad \text{..... (3.5)}$$

Where, S_r= degree of saturation

$$Total\ Unit\ Weight\ (\gamma_t) = \gamma_d(1 + w) \quad \text{(3.6)}$$

3.3.5.3. Specimen mold set up

The split mold with 2.85 inch internal diameter and 5.7 inch length was used for the sample preparation. Silicon grease was applied in the corner and inside the split mold. Latex membrane was mounted inside the split mold and then, the membrane was folded at each end of the split mold. After that, three O rings were rolled into each end and then vacuum was applied at the at the split mold. If folding, twisting was observed during application of vacuum, the membrane was taken out and again folded with due precaution**.**

3.3.5.4. Soil deposition

The split mold was placed at the base of triaxial pedestal containing boiled porous stone. The vacuum at the base was applied to give some confining pressure to the soil in the mold. Then, the sample was deposited in the split mold in six layers using predetermined soil mass for each layer and compacted by tamping to required depth of that layer. Then, the saturated porous stone containing filter paper was placed. After that, top cap was placed over the porous stone. Plastic tubing from the base was inserted into top cap. The rubber membrane was folded at triaxial base, slightly moving up the split mold and O rings were rolled down. Similarly, membrane at the top was folded at the top cap and O-rings were rolled down. After that, vacuum was removed from the split mold and split mold was separated after loosening the screw. Silicon grease was applied at the base and top of cylindrical chamber and placed at the triaxial base. Then, cell top containing the post knobs and the piston was assembled. The piston was tightened at the top cap. The chamber was filled with water. Then, triaxial cell was kept at the load trac II and external

displacement transducer was coupled with piston. After that, piston was connected to the actuator. External cell and sample pressure transducers were coupled with cell and sample, respectively.

3.3.6. Cyclic triaxial test procedure

In order to simulate earthquake loading conditions, cyclic triaxial was conducted at following steps given below.

3.3.6.1. Initialization phase

After flushing the sample with distilled deaired water, the external and internal sensors for sample and cell pump, load were calibrated and the test was started with the input of necessary parameters. The first phase of cyclic triaxial test is initialization, which is conducted for checking any leakage in the system. Cell pressure of 5 psi and sample pressure of 2 psi was applied for 10 minutes. If the applied pressure was maintained and there was no unusual sound, it was assumed that there was no leakage in the system. If leakage was observed, the test was stopped. The system automatically goes to saturation phase, after completion of the initialization phase.

3.3.6.2. De-aeration of water

The water was deaired using the Nold De Aerator (Model 2100), which was manufactured by Geokon. Water is de aired by means of cavitations and nucleation. The agitation is produced by an impeller coupled with a magnetic clutch to an electric motor where as the cavitations occur due to rotation of impeller which vaporizes the liquid into fine mist, which looks like spray (Geokon, 2002). The released gases are hurled outwards by centrifugal forces. The deaeration

system is shown in Figure 3-7. It was suggested to run the pumps for 5 minutes. However, for better deaeration, the equipment was operated for 1.5 hours. The deaired water was used for the sample preparation and filling of the sample pump, which supplies water for the saturation of sample. Distilled water was used for filling cell pump. Cell pump is used for the application of confining pressure to sample.

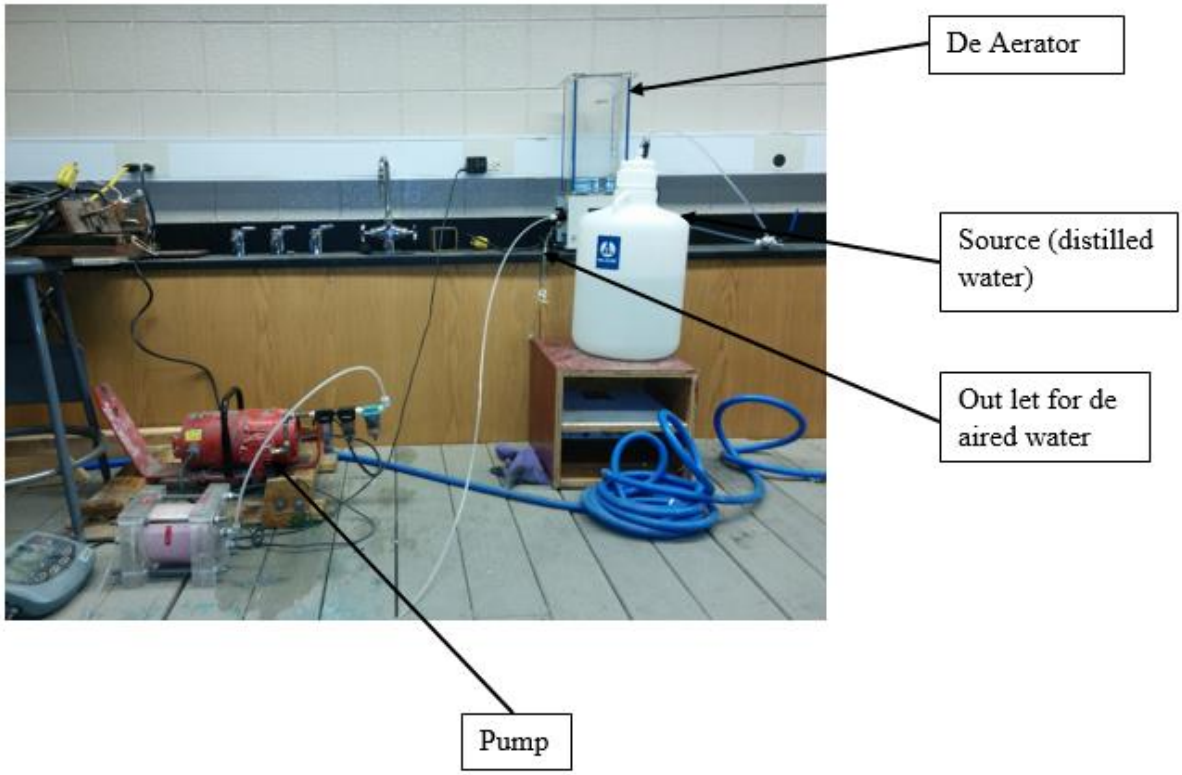

Figure 3-7 De aeration system in Geotechnical lab, SIUC.

3.3.6.3. Saturation with back pressure technique

Initially efforts were made to saturate the sample with back pressure technique (Black and Lee, 1973). The saturation phase starts after initialization phase. This phase consists of incremental increases in cell pressure and pore water pressure at constant effective stress. The cell pressure was increased by 5 psi at each step and maintained for 3 minutes. During the increment of cell

pressure, the system monitors the increase in pore water pressure. At this phase, the system checks the saturation ratio. Then, the system increases the pore water pressure and keeps constant for specified time maintaining a constant effective stress. The back pressure was maintained for 4 minutes. During this process, the air will be dissolved in the water and results in higher B coefficient value. The cell pressure pump is responsible for maintaining confining pressure of the sample. However, water trap chamber is responsible for maintaining constant cell pressure during evacuation of water from cell. Before the beginning of cyclic phase, some space should be created for cyclic load application by evacuating water from the cell. The pressure system available in the lab can apply a maximum cell pressure of 120 psi from the water trap chamber. So maximum 105 psi back pressure can be applied in our lab for the tests conducted at initial effective confining pressure of 15 psi. Therefore, the process of increasing cell pressure and back pressure was continued in a similar way until the cell pressure reaches 100 psi. Further, the pressure regulator does not apply constant confining pressure during cyclic phase, for the pressure above 110 psi. So, for the test conducted at 15 psi effective confining pressure, the cell pressure was increased up to 95 psi. Hence, the total pressure applied is 110 psi and exact pressure can be applied. If the samples were saturated to B - coefficient value greater than 0.95 at back pressure of 100 psi, then, the system automatically would go to consolidation phase. However, with back pressure technique only, lower B value was observed. Then, the system automatically enters into the cyclic phase of increasing and decreasing the cell pressure and continuously measuring the B value. After the target number of cycles and time period for cyclic step of saturation, it will go to consolidation phase. The target number of cycles and time period can be changed depending upon the nature of the specimen. On saturating the sample with 100

psi back pressure and 10 number of cycles, Skempton B coefficient was observed in the range 0.88, which does not satisfy the ASTM requirement.

3.3.6.4. CO_2 percolation

It was not possible to saturate the sample, using the back pressure method only because of system limitations. For the saturation of the specimen, the air has to be removed from the voids and it should be filled back with distilled de-aired water. Since CO_2 has higher value of Henry constant, it easily gets dissolved in water. Therefore, for rapid saturation, CO_2 flushing technique in combination with back pressure technique (suggested by Chaney et al., 1979) was used. Initially, the sample was flushed with de-aired water and then CO_2 for 10 minutes and saturated by using back pressure technique as discussed in Section 3.6.3.3. The saturation ratio obtained by this technique was in the range of 0.91, which also does not satisfy ASTM requirement. The saturation behavior of the sample is shown in Figure 3-8. Finally, the process was reversed, i.e. the sample was initially flushed with CO_2 and then distilled de-aired water. This process resulted in better saturation. The B-coefficient higher than 0.95 was obtained. The saturation progress for final process is shown in Figure 3-9. This procedure was adopted throughout the test program. For the clean sand, CO_2 was percolated about 10 minutes with 2 psi pressure, whereas for sand containing 10, 20 % and fly ash, it was percolated for 15 minutes. The jogging with distilled de-aired water after CO_2 percolation helps to remove the trapped CO_2. The jogging with de-aired water was continued till the clear water comes out of the sample. For sand containing fly ash, it was jogged for 2-3 times after refilling of the pump.

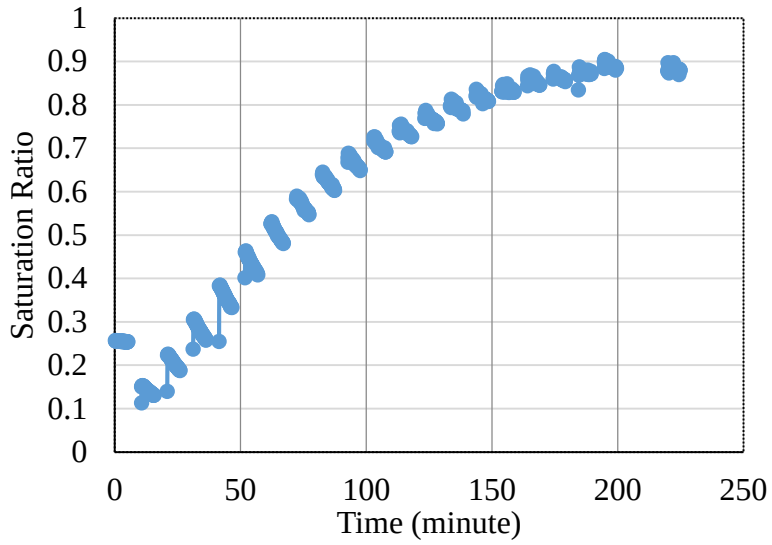

Figure 3-8 Saturation progress of clean sand (initial flushing with deaired water and then CO_2).

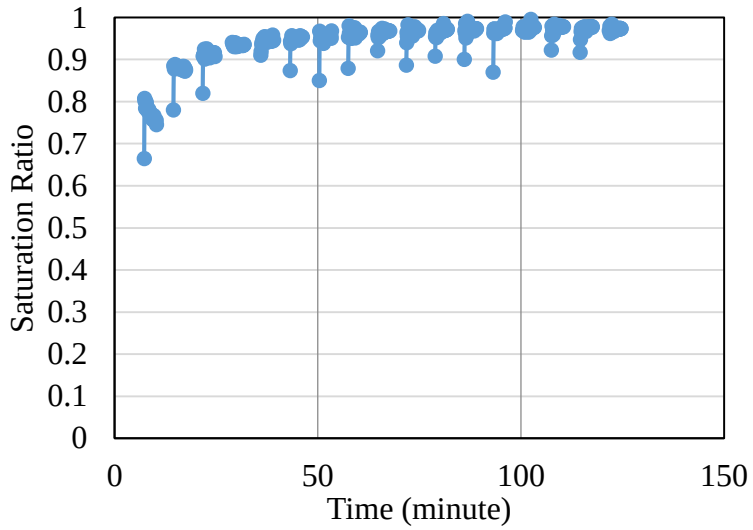

Figure 3-9 Saturation progress of clean sand (initial flushing with CO_2 and then deaired water).

3.3.6.5. Consolidation phase

After saturation, the samples were consolidated applying the desired confining pressure. The primary consolidation for a given effective confining pressure, was completed within 1-2

minutes. The specimen was consolidated for 30 minutes. The stress was increased at the rate of 100 psi per minute. Five, ten and fifteen psi effective confining pressure was used for the consolidation of specimens for conducting different series of tests.

3.3.6.6. Application of cyclic shear stress

Following the consolidation phase, the external displacement transducer was adjusted at the midway setting. For the application of cyclic load, around 100 ml of water was removed to form an air pocket inside the cell. During emptying, the cell pressure may fluctuate. In order to maintain the constant cell pressure; water trap chamber/pressure regulator was used. It supplied constant external pressure. The cyclic software automatically adjusts the position of the cell at the appropriate position. Then, cyclic load of 1 Hz frequency was applied. Twenty data sets were recorded in each cycle.

During the cyclic loading, the stiffness of sample changes frequently. So it is difficult to apply the correct load throughout the test in most of the equipment. In order to apply correct load, the Geo Comp cyclic triaxial equipment uses a PID system for controlling the load. PID stands for Proportional-Integral-Derivative. It calculates the error, which is the difference between the target load and the measured load. According to the error, PID controller automatically adjusts the load throughout the test (Marr et al., 2003).

3.4. Test details

In this research, cyclic triaxial tests were conducted on samples of clean sand, fly ash and sand-fly ash mixtures containing 10 and 20 % fly ash. All samples were prepared at a constant relative density of 50%. The clean sand samples were consolidated by applying initial effective confining pressure of 5, 10 and 15 psi, which resulted in three series of tests. For each initial

effective confining pressure, reversible cyclic shear was applied varying the CSR from 0.1 to 0.5 systematically. Sixteen tests were conducted on clean sand as shown in Table 3-4.

Table 3-2 Cyclic triaxial tests on clean sand (e = 0.61 and γ_d =16.29 kN/m^3)

Effective Confining Pressure (σ_3), psi	CSR	Remarks
5	0.10	Not Liquefied
	0.20	Not Liquefied
	0.25	Liquefied at 20 cycles
	0.30	Liquefied at 11.6 cycles
	0.40	Liquefied at 6.5 cycles
	0.50	Liquefied at 4 cycles
10	0.10	Not Liquefied
	0.20	Liquefied at 22 cycles
	0.30	Liquefied at 7 cycles
	0.40	Liquefied at 3.5 cycles
	0.45	Liquefied at 2.5 cycles
15	0.10	Not Liquefied
	0.20	Liquefied at 9 cycles
	0.30	Liquefied at 4.5 cycles
	0.35	Liquefied at 3.5 cycles
	0.40	Liquefied at 3 cycles

Sand-fly ash mixtures containing 10 and 20 % fly ash were prepared. Similar to clean sand, sand-fly ash mixtures containing 10 and 20 % fly ash were also consolidated by applying initial effective confining pressure of 5, 10 and 15 psi. For each confining pressure, reversible cyclic shear stress was applied varying the CSR from 0.1 to 0.5. Twenty eight tests were conducted on the sand containing 10 and 20 % fly ash as shown in Table 3-4.

Table 3-3 Cyclic triaxial tests on sand-fly ash mixtures.

Sand+ Fly Ash %	Void Ratio (e)	Dry Density (γ_d) kN/m^3	Effective Confining pressure (σ_3) psi	CSR	Remarks
Sand + 10 % Fly Ash	0.5	17.37	5	0.1	Not Liquefied
				0.2	Liquefied at 37 cycles
				0.3	Liquefied at 6 cycles
				0.4	Liquefied at 4.5 cycles
				0.45	Liquefied at 3.5 cycles
			10	0.1	Not Liquefied
				0.2	Liquefied at 10 cycles
				0.3	Liquefied at 3.5 cycles
				0.35	Liquefied at 2.5 cycles
			15	0.1	Liquefied at 234 cycles
				0.2	Liquefied at 7.5 cycles
				0.3	Liquefied at 2.5 cycles
				0.35	Liquefied at 2.2 cycles
				0.4	Liquefied at 2 cycles
Sand + 20 % Fly Ash	0.41	18.35	5	0.1	Not Liquefied
				0.2	Not Liquefied
				0.3	Liquefied at 12 cycles
				0.4	Liquefied at 7 cycles
				0.5	Liquefied at 4 cycles
			10	0.1	Liquefied at 263 cycles
				0.2	Liquefied at 14 cycles
				0.3	Liquefied at 5.5 cycles
				0.4	Liquefied at 2.5 cycles
			15	0.1	Liquefied at 290 cycles
				0.2	Liquefied at 8 cycles
				0.3	Liquefied at 3.5 cycles
				0.35	Liquefied at 2.5 cycles
				0.45	Liquefied at 2.1 cycles

The samples of fly ash were consolidated by applying the initial effective confining pressure of 5 psi only. After consolidation, reversible cyclic shear stress was applied by varying the CSR from 0.1 to 0.4. Four tests were conducted on fly ash as shown in Table 3-4.

Table 3-4 Cyclic triaxial tests on pure fly ash (Void ratio, e =1.137 and γ_d =11.29 kN/m^3).

Effective Confining Pressure (σ_3), psi	CSR	Remarks
5	0.1	Not Liquefied
	0.2	Liquefied at 24 cycles
	0.3	Liquefied at 5.2 cycles
	0.4	Liquefied at 3 cycles

3.5. Summary

In this chapter, the methodology adopted in this research was discussed. The clean sand, fly ash and it's mixtures used in this research were described at the beginning. Next, cyclic triaxial test, Geo Comp cyclic triaxial equipment, the procedures for sample preparation and test procedure were discussed. Finally, tests information were presented.

CHAPTER 4

RESULTS AND DISCUSSIONS

4.1 Introduction

This chapter presents the results of cyclic triaxial tests on samples of sand, fly ash, and sand-fly ash mixtures. Details of tests conducted are given in Table 3-2 to Table 3-4. The properties of the materials used in this research are presented at the beginning. Some typical results dealing with effects of reversible shear stresses and confining pressure on rate of pore water pressure generation and axial strain on saturated clean sand are discussed first. This is followed by results for sand containing 10 and 20 % fly ash and pure fly ash. Similar to the case of clean sand, effects of addition of fly ash on liquefaction resistance is also evaluated in terms of effective confining pressure, pore water pressure generation and deformation. Finally, results on Youngs modulus and damping ratio are presented. Effects of confining pressures and fly ash contents are also evaluated on Youngs modulus and damping ratio.

4.2 Material properties

The Ottawa (20-30) sand was used in this research. The index properties of clean sand were determined as described in Chapter 3. The index properties of clean Ottawa sand and fly ash are given in Table 4-1 and Table 4-2, respectively.

Table 4-1 Index properties of clean Ottawa (20-30) sand.

Properties	Values
D_{10} (mm)	0.62
D_{30} (mm)	0.65
D_{50} (mm)	0.70
D_{60} (mm)	0.75
Uniformity Coefficient (C_u)	1.21
Coefficient of Curvature (C_c)	0.91
Maximum void ratio (e_{max})	0.72
Minimum void ratio (e_{min})	0.51
Specific Gravity (G_s)	2.66
Minimum dry density ($\gamma_{d,min}$) kN/m^3	15.33
Maximum dry density ($\gamma_{d,min}$) kN/m^3	17.4

Table 4-2 Index properties of fly ash.

Properties	Values
D_{10} (mm)	0.0015
D_{30} (mm)	0.008
D_{50} (mm)	0.015
D_{60} (mm)	0.025
Uniformity Coefficient (C_u)	16.67
Coefficient of Curvature (C_c)	1.70
Maximum void ratio (e_{max})	1.60
Minimum void ratio (e_{min})	0.68
Specific Gravity (G_s)	2.46
Minimum dry density ($\gamma_{d,min}$) kN/m^3	9.30
Maximum dry density ($\gamma_{d,min}$) kN/m^3	14.38

The index properties of the sand containing various percentages of fly ash are shown in Table 4-3.

Table 4-3 Index properties of sand-fly ash mixtures.

Measured properties	Sand+10 % Fly Ash	Sand+20 % Fly Ash
Specific Gravity (G_s)	2.65	2.63
Maximum void ratio (e_{max})	0.62	0.56
Minimum void ratio (e_{min})	0.38	0.26
Maximum dry density ($\gamma_{d,max}$) kN/m^3	18.85	20.46
Minimum dry density ($\gamma_{d,min}$) kN/m^3	16.09	16.58

4.3 Test results on clean sand

The results of cyclic triaxial tests conducted on clean sand are presented first. The cyclic triaxial tests on clean sand were performed at three different effective confining pressures as listed in Table 3-4. For each series of these tests, CSR was varied from 0.1 to 0.5. Sixteen tests were performed with clean sand. Effects of reversible shear stresses and confining pressure on the liquefaction resistance were evaluated in terms of pore water pressure generation and axial deformation.

4.3.1 Typical test results

The typical results of the effect of application of cyclic shear stress on a sand sample are shown in Figure 4-1. The initial effective confining pressure used in this test was 5 psi and cyclic shear stress of 1.5 psi was applied. The excess pore water pressure represents the increase in pressure within voids on application of the cyclic load. It can be clearly observed from Figure 4-1 that, the pore water pressure build up is a function of the number of cycles of loading. The excess pore water pressure did not show an appreciable increase till the end of first cycles. It is seen to

increase gradually with application of load cycles. After fourth cycles, it started to increase rapidly. Finally, the excess pressure became equal to the initial effective confining pressure of 5 psi at the beginning of eleventh cycles and the sand sample came to stage of initial liquefaction. The excess pore pressure remained constant on further application of cyclic load. Similar types of graphs were obtained in tests on other clean sand samples.

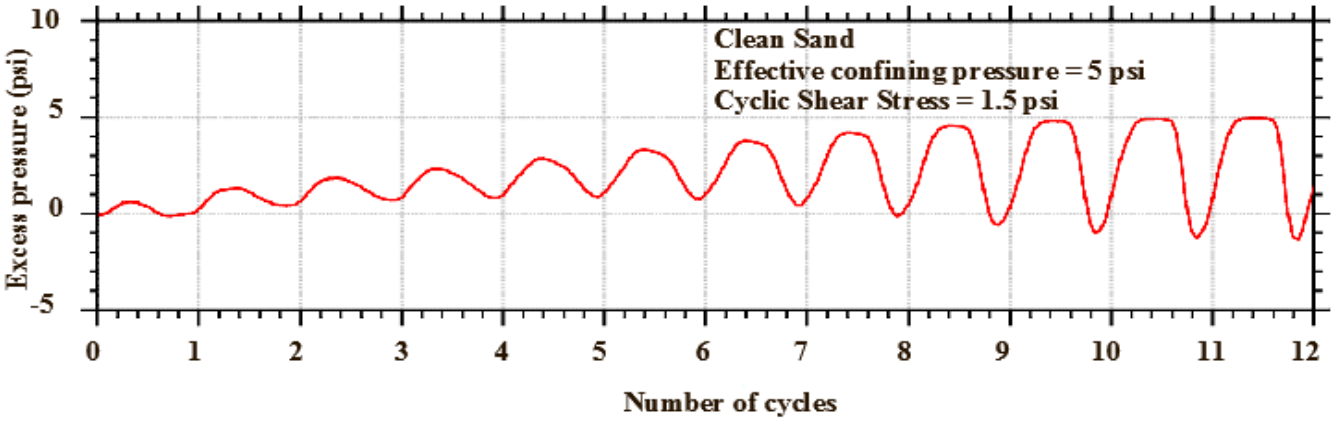

Figure 4-1 Typical variation of pore water pressure with number of cycles for clean sand sample.

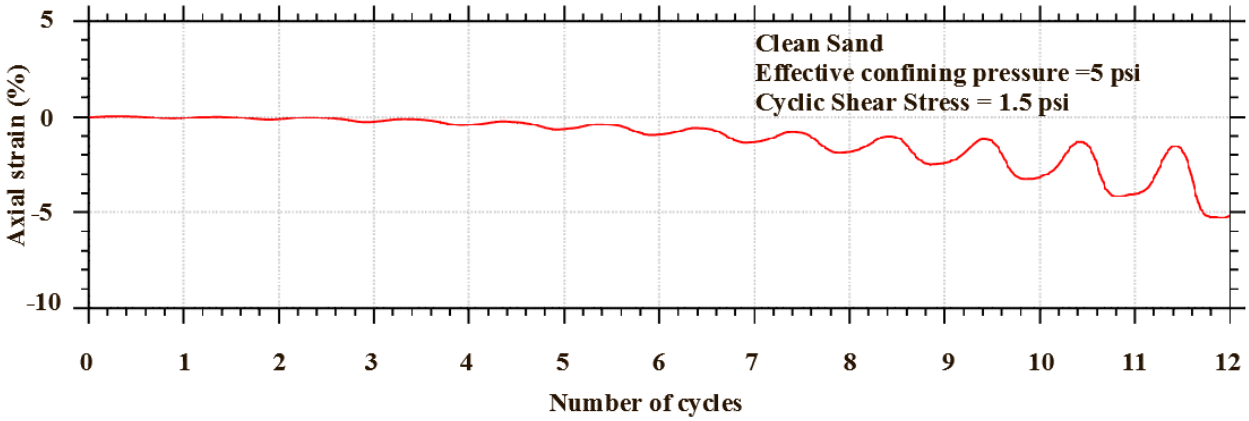

Figure 4-2 Typical variation of axial strain with number of cycles for clean sand sample.

Figure 4-2 shows the axial deformation of the clean sand sample on cyclic load applications for a test using initial effective confining pressure of 5 psi and cyclic shear stress of 1.5 psi. It shows the deformation of the specimen in terms of axial strain with subsequent cycles. Similar to the

case of pore water pressure generation, axial strain is also a function of the number of cycles of loading. It can be clearly observed from Figure 4-2 that the sand sample did not show any significant deformation during about first four cycles. However, sample started to deform slowly after fourth cycles. Rate of deformation increased rapidly after sixth cycles. The sample developed axial strain of 4.05 % at the end of eleventh cycle, which coincides with the stage of initial liquefaction. At the end of twelfth cycles, 5 % axial strain was reached. Beyond that, the specimen continued to deform rapidly.

Other clean sand samples used in the tests also showed similar deformation behavior in general. During liquefaction, the sample showed large deformation depending on the value of cyclic shear stress or cyclic stress ratio (CSR).

4.3.2 Effects of confining pressure

The soil element at any depth is subjected to effective overburden pressure corresponding to weight of soil, any surcharge and position of water table. In addition to overburden pressure, it is subjected to lateral earth pressure, which depends upon the coefficient of lateral earth pressure. The overburden pressure and lateral earth pressure acts as confinement for the soil. Depending upon the depth of soils, the cyclic triaxial tests are conducted by using appropriate confining pressures. In this research, cyclic triaxial tests were conducted at initial effective confining pressures of 5, 10 and 15 psi as shown in Table 3-4.

The effects of confining pressure were evaluated in terms of pore water pressure generation as well as deformation during cyclic loading.

4.3.2.1 Effect of confining pressure on generation of pore water pressure

For the evaluation of effects of confining pressure in terms of pore water pressure generation, the number of cycles required for initial liquefaction was determined for each specimen as discussed in Section 4.3.1. After that, the cyclic shear stress was plotted against the number of cycles required for initial liquefaction as shown in Figure 4-3. It shows three series of curves for the test conducted after consolidating the samples at initial effective confining pressures of 5, 10, and 15 psi, respectively. It can be observed that, the cyclic shear stress required for initial liquefaction increases with an increase in effective confining pressure for any given number of cycles. For instance, the reversible shear stress required for the initial liquefaction in ten cycles are 1.7, 2.7 and 2.8 psi for the samples consolidated at effective confining pressures of 5, 10, and 15 psi, respectively.

For a clean sand sample consolidated with certain initial effective confining pressure, it is seen that the number of cycles required for initial liquefaction decreases with an increase in cyclic shear stress. For example, the clean sand sample consolidated with 5 psi initial effective confining pressure liquefied at 20 cycles on applying reversible cyclic shear stress of 1.25 psi, whereas it liquefied at 4 cycles on the application of reversible cyclic shear stress of 2.5 psi.

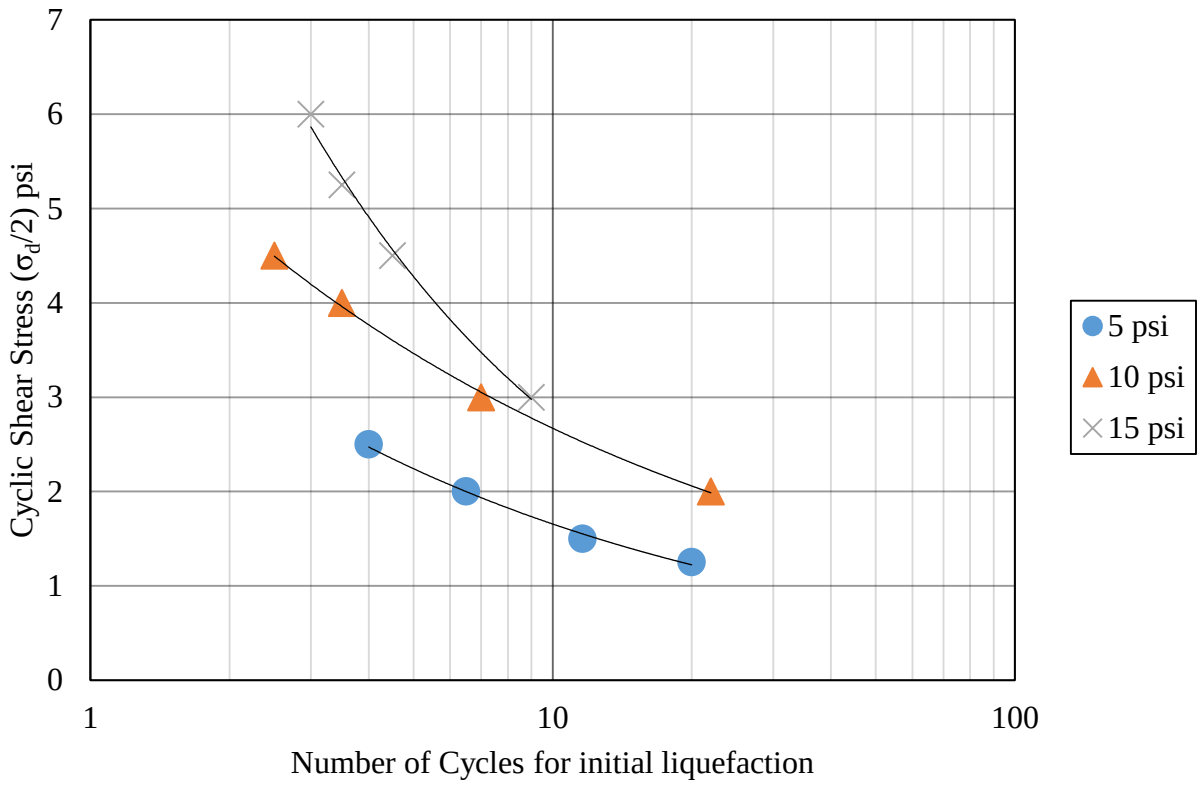

Figure 4-3 Variation of cyclic shear stress with number of cycles for initial liquefaction at initial effective confining pressures of 5, 10, and 15 psi for clean sand.

The effects of confining pressure on the liquefaction resistance are generally presented in terms of CSR versus number of cycles to develop any failure condition. The plot of CSR versus number of cycles for initial liquefaction is shown in Figure 4-4. The plot shows three series of tests on clean sand conducted after consolidating the samples at an initial effective confining pressure of 5, 10, and 15 psi, respectively. Figure 4-4 shows that, as the initial confining pressure increases, the CSR required for the initial liquefaction for any given number of cycles decreases. For instance, the CSR required for the initial liquefaction in ten cycles are 0.32, 0.26, and 0.18 for the clean sand samples consolidated with 5, 10, and 15 psi effective confining pressure, respectively.

Similar to the cyclic shear stress, the number of cycles required for initial liquefaction decreases with increasing CSR for any given confining pressure. For example, the clean sand sample consolidated at an initial effective confining pressure of 5 psi liquefied in twenty stress cycles on the application of cyclic shear stress corresponding to CSR of 0.25, whereas it liquefied in four stress cycles on the application of cyclic shear stress corresponding to CSR of 0.5.

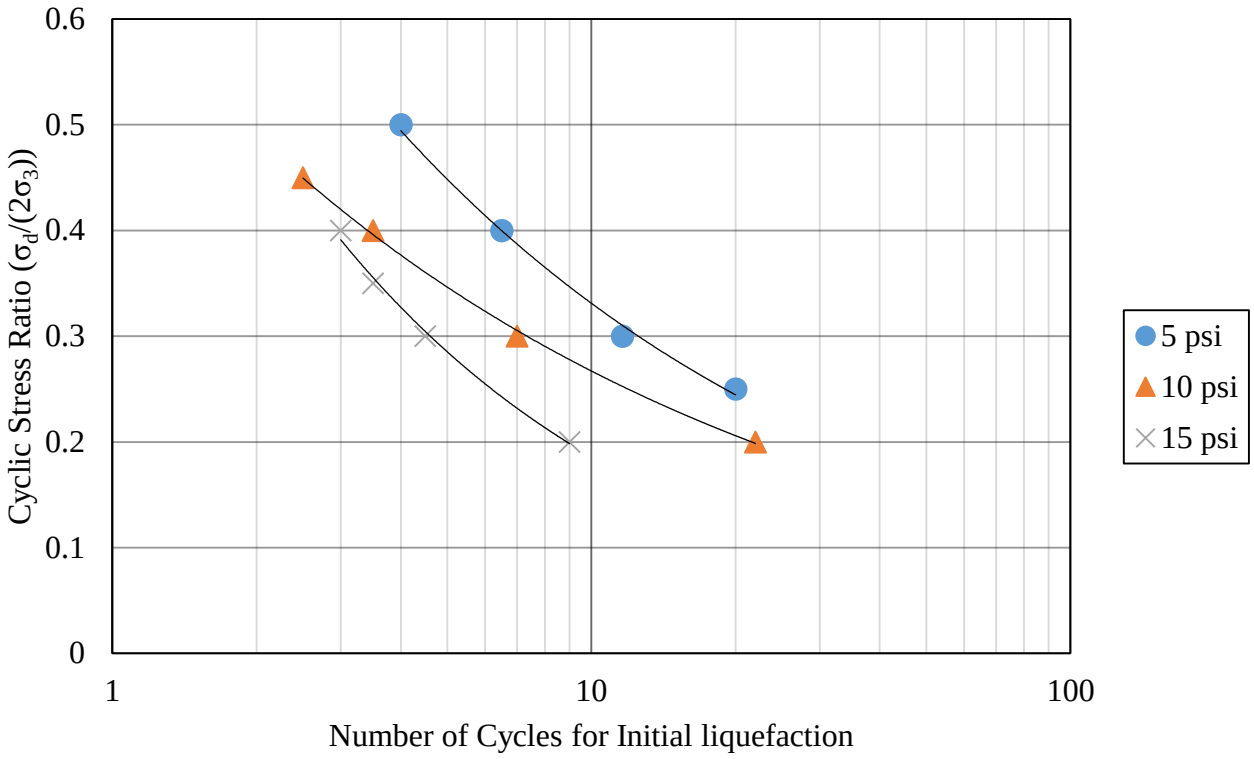

Figure 4-4 Variation of CSR with number of cycles for initial liquefaction at initial effective confining pressures of 5, 10, and 15 psi for clean sand.

4.3.2.2 Effects of confining pressure on axial deformation

Figure 4-5 shows the effects of confining pressure, reversible shear stresses, and the number of cycles of load application on axial deformation of the sample. The number of cycles required for 2.5 % and 5 % DA strain was noted. The cyclic shear stress and corresponding number of cycles for 2.5 % DA strain are plotted as shown in Figure 4-5. An increase in confining pressure is

seen to increase cyclic shear stress inducing 2.5 % DA (Double Axial) strain for any given number of cycles. For instance, the cyclic shear stress required for the development of 2.5 % DA strain are 1.5, 2.5, 2.8 psi for the samples consolidated with initial effective confining pressure of 5, 10, and 15 psi, respectively. As expected, for a samples consolidated with certain initial effective confining pressure, the number of stress cycles required for 2.5 % DA strain is found to decrease with an increase in cyclic shear stress. The number of cycles required for the development of 2.5 % DA strain decreases from 18 to 2.2, with increasing the cyclic shear stress from 1.25 to 2.5 psi.

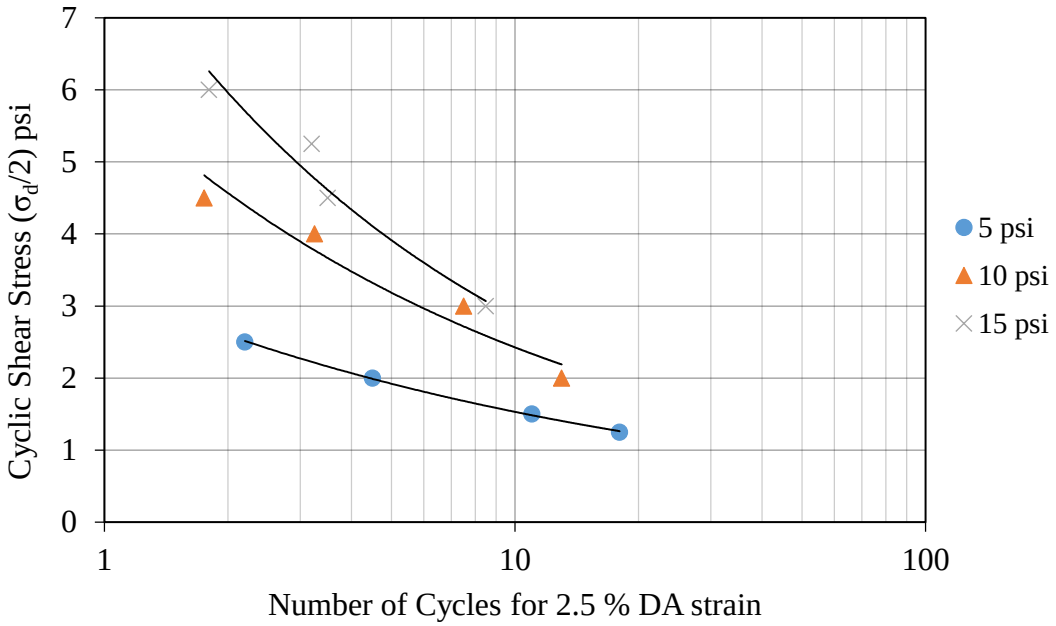

Figure 4-5 Variation of cyclic shear stress with number of cycles for 2.5 % DA at initial effective confining pressures of 5, 10, and 15 psi for clean sand.

Figure 4-6 presents the effects of initial confining pressure on cyclic shear stress inducing 5 % DA strain in a given number of stress cycles. It can be seen that the higher the initial effective confining pressure, the greater is the cyclic shear stress required to induce 5 % DA strain at any given number of stress cycles. For example, the cyclic shear stress required for the development

of 5 % DA strain for the samples consolidated with 10 and 15 psi initial effective confining pressure in ten cycles are 55 % and 61 % higher than that of sample consolidated with 5 psi effective confining pressure. Moreover, it can be observed that, the number of stress cycles required for the development of 5 % DA strain decreases with an increase in cyclic shear stress. With increasing the cyclic shear stress from 1.25 to 2.5, the number of cycles required for the development of 5 % DA strain decreases from 19 to 3.

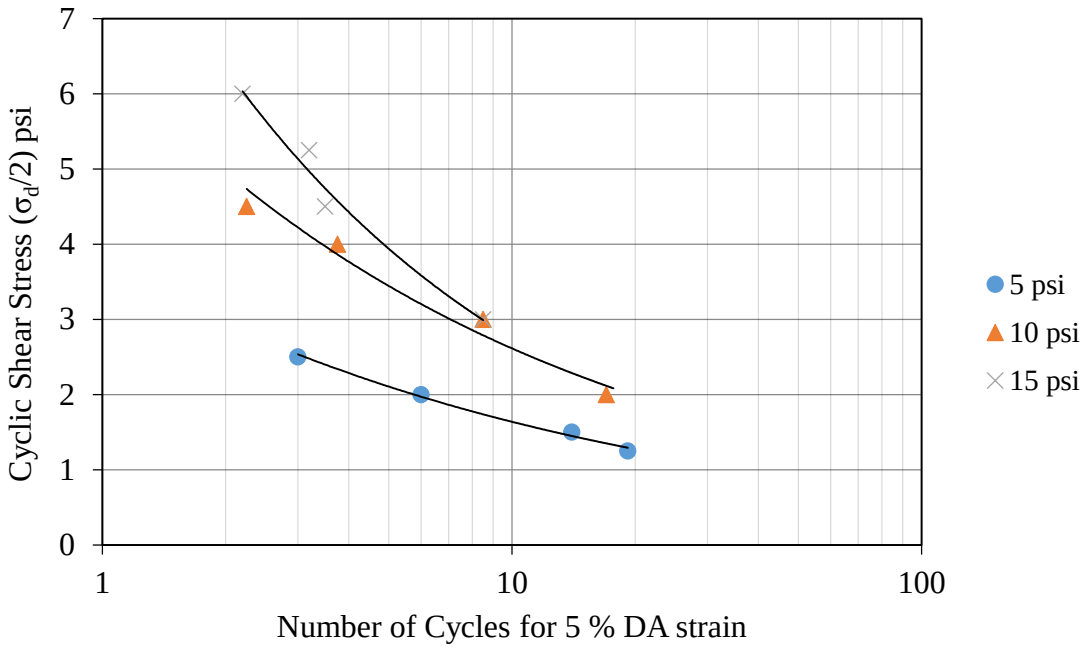

Figure 4-6 Variation of cyclic shear stress with number of cycles for 5 % DA at initial effective confining pressures of 5, 10, and 15 psi for clean sand.

The plots of CSR against the number of cycles required for 2.5 % DA strain is shown in Figure 4-7. It shows the effects of variation of initial effective confining pressure on CSR. As the initial effective confining pressure increases, the CSR required for the development of 2.5 % DA strain at a certain number of stress cycles decreases. The CSR required for the development of 2.5 % DA strain at ten stress cycles for the sample consolidated with initial effective confining pressure of 5 and 10 psi are 63 % and 26 % higher than that of sample consolidated with 15 psi. Similar to

pore water pressure generation, the number of cycles required to induce 2.5 % DA strain are found to decrease with an increase in CSR. With increase in CSR from 0.25 to 0.5, the number of cycles required for the development of 2.5 % DA strain decreases from 18 to 2.

Figure 4-8 shows the effects of initial effective confining pressure on CSR inducing 5 % DA strain. It can be observed that, the CSR required for the development of 5 % DA strain decreases with an increase in confining pressure for a given number of cycles. It is similar to the case of development of 2.5 % DA strain. For example, the CSR required for the development of 5 % DA strain at ten cycles are 0.18, 0.26, and 0.33 for the samples consolidated with effective confining pressure of 15, 10, and 5 psi, respectively. It is also noted that, the number of cycles required for the development of 5 % DA strain, gradually decreases with an increase in CSR. For instance, on increasing the CSR from 0.25 to 0.5, the number of cycles required for the development of 5 % DA strain, decreases from 19 to 3 for the clean sand sample consolidated with effective confining pressure of 5 psi.

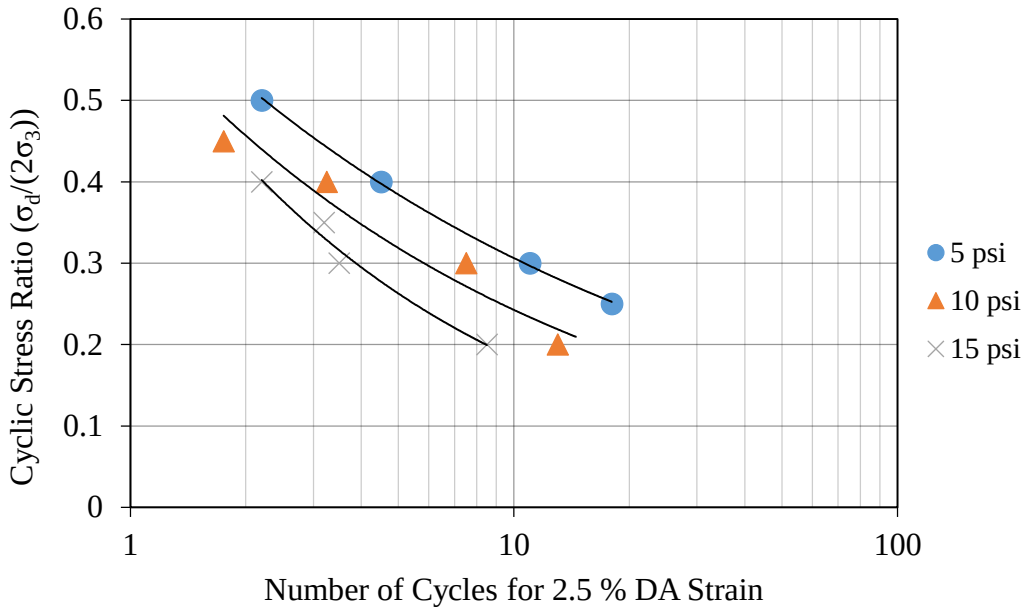

Figure 4-7 Variation of CSR with number of cycles for 2.5 % DA at initial effective confining pressures of 5, 10, and 15 psi for clean sand.

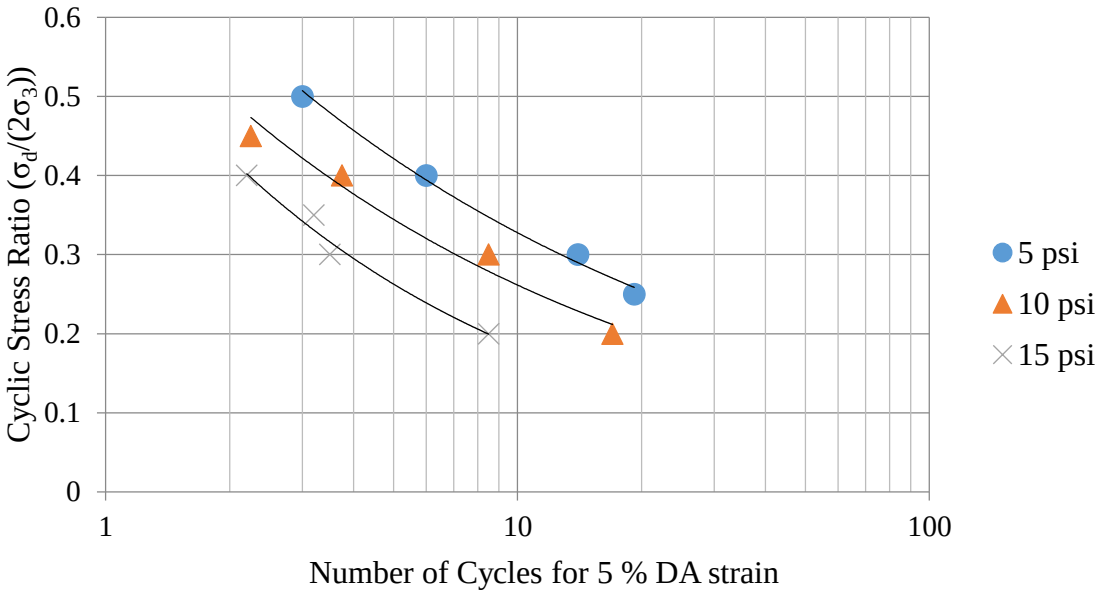

Figure 4-8 Variation of CSR with number of cycles for 5 % DA at initial effective confining pressures of 5, 10, and 15 psi for clean sand.

4.4 Test results on sand containing 10 % fly ash

The results of cyclic triaxial tests conducted on sand containing 10 % fly ash are presented in this section. Similar to cyclic triaxial tests on clean sand, three series of tests were performed at 5, 10 and 15 psi effective confining pressures as listed in Table 3-3. The CSR was varied systematically from 0.1 to 0.5 for each series of these tests. Effects of reversible shear stress and confining pressure on the liquefaction resistance were evaluated in terms of pore water pressure generation and axial deformation as for the case of clean sand.

4.4.1 Typical test results

Figure 4-9 shows the typical results of the application of cyclic shear stress on a sand + fly ash sample. The amount of fly ash in the sample was 10 %. In this test cyclic shear stress of 1.5 psi was applied at a frequency of 1 Hz. The effective confining pressure for the test was 5 psi. The resulting axial strain and pore-water pressure were recorded. The plot in Figure 4-9 show that, the pore water pressure increases slowly initially, but the pace of build up of pore water pressure increases on subsequent cyclic loadings. Finally, the generated excess pore water pressure on specimen was equal to applied initial effective confining pressure at the end of fifth cycles and the stage of initial liquefaction developed.

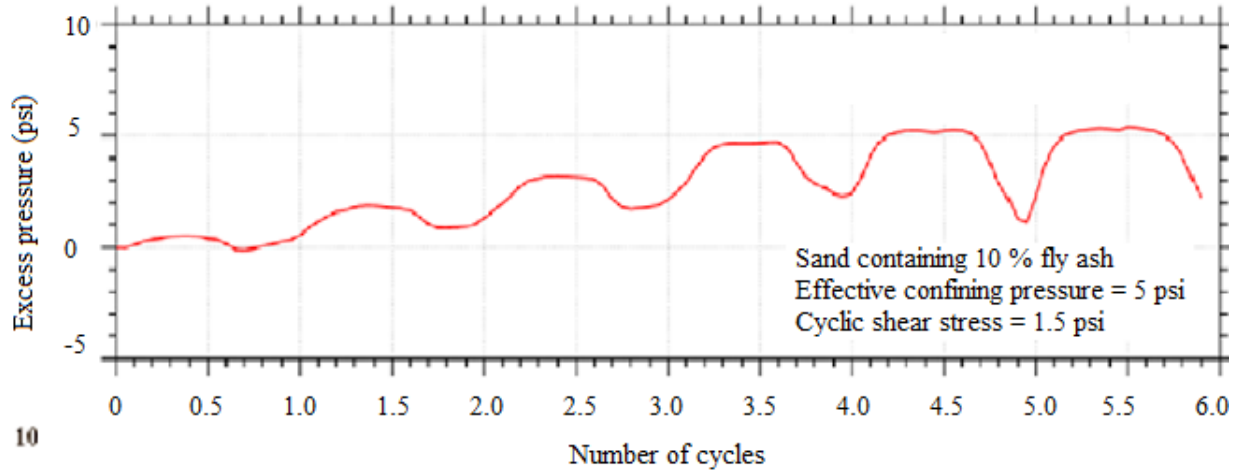

Figure 4-9 Typical variation of pore water pressure with number of cycles for Sand + 10 % fly ash sample.

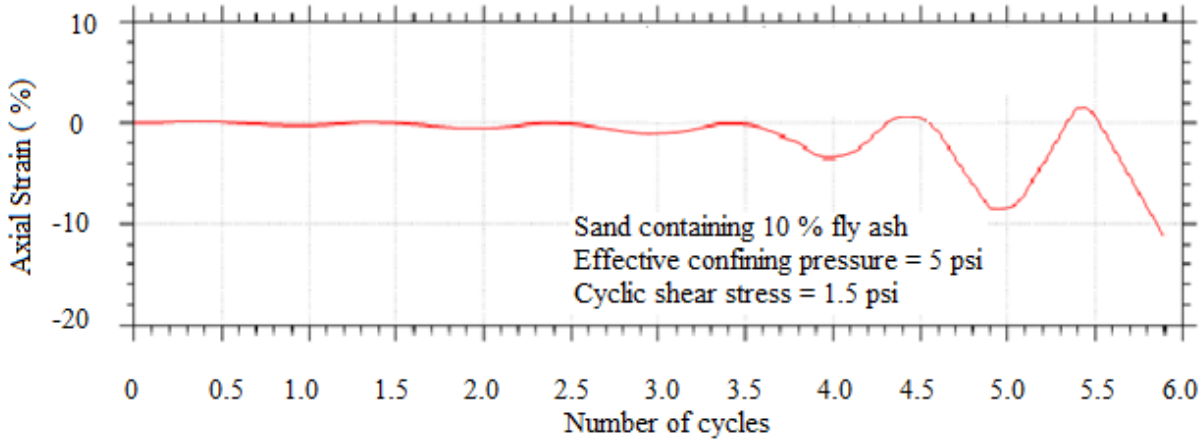

Figure 4-10 Typical variation of axial strain with number of cycles for sand + 10 % fly ash sample.

Figure 4-10 shows the typical axial deformation of a sand containing 10 % fly ash samples with cycles of load application. The sample was consolidated at an initial effective confining pressure of 5 psi and then cyclic shear stress of 1.5 psi was applied. It is observed from Figure 4-10 that the sample showed no noticeable deformation for first three cycles of load application, although

the pore water pressure builds up gradually (Figure 4-9). After that the sample started to deform rapidly. The axial deformation of samples exceeded 10 % at the end of fifth cycles.

4.4.2 Effect of confining pressure on liquefaction resistance

Similar to clean sand, the effects of confining pressure for sand containing 10 % fly ash were evaluated in terms of pore water pressure generation as well as deformation during cyclic loading.

4.4.2.1 Effects of confining pressure on generation of pore water pressure

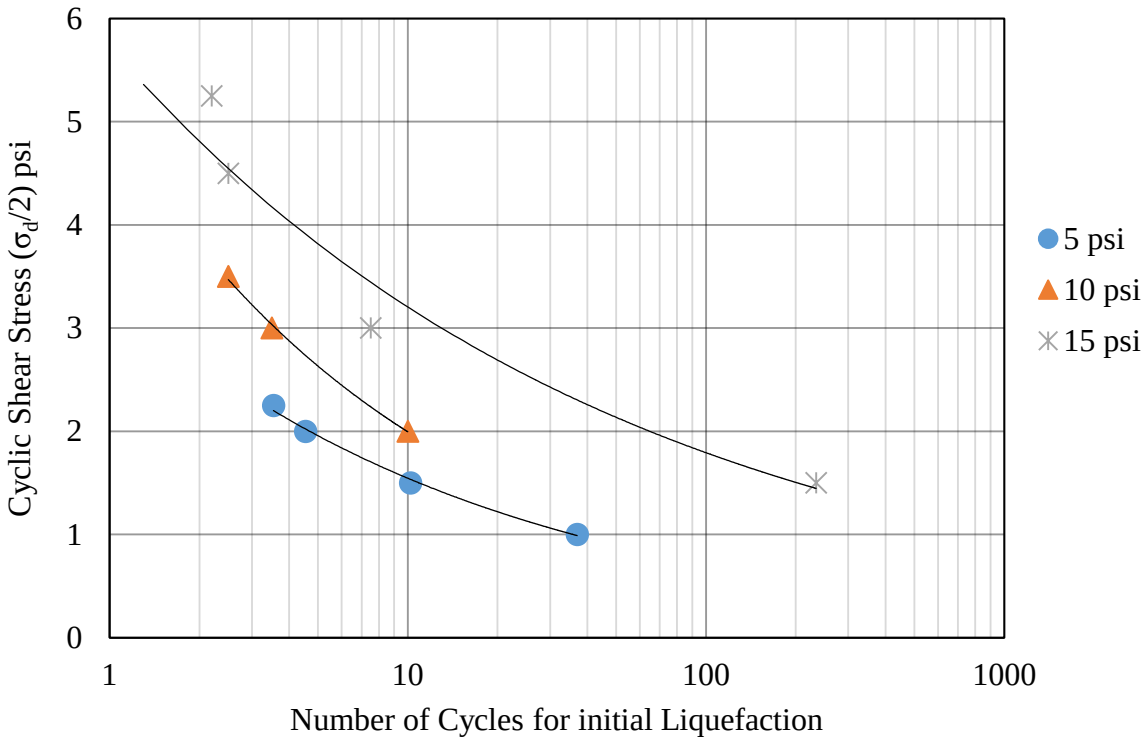

Figure 4-11 Variation of cyclic shear stress with number of cycles for initial liquefaction at initial effective confining pressures of 5, 10, and 15 psi for sand + 10 % fly ash samples.

Figure 4-11 shows the relationship between applied cyclic shear stress and the number of cycles for initial liquefaction. The plot presents three series of tests conducted at initial effective confining pressures of 5, 10 and 15-psi. It can be observed that, the higher the initial effective

confining pressure, the greater is the cyclic shear stress required for initial liquefaction for any given number of stress cycles. For instance, the cyclic shear stress required for the initial liquefaction in ten cycles for the sample consolidated at initial effective confining pressures of 5, 10, and 15 psi are 1.5, 2, and 3.2 psi, respectively. As in the case of clean sand, the number of cycles for initial liquefaction decreases with an increase in cyclic shear stress. For example, the sample consolidated at 5 psi initial effective confining pressure, the number of cycles for initial liquefaction decreases from 37 to 3.5 with an increase in cyclic shear stress from 1 to 2.25 psi. The plot of CSR versus the number of cycles for initial liquefaction for sand +10 % fly ash is shown in Figure 4-12. It is seen from the figure that, the CSR required for initial liquefaction at any given number of cycles decreases with an increase in confining pressure which is similar to the case of clean sand. For instance, the CSR required for the initial liquefaction in ten cycles for the sample consolidated at initial effective confining pressures of 5, 10, and 15 psi are 0.3, 0.2, and 0.19, respectively. In addition, the number of cycles required for initial liquefaction at any given confining pressure decreases as the CSR increases. For instance, the sand containing 10 % fly ash sample consolidated at an initial effective confining pressure of 5 psi liquefied at 37 cycles during the application of cyclic shear stress at CSR = 0.2, whereas it liquefied at 10 cycles during the application of cyclic shear stress at CSR = 0.3.

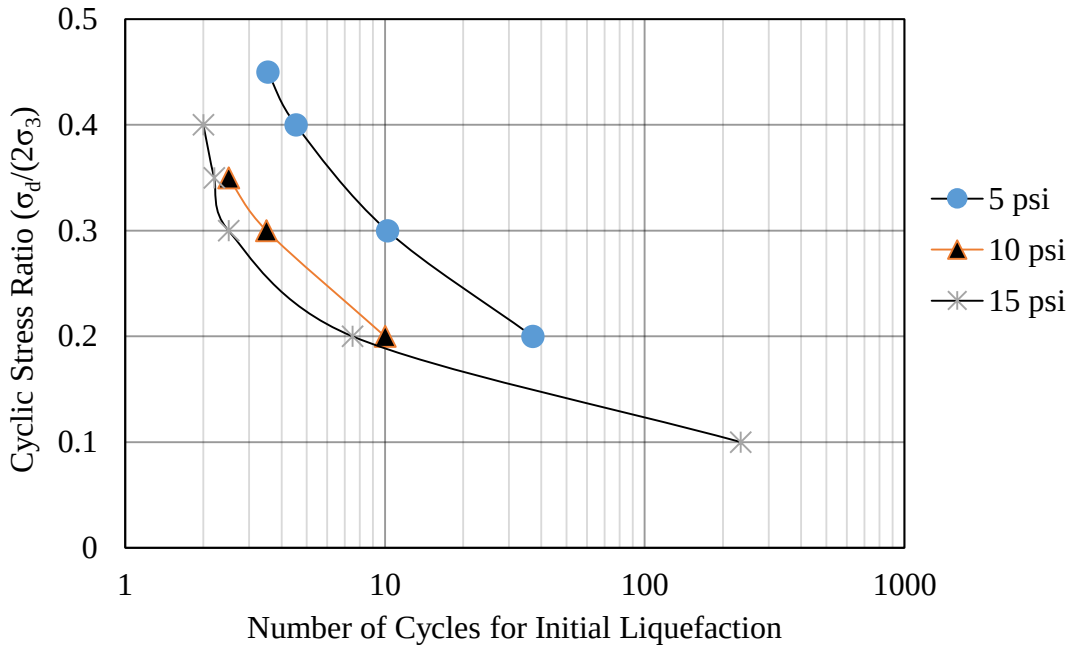

Figure 4-12 Variation of CSR with number of cycles for initial liquefaction at initial effective confining pressures of 5, 10, and 15 psi for sand + 10 % fly ash samples.

4.4.2.2 Effects of confining pressure on axial deformation

Figure 4-13 shows the relationship between the cyclic shear stress applied and number of cycles required to induce 2.5 % DA strain in sample consolidated at $\overline{\sigma 3}$ = 5, 10 and 15 psi. On increasing the confining pressure, the cyclic shear stress required to induce 2.5 % DA strain for a given number of stress cycles, also increases. For example, the cyclic shear stress required to induce 2.5 % DA strain are 1.6, 2.7, and 3.2 psi for the sample consolidated at initial effective confining pressures of 5, 10, and 15 psi, respectively. Similar to the case of pore water pressure build up, the number of cycles required to induce 2.5 % DA strain decreases with an increase in cyclic shear stress for the sample consolidated at any effective confining pressure. For example, the number of cycles required for the development of 2.5 % DA strain in sample consolidated at

an initial effective confining pressure of 5 psi decreases from nineteen to three on increasing the cyclic shear stress from 1.25 to 2.5 psi.

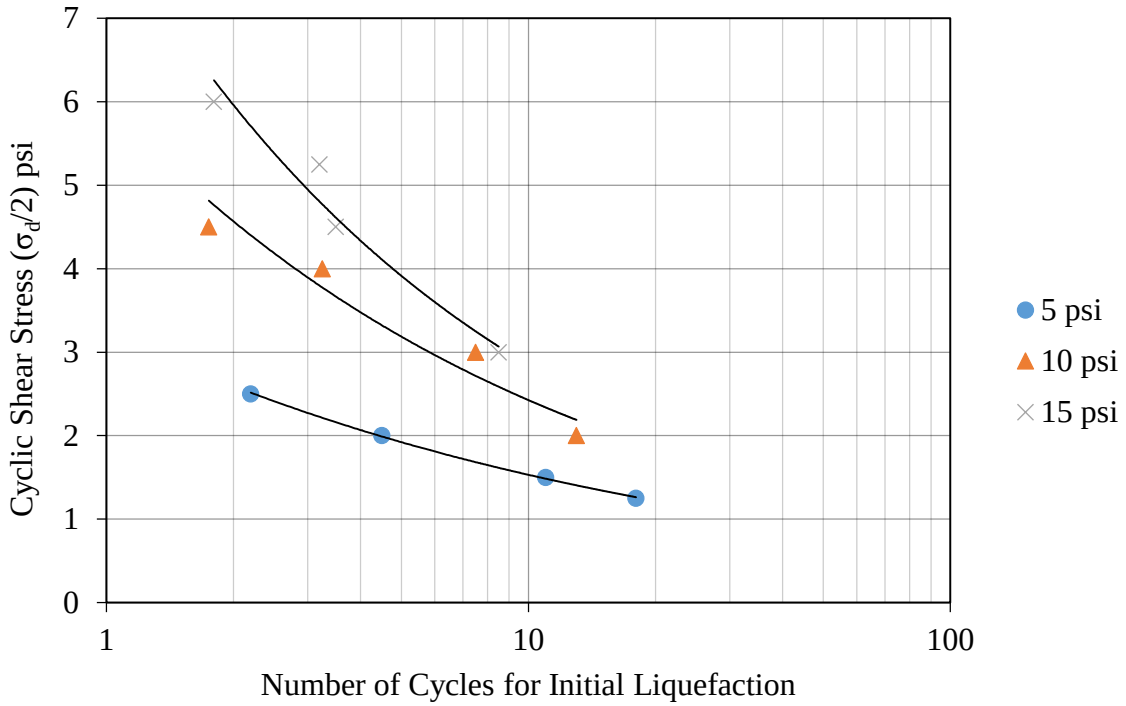

Figure 4-13 Variation of cyclic shear stress with number of cycles for 2.5 % DA strain at initial effective confining pressures of 5, 10, and 15 psi for sand + 10 % fly ash samples.

Figure 4-14 presents the effects of initial confining pressure on cyclic shear stress inducing the 5 % DA strain in a given number of stress cycles. It can be observed that, the cyclic shear stress required to induce 5 % DA strain at any given number of stress cycles increases with an increase in initial effective confining pressure. For the development of 5 % DA strain in the samples consolidated at effective confining pressures of 5, 10, and 15 psi in ten cycles, cyclic shear stresses required are 1.5, 2.5, and 2.8 psi, respectively. Moreover, the number of cycles required to induce 5 % DA strain in the sample consolidated at any given effective confining pressure decreases with an increase in cyclic shear stress. For instance, the number of cycles required to

induce 5 % DA strain in the sample consolidated at an initial effective confining pressure of 5 psi decreases from 37 to 2 , on increasing cyclic shear stress from 1 to 2.5 psi.

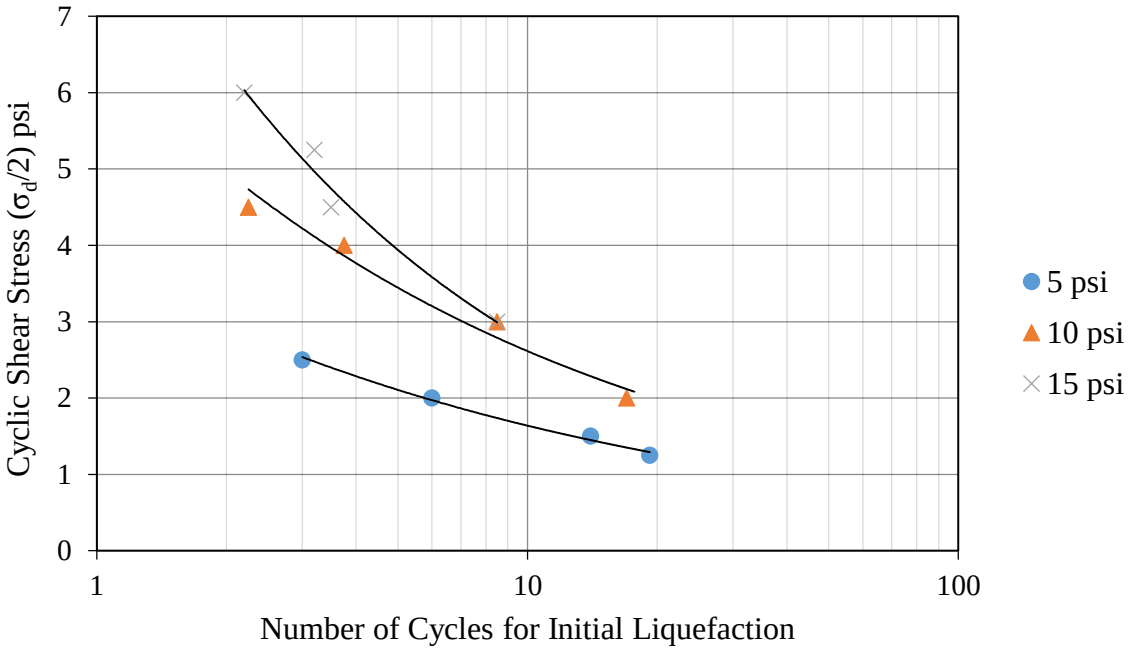

Figure 4-14 Variation of cyclic shear stress with number of cycles for 5 % DA strain at initial effective confining pressures of 5, 10, and 15 psi for sand + 10 % fly ash.

The plots of CSR versus the number of cycles required to induce 2.5 % DA strain are shown in Figure 4-15. It can be seen that, the CSR required to induce 2.5 % DA strain in the sand containing 10 % fly ash sample for any given number of stress cycles decreases with an increase in effective confining pressure. For example, the CSR required to induce 2.5 % DA strain in sand containing 10 % fly ash sample consolidated at effective confining pressures of 5, 10, and 15 psi at ten stress cycles are 0.28, 0.19, and 0.16, respectively. The number of stress cycles required to induce 2.5 % DA strain in a sample consolidated at any effective confining pressure also decreases with an increase in cyclic shear stress. For example, the samples consolidated at an

effective confining pressure of 5 psi, the number of cycles required to induce 2.5 % DA strain decreases from 35 to 2, on increasing the CSR 0.2 to 0.45.

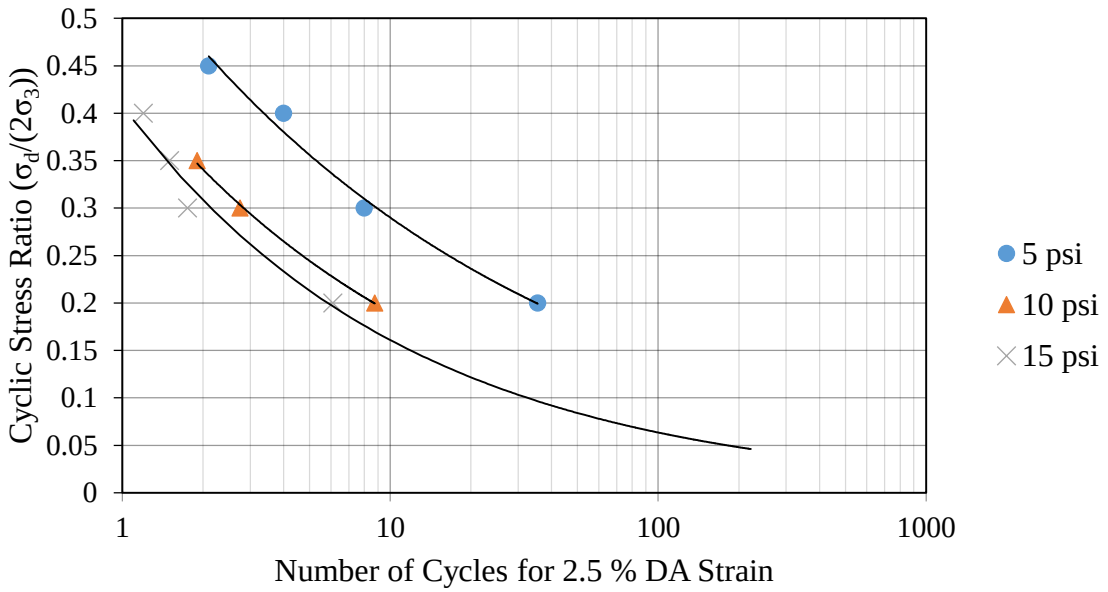

Figure 4-15 Variation of cyclic shear stress with number of cycles for 2.5 % DA strain at initial effective confining pressures of 5, 10, and 15 psi for sand + 10 % fly ash samples.

Figure 4-16 shows the effects of initial effective confining pressure on CSR inducing 5 % DA strain in the sand sample containing 10 % fly ash. It can be observed that, the CSR required to induce 5 % DA strain in the sand sample containing 10 % fly ash for any given number of stress cycles decreases as the confining pressure increases. The number of stress cycles required to induce 5 % DA strain in the sand containing 10 % fly ash sample also decreases with an increase in CSR.

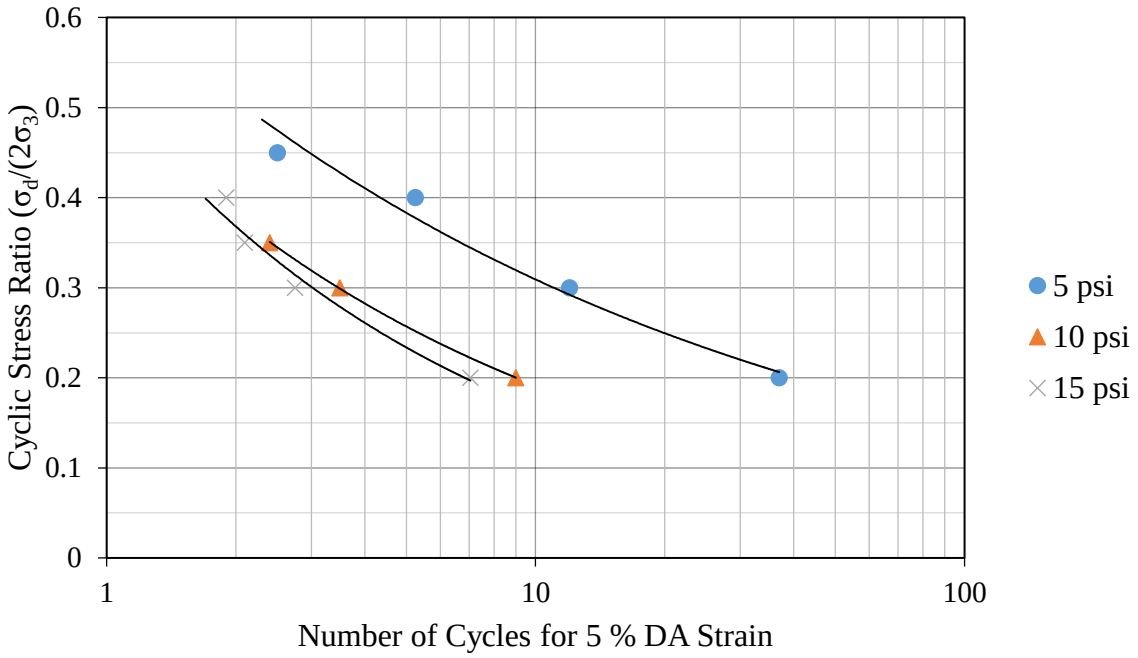

Figure 4-16 Variation of cyclic shear stress with number of cycles for 5 % DA strain at initial effective confining pressures of 5, 10, and 15 psi.

4.5 Test results on sand containing 20 % fly ash

This section presents the results of the tests conducted on sand containing 20 % fly ash. Three series of tests were performed after consolidating the sample at initial effective confining pressures of 5, 10 and 15 psi. For each consolidation pressure, the cyclic load was varied, changing the CSR from 0.1 to 0.5, as shown in Table 3-3.

Effects of confining pressure on the liquefaction resistance were evaluated in terms of pore water pressure generation as well as axial deformation.

4.5.1 Typical test results of sand containing 20 % Fly ash

The typical result of the effect of application of cyclic shear stress in terms of pore water pressure generation on a sand containing 20 % fly ash sample is shown in Figure 4-17.

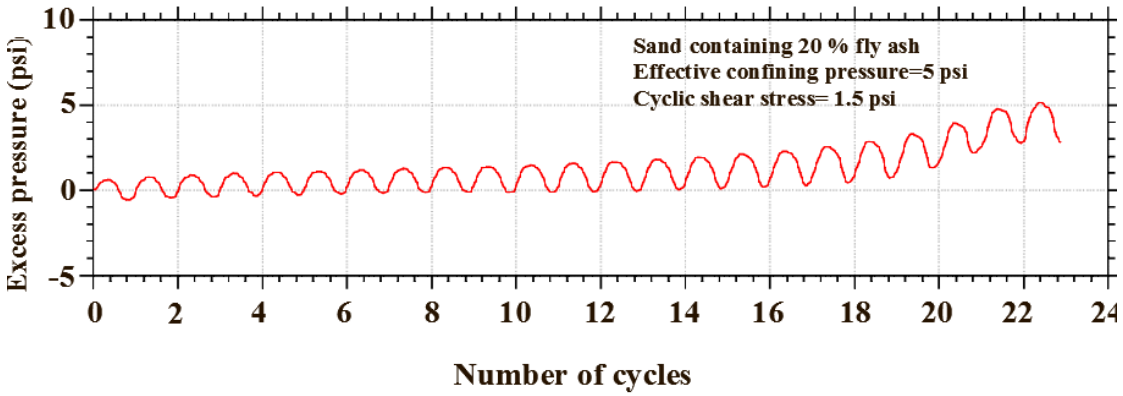

Figure 4-17 Typical variation of pore water pressure with number of cycles for sand + 20 % fly ash sample.

In this case, sand containing 20 % fly ash sample was consolidated at an initial effective confining pressure of 5 psi and then subjected a cyclic shear stress of 1.5 psi. The pore water pressure and axial strain were measured and potted as shown in Figure 4-17 and Figure 4-18, respectively. The plot in Figure 4-17 shows the rate of development of excess pore water pressure. In comparison to the clean sand samples and sand samples containing 10% fly ash, the excess pore water pressure build up for sand samples with 20 % fly ash developed slowly. The excess pore water pressure started to increase rapidly after sixteenth cycles and began to approach the externally applied effective confining pressure after the twenty-third cycles. Similar types of plots were obtained in other test on sand samples containing 20 % fly ash.

The response of axial deformation on cyclic loading is shown in Figure 4-18. The graph shows that the sample withstood 18 stress cycles without significant deformation. After that sample

started to deform rapidly and immediately exceeded the 10 % axial strain at the end of 23rd cycles. The sample deformed suddenly after the stage of initial liquefaction, which also occurred at the end of 23rd cycles (Figure 4-18). Similar type of graphs were obtained for the tests on sand containing 20 % fly ash.

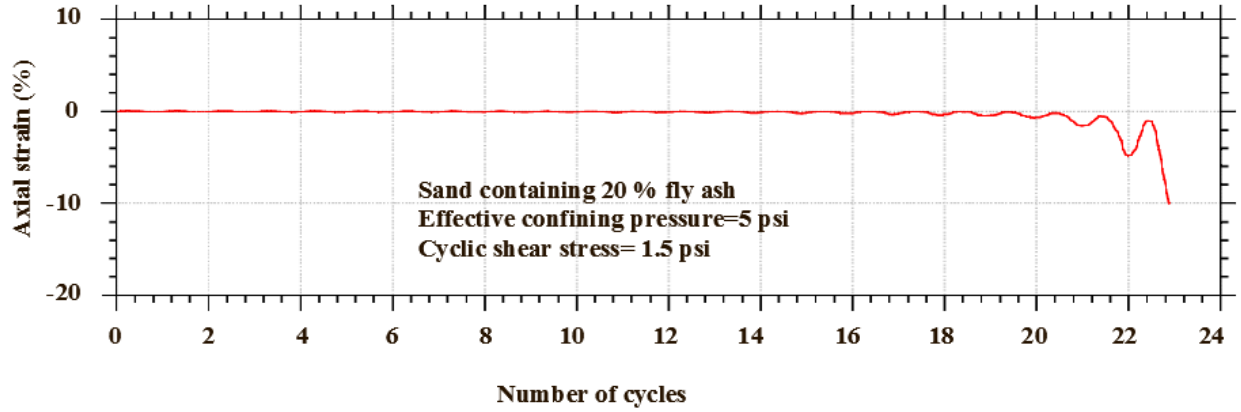

Figure 4-18 Typical variation of axial strain with number of cycles for sand + 20 % fly ash sample.

4.5.2 Effects of confining pressure

4.5.2.1 Effects of confining pressure on generation of pore water pressure

Figure 4-19 presents the relationship between cyclic shear stress versus number of stress cycles for the confining pressures used in this study. As in the case of clean sand and sand containing 10 % fly ash, the cyclic shear stress required for initial liquefaction at any given number of stress cycles of sand containing 20 % fly ash sample increases with an increase in effective confining pressure. For example, the cyclic shear stress required for the initial liquefaction of sample consolidated at initial effective confining pressures of 5, 10, and 15 psi at ten stress cycles are 2, 2.5, and 2.8 psi, respectively.

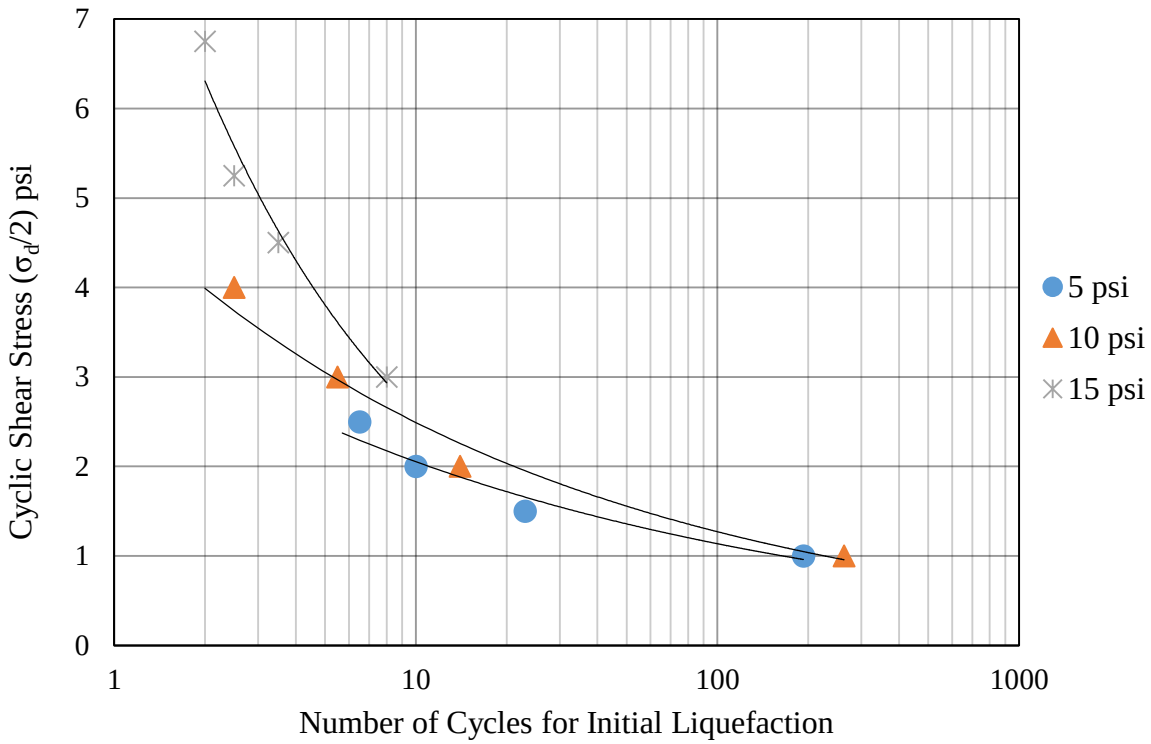

Figure 4-19 Variation of cyclic shear stress with the number of cycles for initial liquefaction at initial effective confining pressures of 5, 10, and 15 psi for sand containing 20 % fly ash.

In addition, it can be observed that, as the cyclic shear stress applied increases, the number of stress cycles required for initial liquefaction of sand containing 20 % fly ash consolidated at any effective confining pressure decreases. For the sample consolidated at an initial effective confining pressure of 5 psi, liquefied in 193 stress cycles during the application of the cyclic shear stress of 1psi , whereas it liquefied in 6.5 cycles on the application of cyclic shear stress of 2.5 psi.

The plots of CSR and the number of stress cycles for initial liquefaction are shown in Figure 4-20**.** It may be observed from the figure that the CSR required for initial liquefaction of the sand sample containing 20 % fly ash at any given number of stress cycles decreases with an increase in effective confining pressure. The pattern is similar to clean sand and sand containing 10 % fly

ash. For example, the CSR required for the initial liquefaction of the sand containing 20 % fly ash sample consolidated at initial effective confining pressures of 5, 10, and 15 psi at ten stress cycles are 0.4, 0.23, and 0.18, respectively. It is also noticed that, as the applied shear stress is increased by increasing the CSR, the number of stress cycles required for initial liquefaction of sand containing 20 % fly ash sample consolidated at any given effective confining pressure also decreases.

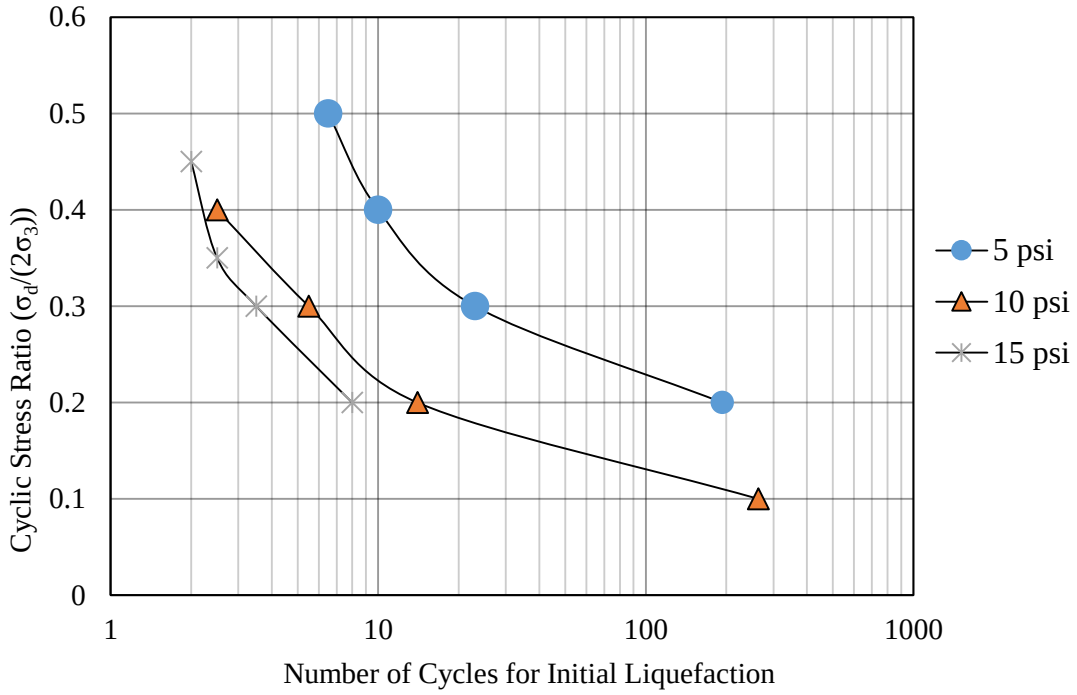

Figure 4-20 Variation of CSR with the number of cycles for initial liquefaction at initial effective confining pressures of 5, 10, and 15 psi for sand containing 20 % fly ash.

4.5.2.2 Effects of confining pressure on axial deformation

The relationship between the cyclic shear stress applied and number of stress cycles required to induce 2.5 % and 5 % DA strain is shown in Figure 4-21 and Figure 4-22, respectively. It can be seen from Figure 4-21 that, as the confining pressure is increased, the cyclic shear stress required

to induce 2.5 % DA strain in the sample of sand containing 20 % fly ash, at any given number of cycles also increases. The sand containing 20 % fly ash sample consolidated at effective confining pressures of 5, 10, and 15 psi requires cyclic shear stress of 2.4, 2.6, and 3 psi, respectively to induce 2.5 % DA strain. Further, it can be observed that, with an increase in cyclic shear stress, the number of stress cycles required to induce 2.5 % DA strain in sand samples containing 20 % fly ash consolidated at any given effective confining pressure also decreases.

It may be noted from the Figure 4-22, the cyclic shear stress required to induce 5 % DA strain in a sand sample containing 20% fly ash at any given stress cycle increases with an increase in effective confining pressure. It is also observed that, the number of stress cycles required to induce 5 % DA strain decreases with an increase in cyclic shear stress.

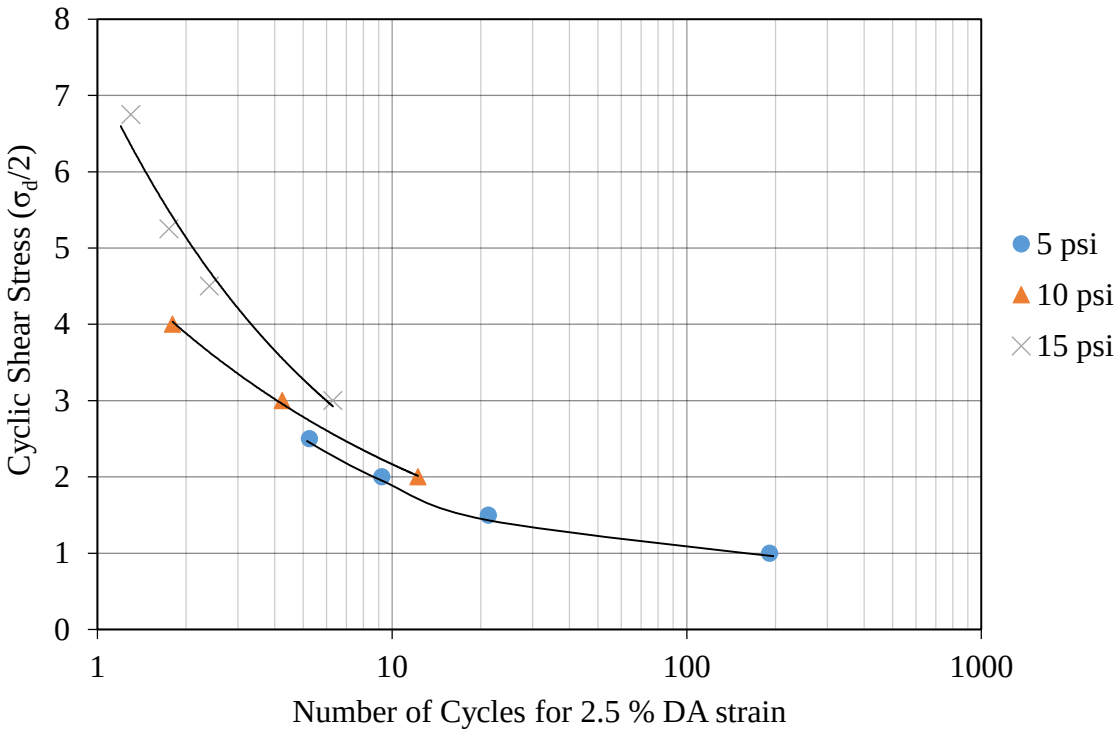

Figure 4-21 Variation of CSR with the number of cycles for 2.5 % DA strain at initial effective confining pressures of 5, 10, and 15 psi for sand containing 20 % fly ash.

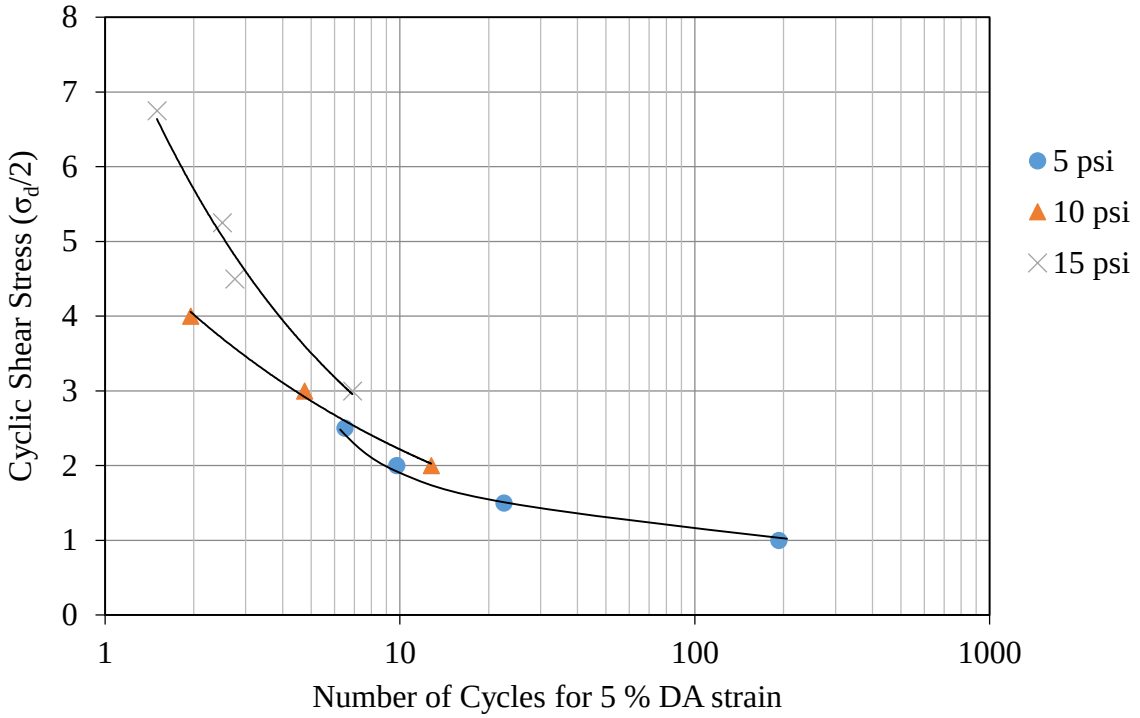

Figure 4-22 Variation of cyclic shear stress with number of cycles for 5 % DA strain at initial effective confining pressures of 5, 10, and 15 psi for sand containing 20 % fly ash.

The relationship between CSR and the number of cycles required for 2.5 % and 5 % DA strain at different confining pressures is shown in Figure 4-23 and Figure 4-24, respectively. The results indicate that, CSR required to induce 2.5 % DA strain in a sample of sand containing 20% fly ash at any stress cycle decreases with an increase in effective confining pressure. For instance, the CSR required to induce 2.5 % DA strain in a sand sample containing 20 % fly ash at ten stress cycles consolidated at effective confining pressures of 5, 10, and 15 psi are 0.38, 0.22, and 0.16, respectively. It is also noted that, the number of stress cycles required to induce 2.5 % DA strain in a sand sample containing 20 % fly ash sample decreases with an increase in CSR. For example, the stress cycles required to induce 2.5 % DA strain in a sample consolidated at 5 psi

effective confining pressure during the application of CSR=0.2 is 193, whereas same DA strain was induced at 6.5 stress cycles on applying CSR=0.5.

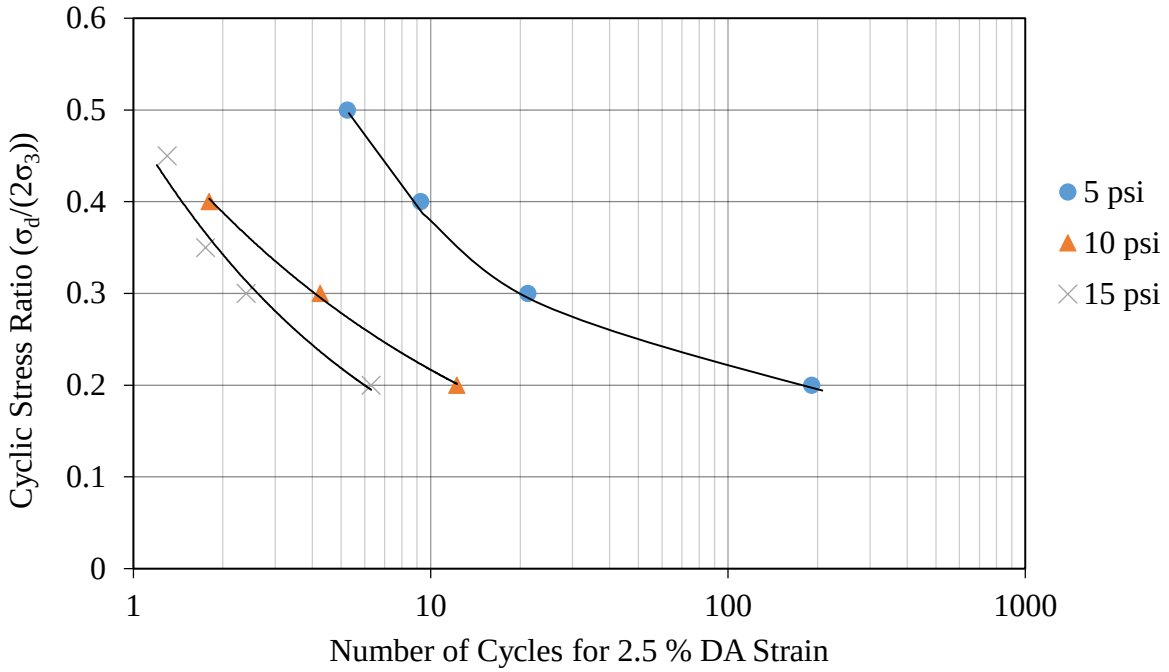

Figure 4-23 Variation of CSR with the number of cycles for 2.5 % DA strain at initial effective confining pressures of 5, 10, and 15 psi for sand containing 20 % fly ash.

It may be observed from Figure 4-24 that as the effective confining pressure increases, the number of cycles inducing 5 % DA strain at a given CSR decreases.

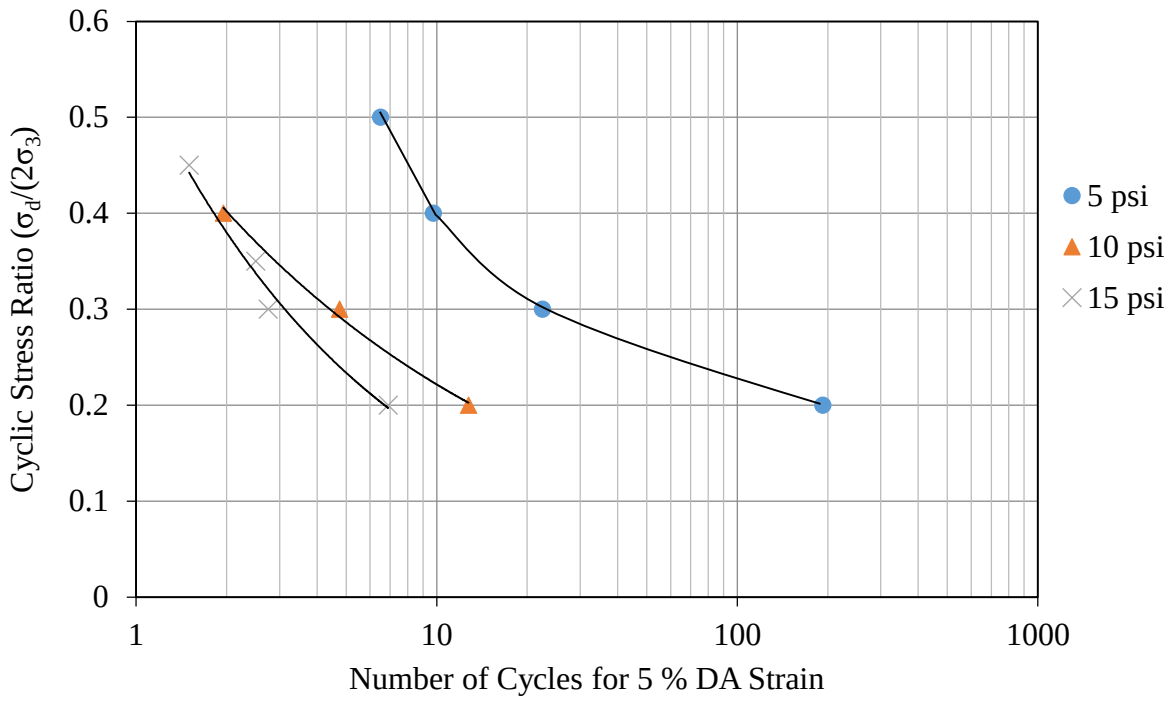

Figure 4-24 Variation of CSR with the number of cycles for 5 % DA strain at initial effective confining pressures of 5, 10, and 15 psi for sand containing 20 % fly ash.

4.6 Test results on fly ash

The cyclic triaxial test results on fly ash will now be discussed. Four tests were conducted after consolidating the samples at an initial effective confining pressure of 5 psi and varying the CSR from 0.1 to 0.4.

The typical test results of the effect of application of cyclic shear stress on a sample are shown in Figure 4-25 and Figure 4-26. In this case, the fly ash sample was consolidated at an initial effective confining pressure of 5 psi and then cyclic shear stress of 1.5 psi was applied. Figure 4-25 shows the excess pore water pressure generated on cyclic loading. The pore water pressure started to build up from the beginning of the first cycle. It gradually increases on subsequent cyclic stress application. Finally, at the end of fifth stress cycles the excess pore water pressure

became equal to externally applied effective confining pressure and the sample came to the stage of initial liquefaction. Similar excess pressure generations were observed on other fly ash samples tested as a part of this study.

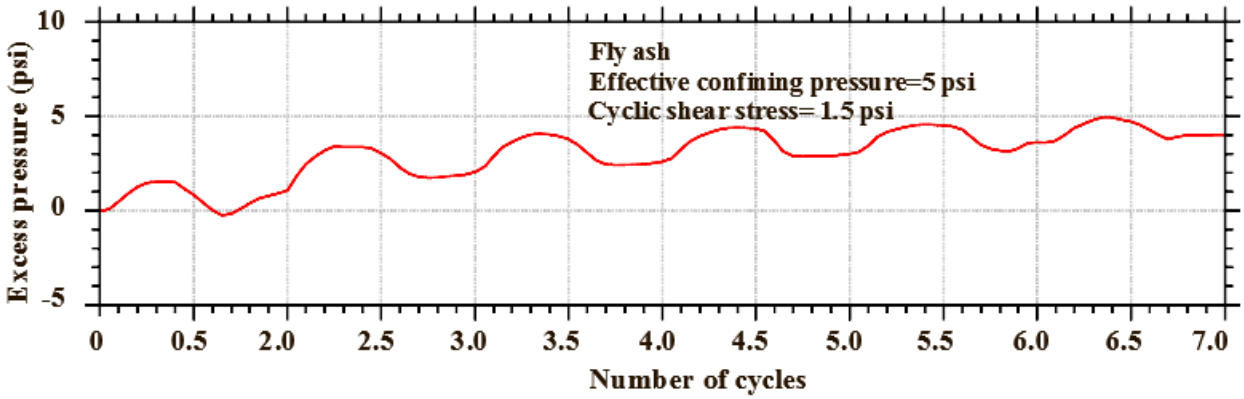

Figure 4-25 Typical variation of pore water pressure with number of cycles for fly ash sample.

The typical deformation behavior of fly ash sample on cyclic loading is shown in Figure 4-26. The fly ash sample was not deformed until the application of three stress cycles. After that, it started to deform slowly. The rate of deformation started to increase rapidly after 4.5 cycles and axial strain of 4 % occurred in 6 cycles. The sample started deforming excessively, just when the initial liquefaction occurred in the 5^{th} cycles. During the stage of initial liquefaction, the axial deformation of the specimen exceeded 8 %.

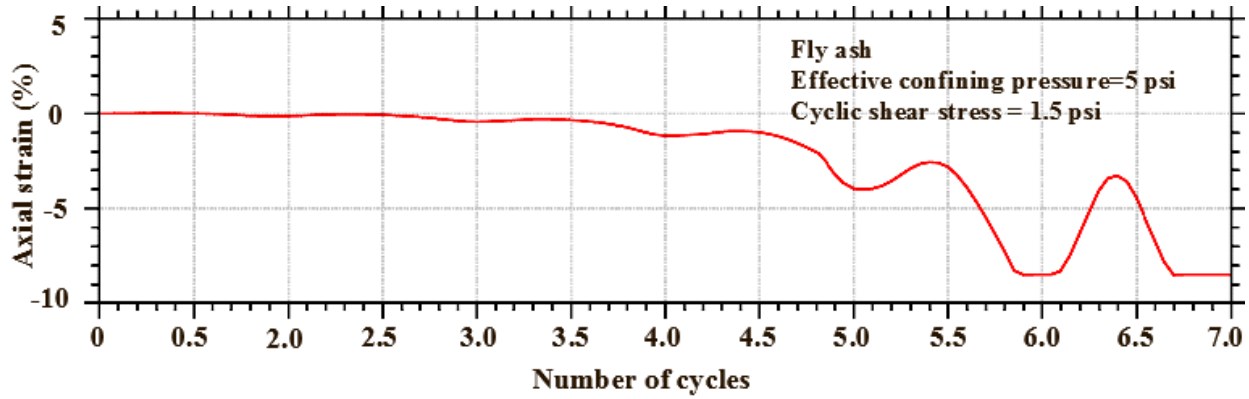

Figure 4-26 Typical variation of axial deformation with number of cycles for pure fly ash sample.

The variation of cyclic shear stress with numbers of cycles for initial liquefaction on the fly ash sample consolidated at an initial effective confining pressure of 5 psi is shown in Figure 4-27. It can be seen that, as higher the cyclic shear stress is applied, the lesser the number of stress cycles are required for the initial liquefaction. For example, during the application of 2 psi cyclic shear stress, the fly ash sample liquefied in 3 stress cycles, whereas it liquefied in 24 stress cycles when cyclic shear stress of 1 psi was applied.

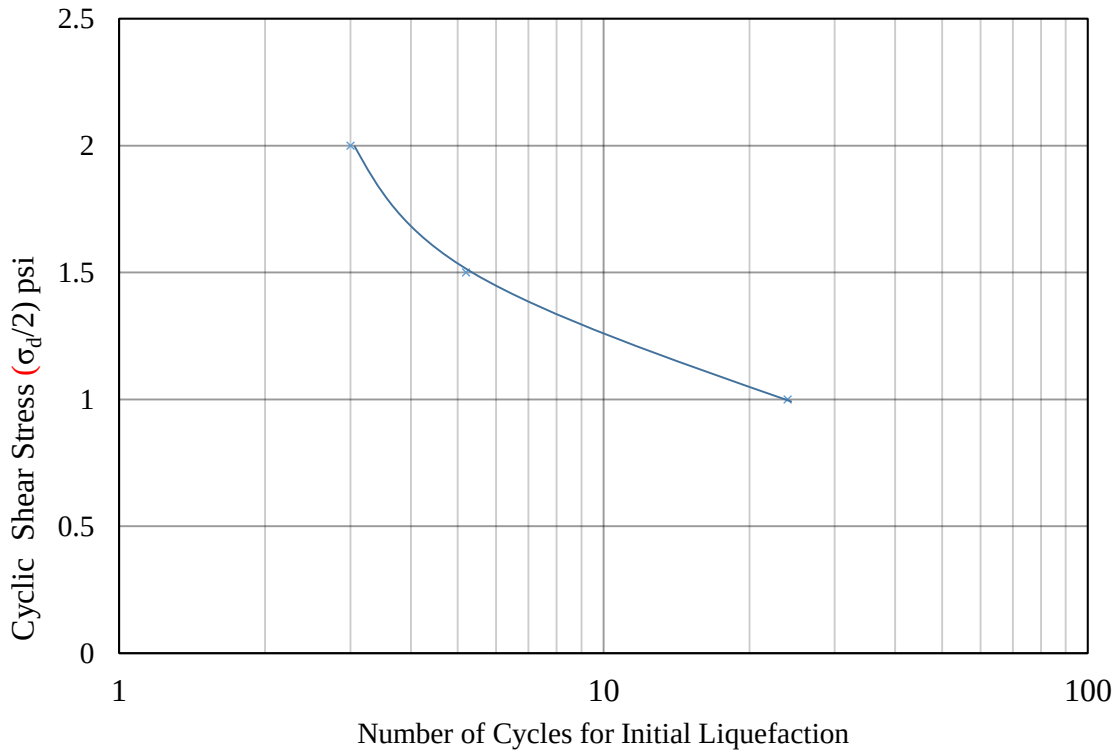

Figure 4-27 Variation of cyclic shear stress with number of cycles for initial liquefaction at 5 psi effective confining pressure for fly ash.

Figure 4-28 presents the variation of CSR with numbers of cycles for initial liquefaction. As in the case of other tests, on increasing CSR, the number of stress cycles required for initial liquefaction decreases. For example, the fly ash sample liquefied during the application of 24 stress cycles, when CSR was 0.2, whereas it liquefied in 3 cycles when CSR = 0.4 was used.

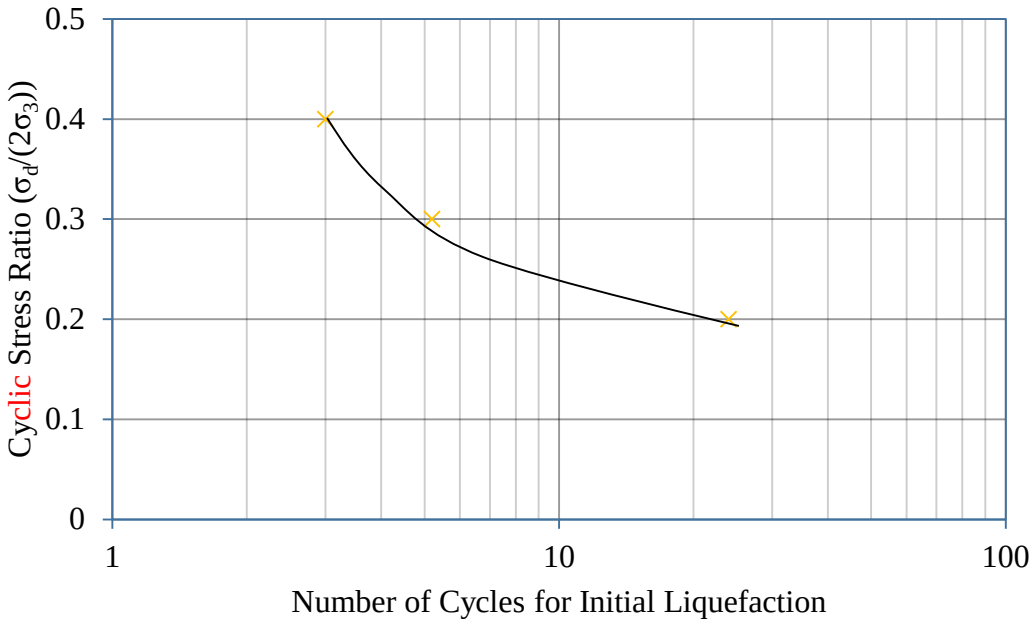

Figure 4-28 Variation of CSR with number of cycles for initial liquefaction at 5 psi effective confining pressure for fly ash.

The variation of CSR required to induce 2.5 % DA strain in fly ash samples consolidated at 5 psi effective confining pressure is shown in Figure 4-29. It can be observed that, as the CSR is increased, the number of cycles required to induce 2.5 % DA strain decreases. For example, under the application of cyclic load corresponding to CSR= 0.2, the sample was deformed by 2.5 % DA strain at 22.25 stress cycles, whereas same deformation was observed at 1.25 stress cycles when CSR=0.4.

Figure 4-30 displays the variation of CSR with the number of stress cycles required to induce 5 % DA strain in fly ash sample consolidated at an initial effective confining pressure of 5 psi. The number of cycles required to induce 5 % DA strain is found to decrease with an increase in CSR.

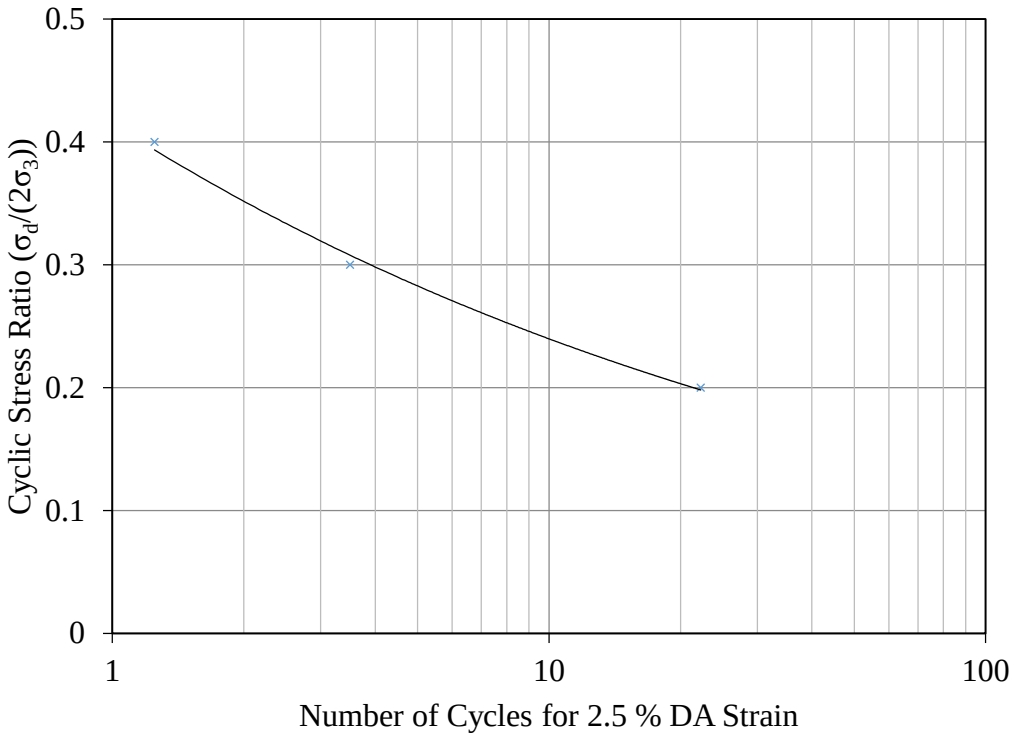

Figure 4-29 Variation of cyclic stress required to induce 2.5 % DA strain to fly ash at 5 psi effective confining pressure.

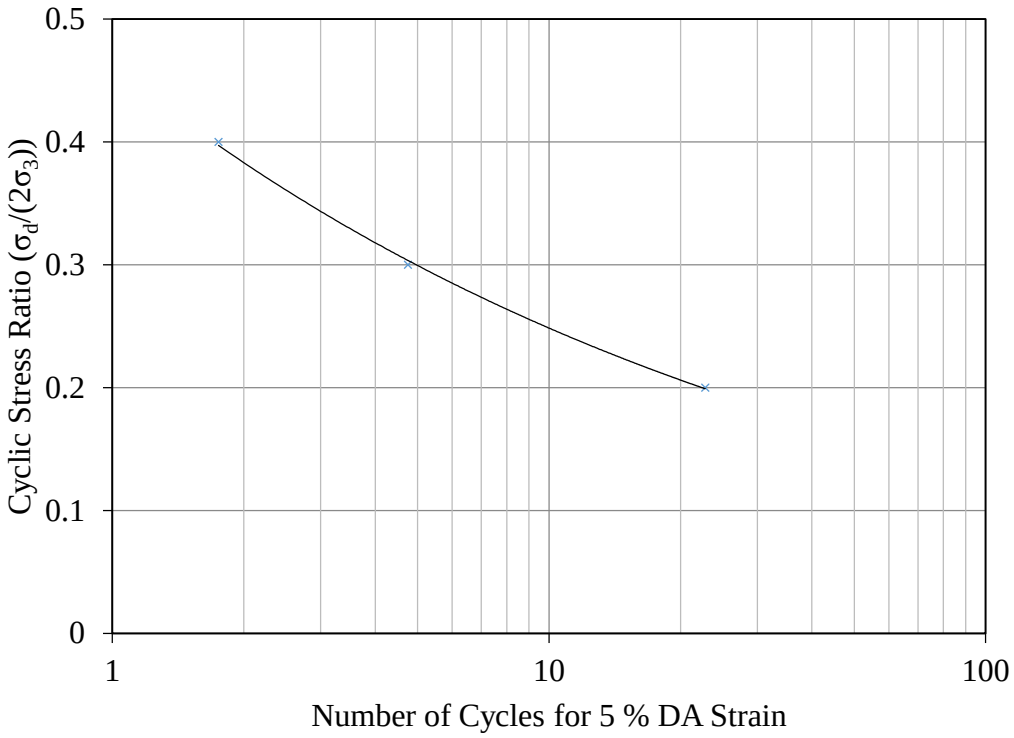

Figure 4-30 Variation of cyclic stress required to induce 5 % DA strain to fly ash at 5 psi effective confining pressure.

4.7 Effects of addition of fly ash on index properties of sand

With the addition of fly ash to sand a reduction in the void ratio was observed. Both maximum and minimum void ratios decreased with the addition of 10 and 20 % fly ash, as shown in Figure 4-31. The reduction in minimum void ratio was more compared to reduction of maximum void ratio. The reduction in the void ratio represents that, the added fly ash is utilized for the filling voids in sand. The results of (Regmi, 2014) is also combined for the study of variation of void ratios at higher fly ash contents (25, 30, and 50 % fly ash). It can be seen that, addition of 25 % fly ash slightly decreased maximum and minimum coid ratios. It was almost constant at 30 % fly ash. Maximum void ratio started to increase after 50 % but minimum void ratio is almost constant at 50 % after that, it increases.

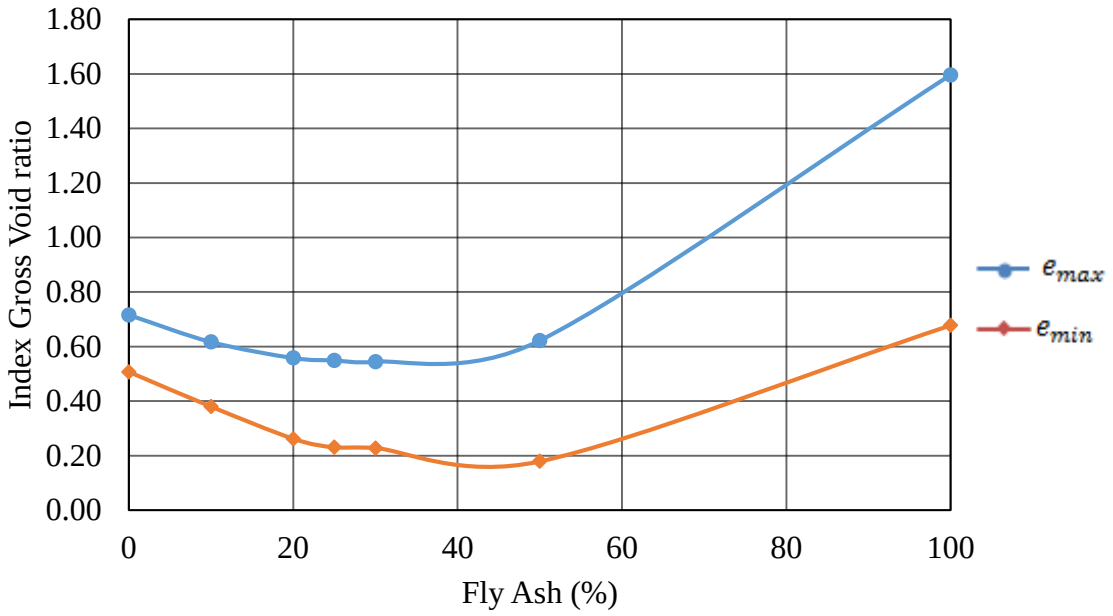

Figure 4-31 Variation of index void ratio with fly ash contents.

As described in Chapter 3, the specific gravity was found to decrease with the addition of fly ash. The clean sand has highest specific gravity (G_s = 2.66) whereas sand containing 20 % fly ash has a lower specific gravity (G_s = 2.63). Due to changes in specific gravity, the void ratio and the dry density also changes with the fly ash additions. The variation in the dry density at a relative density of 50 % is shown in Figure 4-32. The sand containing 20 % fly ash has the highest dry density.

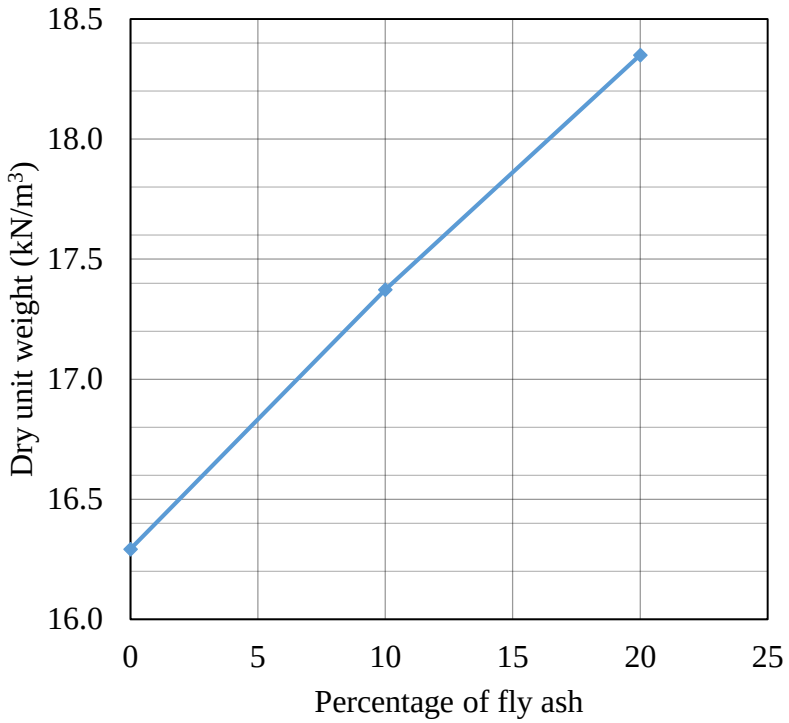

Figure 4-32 Variation of dry unit weight with various fly ash contents at 50 % relative density.

4.8 Effects of addition of fly ash on liquefaction resistance of sand

In order to evaluate the effects of addition of fly ash on liquefaction resistance of sand, the tests conducted by the addition of 10 % and 20 % fly ash are used here. The effects on liquefaction resistance were evaluated at three effective confining pressure of 5, 10 and 15 psi. Both pore water pressure generation and axial deformation of samples are considered as the basis of comparison. The initial liquefaction is used as the basis of comparison in terms of pore water pressure generation. The number of cycles required to induce 2.5 % and 5% DA strain is considered for the comparison of liquefaction resistance in terms of deformation.

4.8.1 Liquefaction resistance of clean sand and fly ash

The CSR required for initial liquefaction of samples of clean sand and fly ash consolidated at an initial effective confining pressure of 5 psi is shown in Figure 4-33. Figure 4-33 shows that, the CSR required for the initial liquefaction of clean sand at any given number of stress cycle is more than that for fly ash. For example, CSR required for the initial liquefaction of clean sand

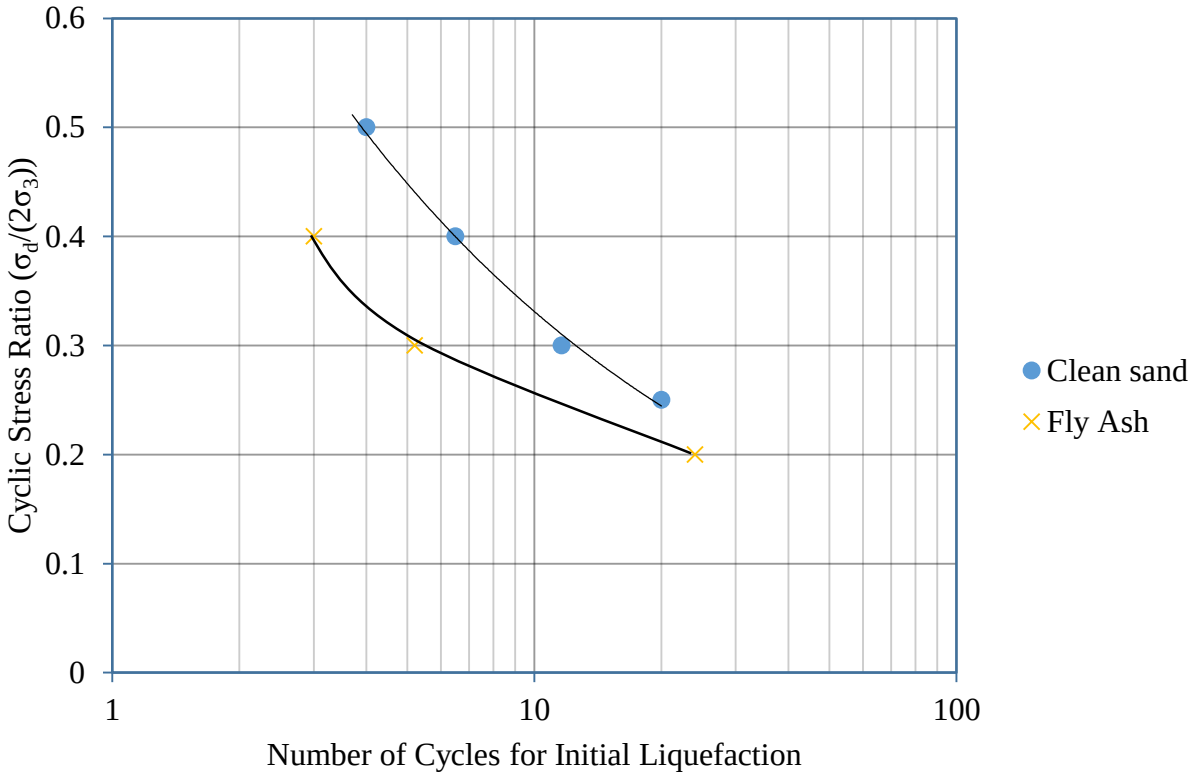

Figure 4-33 Liquefaction resistance of clean sand and pure fly ash at 5 psi effective confining pressure in terms of pore water pressure generation.

sample in 10 stress cycle is 0.32, whereas the CSR required for the initial liquefaction fly ash sample at ten stress cycles is 0.25.

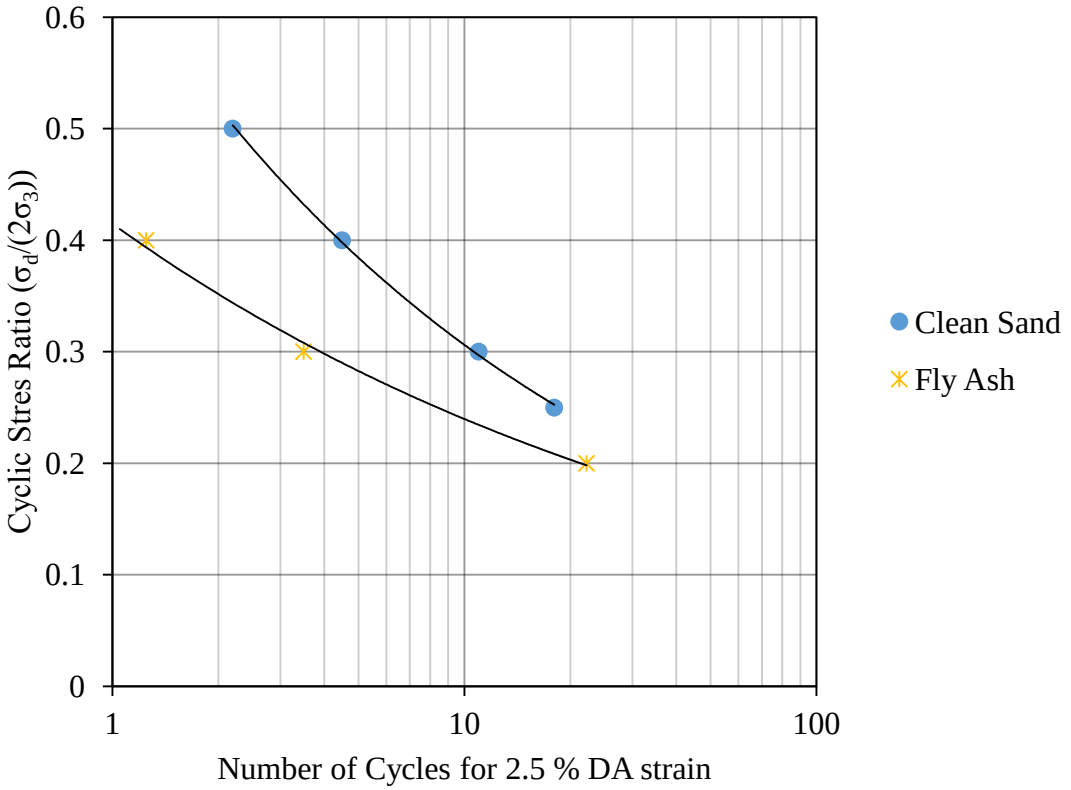

Figure 4-34 Liquefaction resistance of clean sand and pure fly ash samples at 5-psi effective confining pressure at 2.5 % deformation.

The CSR required for the development of 2.5 % and 5 % DA strain in a sample of clean sand and pure fly ash consolidated at an initial effective confining pressure of 5 psi is shown in Figure 4-34 and Figure 4-35, respectively. It can be seen in Figure 4-34 that, CSR required for the development of 2.5 % in the clean sand sample at any stress cycle is higher than that of pure fly ash. For example, CSR required for development of 2.5 % DA strain in a clean sand sample and fly ash sample are 0.31 and 0.25, respectively. As in the case of 2.5 % DA strain, CSR required for the development of 5 % DA strain in a clean sand sample at any stress cycle is also greater than that of pure fly ash sample as shown in Figure 4-35.

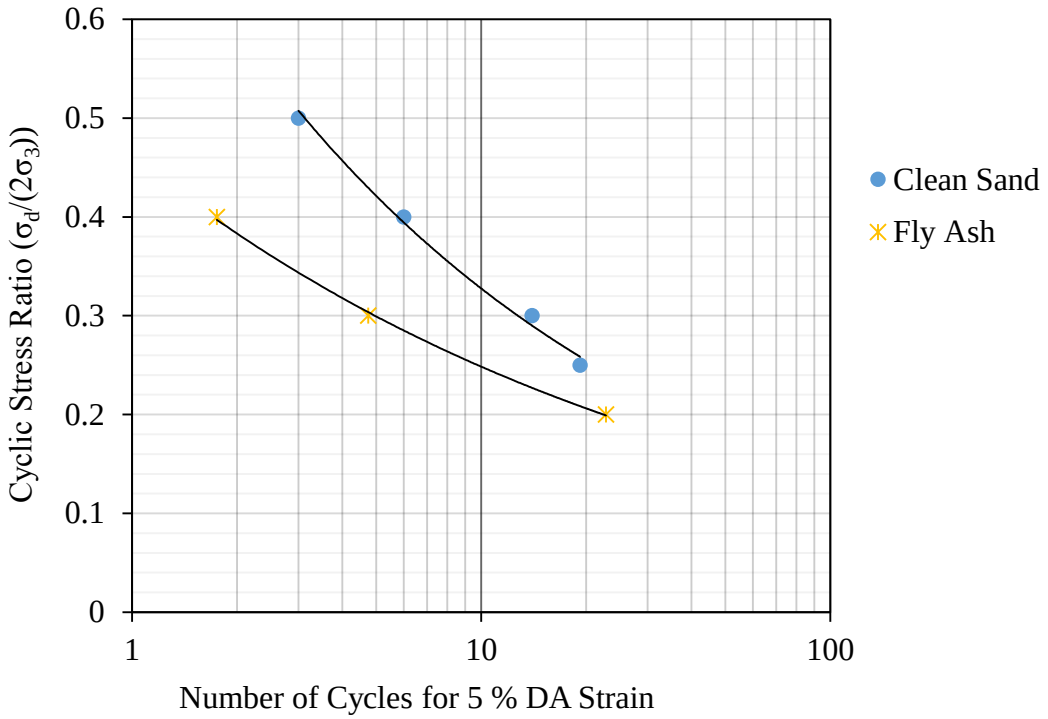

Figure 4-35 Liquefaction resistance of clean sand and pure fly ash samples at 5-psi effective confining pressure at 5 % deformation.

4.8.2 Effective confining pressure of 5 psi

The results of cyclic triaxial tests conducted at an initial effective confining pressure of 5-psi at different fly ash contents for clean sand used in this research are presented in Figure 4-36. The liquefaction resistance is compared in terms of initial liquefaction defined by $u = \overline{\sigma_3}$ condition. The plots in Figure 4-36 indicate that the liquefaction resistance decreases on adding 10 % fly ash. On the other hand, an addition of 20 % fly ash, increases liquefaction resistance significantly which is higher than that for clean sand. Further, the pure fly ash shows the lowest liquefaction resistance among the clean sand, sand containing 10 and 20 % fly ash and pure fly ash sample. The CSR required for initial liquefaction of clean sand, sand containing 10 and 20 % fly ash, pure fly ash samples at ten stress cycles are 0.32, 0.28, 0.4, 0.25, respectively.

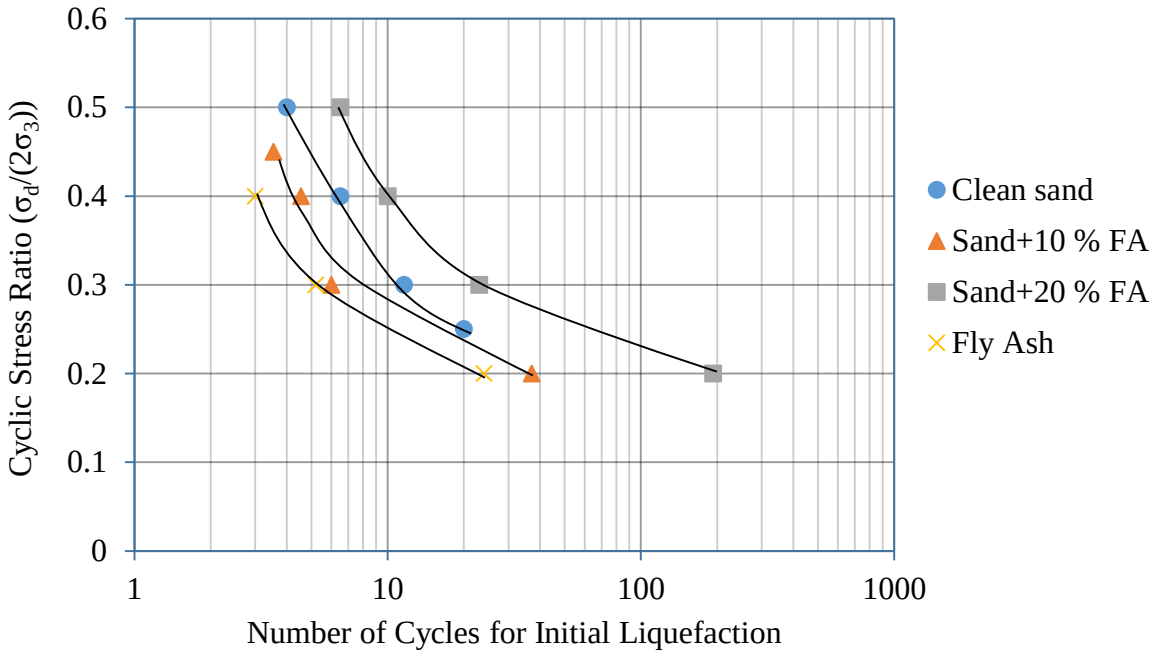

Figure 4-36 Liquefaction resistance of sand containing various percentages of fly ash at 5 psi effective confining pressure in terms of pore water pressure generation.

Figure 4-37 and Figure 4-38 demonstrates the effects of fly ash addition on axial deformation under cyclic load. The variation of number of cycles required to induce 2.5 % DA strain at various CSR values is shown in Figure 4-37. The deformation behavior is also similar to pore water pressure generation behavior. On addition of 10 % fly ash in sand, the resistance to deformation decreases. Moreover, the addition of 20 % fly ash increases the resistance to deformation, which is higher than that of clean sand. The fly ash sample has a lower resistance to deformation in comparison to clean sand, sand containing 10 and 20 % fly ash. For example, the CSR required to induce 2.5 % DA strain in samples of clean sand, sand containing 10 and 20 % fly ash, and pure fly ash at ten cycles are 0.31, 0.29, 0.39, 0.25, respectively. Similar trend can be observed for 5 % DA strain in Figure 4-38. By observing the pore water pressure generation as well as deformation behavior, it can be concluded that, at 5 psi confining pressure, the

liquefaction resistance initially decreases on the addition of 10 % fly ash to sand, and then increases on addition of 20 % fly ash as compared to case of clean sand.

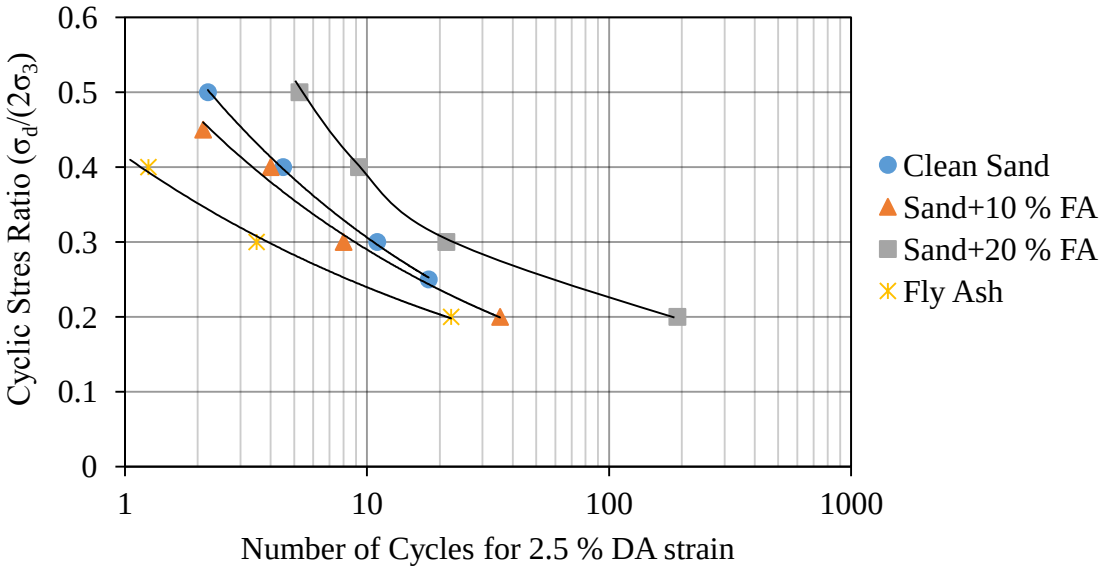

Figure 4-37 Liquefaction resistance of sand containing various percentages of fly ash at 5-psi effective confining pressure in terms of deformation.

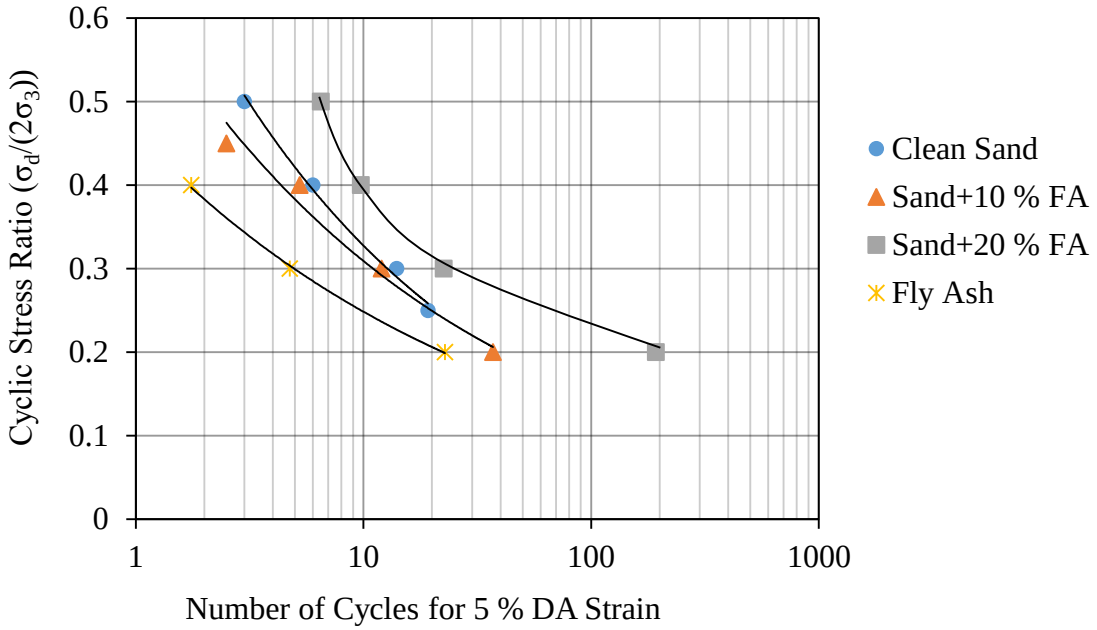

Figure 4-38 Liquefaction resistance of sand containing various percentages of fly ash at 5-psi effective confining pressure in terms of deformation.

4.8.3 Effective confining pressure of 10 psi

Figure 4-39 shows the effects of fly ash on liquefaction resistance in terms of pore water pressure generation, at 10-psi effective confining pressure. On addition of 10 % fly ash, liquefaction resistance decreases. However, on addition of 20 % fly ash, liquefaction resistance increases. In contrast to specimen consolidated at an initial effective confining pressure of 5-psi, liquefaction resistance of sand containing 20 % fly ash was lower than clean sand at an effective confining pressure of 10 psi. The CSR required for the initial liquefaction of clean sand, sand containing 10 and 20 % fly ash samples at ten stress cycles are 0.27, 0.2, and 0.23, respectively.

The effects of fly ash addition on liquefaction resistance in terms of deformation are shown in Figure 4-40 and Figure 4-41. It appears that resistance to deformation decreases, on the addition of 10 % fly ash to clean sand, after that it increases on addition of 20 % fly ash. For example, CSR required to induce 2.5 % DA strain at 10 stress cycles in the samples of clean sand, sand containing 10 and 20 % fly ash are 0.27, 0.23, and 0.2, respectively. The response on deformation is similar to pore water pressure generation. Furthermore, the liquefaction resistance behavior for both 2.5 % DA strain and 5 % DA strain are also similar.

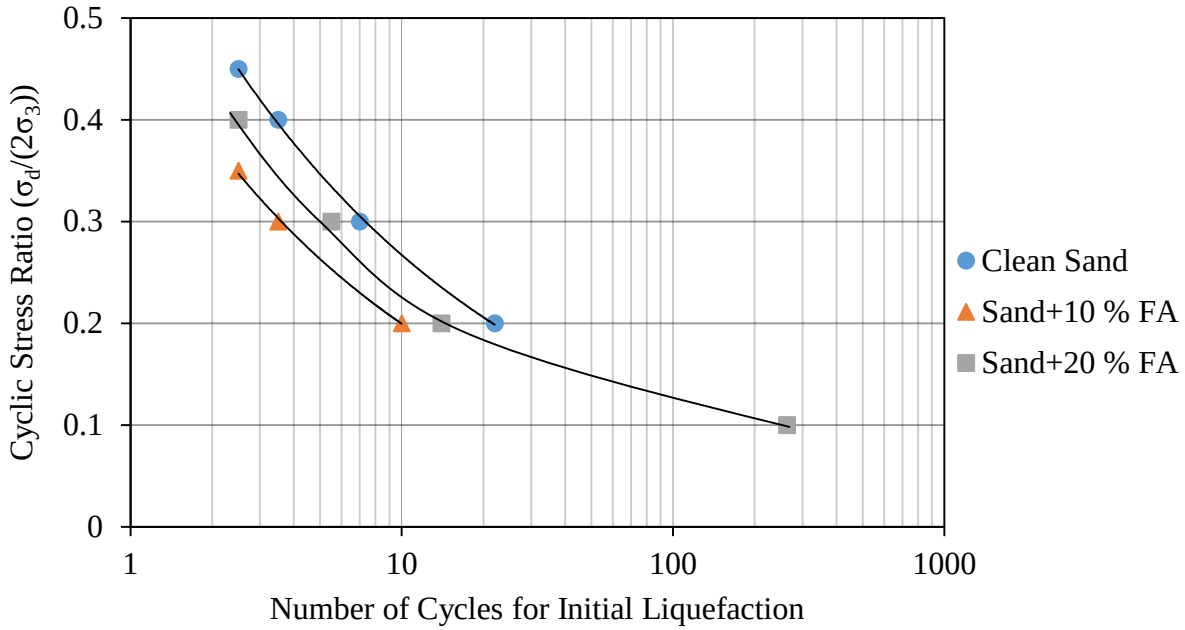

Figure 4-39 Liquefaction resistance of sand containing various percentages of fly ash at 10-psi effective confining pressure in terms of pore water pressure generation.

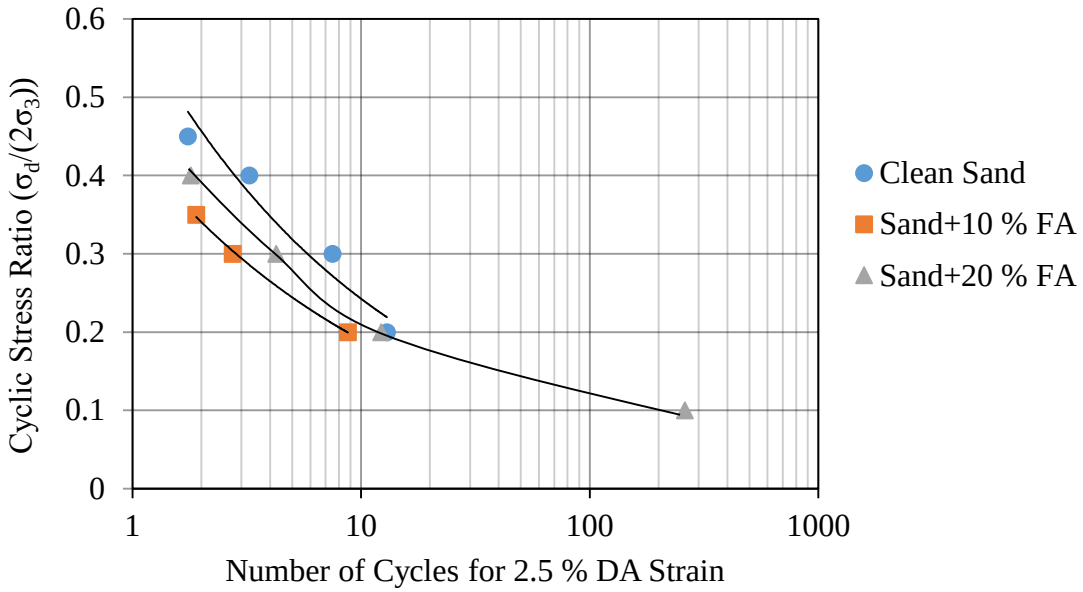

Figure 4-40 Liquefaction resistance of sand containing various percentages of fly ash at 10-psi effective confining pressure in terms of deformation.

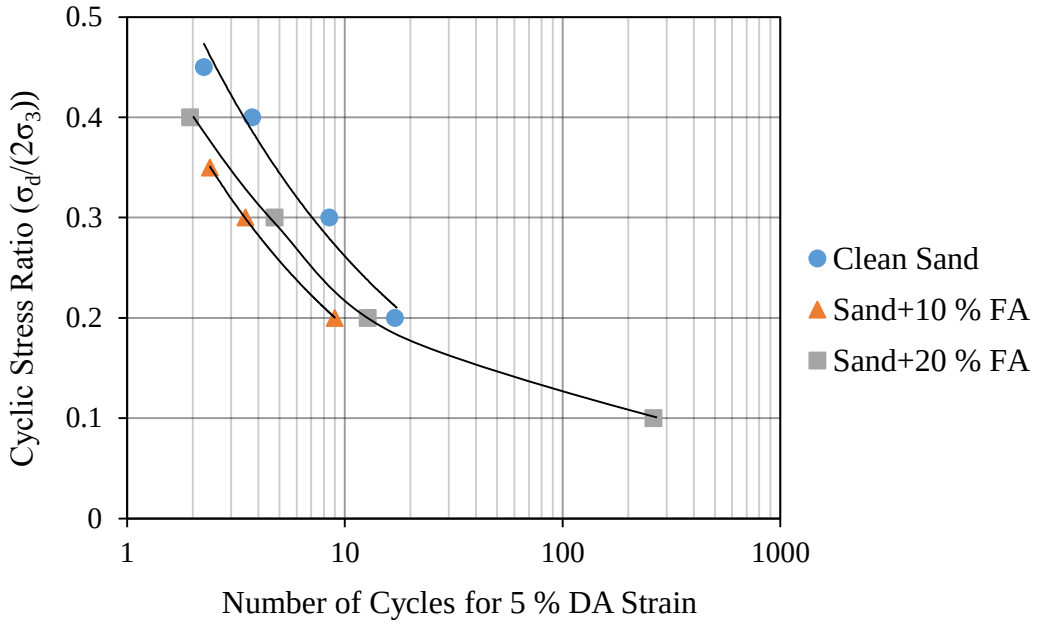

Figure 4-41 Liquefaction resistance of sand containing various percentages of fly ash at 10-psi effective confining pressure in terms of deformation.

4.8.4 Effective confining pressure of 15 psi

The effects of addition of fly ash were also evaluated at an initial effective confining pressure of 15- psi. The effects of liquefaction resistance in terms of pore water pressure generation is shown in Figure 4-42. The graph indicates that sand with 10 % fly ash has lower liquefaction resistance than clean sand. Further, sand with 20 % fly ash has higher liquefaction resistance than sand with 10 % fly ash. Which is similar to the effect of fly ash addition at 10-psi effective confining pressure. The sand samples containing various amounts of fly ash liquefied almost in similar cycles. For example, during the application of cyclic shear stress corresponding to CSR=0.3, the clean sand, fly ash containing 10 and 20 % fly ash samples were liquefied at 7.0, 2.5, 3.5 cycles, respectively. The clean sand sample, sand containing 10 and 20 % fly ash do not possess significant difference in liquefaction resistance.

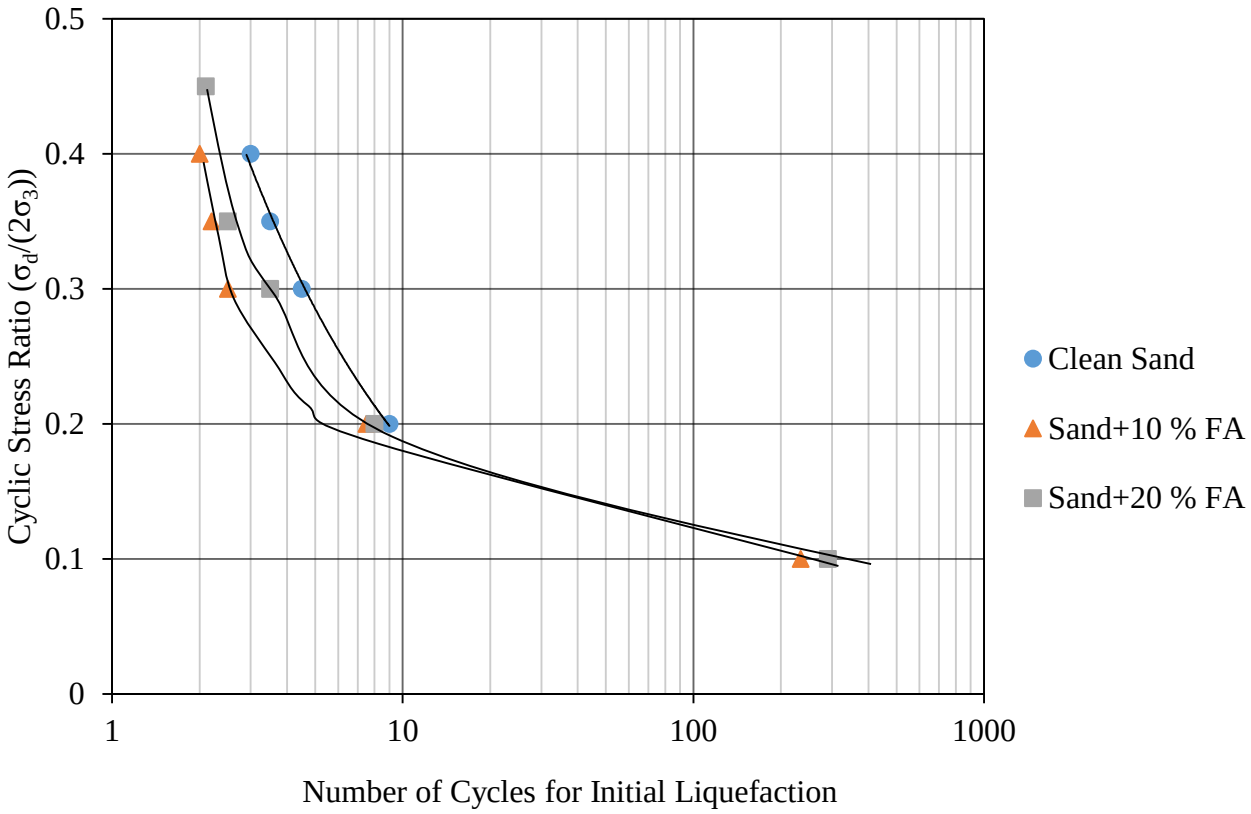

Figure 4-42 Liquefaction resistance of sand containing various percentages of fly ash at 15-psi effective confining pressure in terms of pore water pressure generation.

The number of cycles required for 2.5 % DA strain with corresponding CSR are presented in Figure 4-43. The figure indicates that liquefaction resistance decreases on addition of 10 % fly ash. The addition of 20 % fly ash increases the liquefaction resistance. For example, CSR required to induce 2.5 % DA strain at ten stress cycles in the samples of clean sand, sand containing 10 and 20 % fly ash are 0.19, 0.175, and 0.18, respectively. A similar trend was observed when comparing the effects of fly ash at 5 % DA strain (Figure 4-44). The difference, however, is small and all samples experiences liquefaction in almost similar number of cycles for a given CSR. Hence, it can be noted that, at 15-psi effective confining pressure, the liquefaction resistance is less sensitive to addition of fine content as observed during the tests.

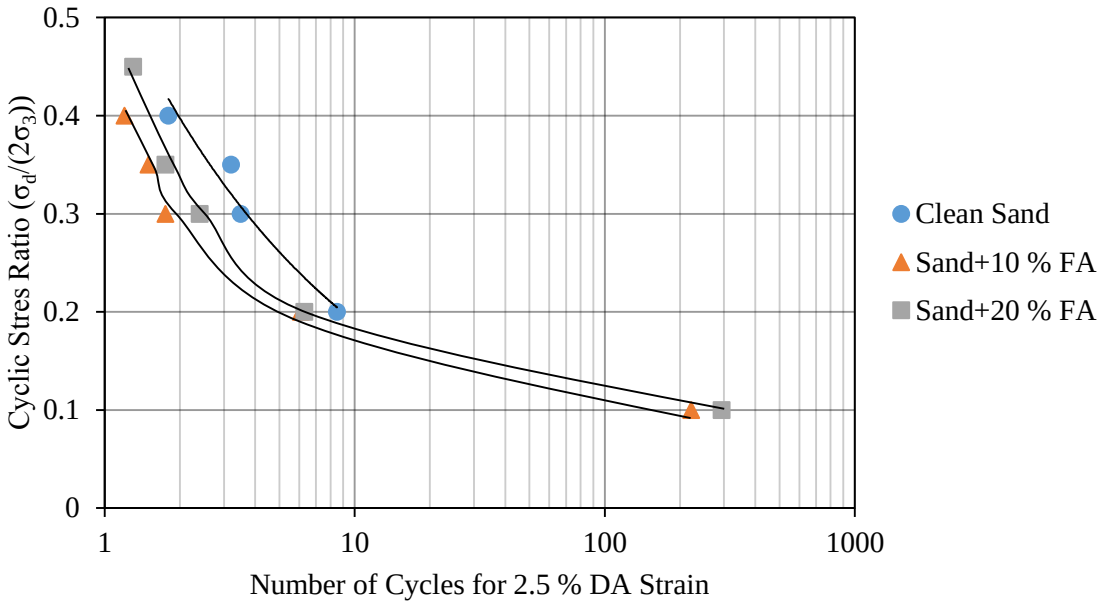

Figure 4-43 Liquefaction resistance of sand containing various percentages of fly ash at 15-psi effective confining pressure in terms of deformation.

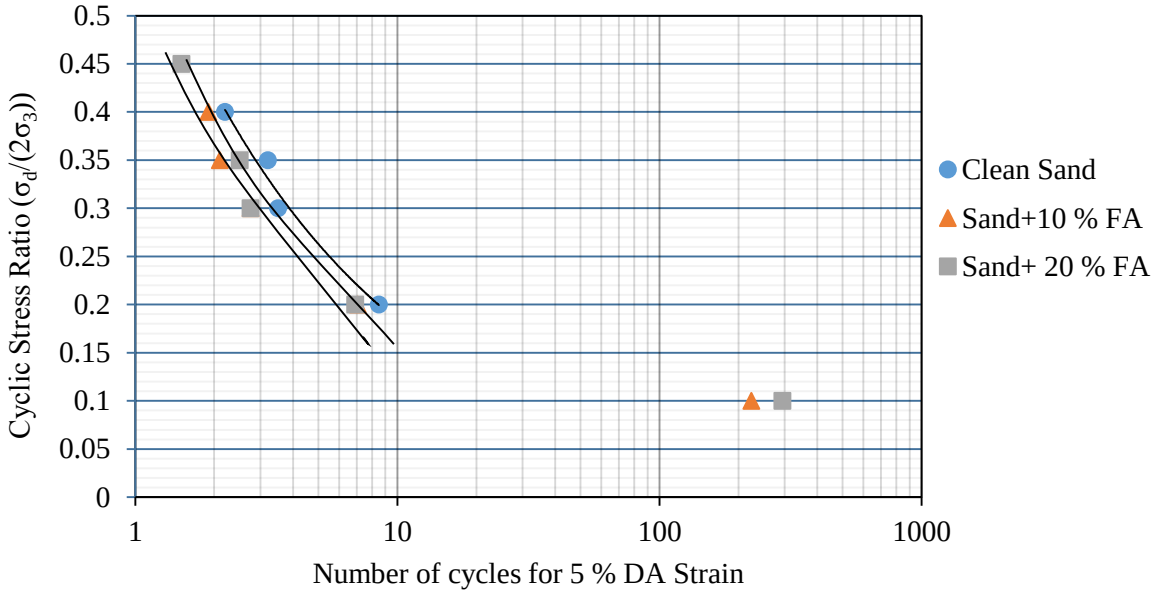

Figure 4-44 Liquefaction resistance of sand containing various percentages of fly ash at 15-psi effective confining pressure in terms of deformation.

4.9 Liquefaction resistance of sand-fly ash mixtures at higher percentages of fly ash

The CSR required for causing initial liquefaction of clean sand, sand containing 10 and 20 % fly ash and pure fly ash samples in 10 cycles were determined from Figure 4-36 for the effective confining pressure of 5 psi. For higher percentages of fly ash (25, 30 and 50 %) results of (Regmi, 2014) are included here. Similarly, CSR required for the initial liquefaction of clean sand, sand containing 10 and 20 % fly ash samples in 10 cycles were determined for effective confining pressure of 10 and 15 psi from Figure 4-39 and Figure 4-42, respectively. For sand containing 25, 30, and 50 % fly ash, CSR are taken from (Regmi, 2014). The CSR values causing intial liquefaction in 10 cycles are plotted against percentages of fly ash for confining pressures of 5, 10, and 15 psi as shown in Figure 4-45. It can be observed from Figure 4-45 that, the addition of 10 % fly ash decreases the liquefaction resistance slightly. Further, addition of fly ash beyond 10 %, increases the liquefaction resistance and attains a maximum value for a fly ash contents of 25. The liquefaction resistance is seen to decrease when the fly ash content exceeds about 25 %.

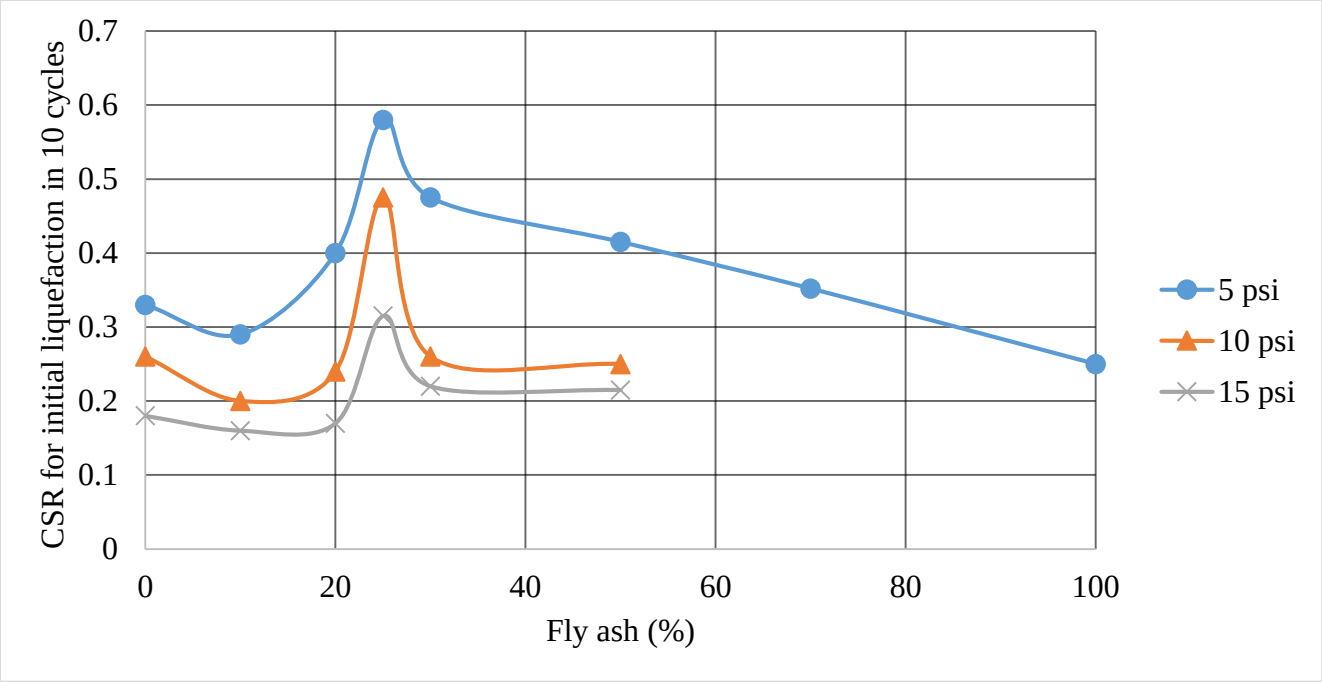

Figure 4-45 Variation in liquefaction resistance (initial liquefaction) of sand with fly ash contents at confining pressure of 5, 10 and 15 psi.

Similarly, liquefaction resistance is also compared in terms of CSR required to develop 2.5 % and 5 % DA strain. The CSR values required for 2.5 % DA strain in 10 cycles are taken from Figure 4-37, Figure 4-40, and Figure 4-43 for effective confining pressures of 5, 10, and 15 psi, respectively. Similarly CSR required for 5 % DA strain in 10 cycles are taken from Figure 4-38, Figure 4-41, and Figure 4-44 for effective confining pressures of 5, 10 and 15 psi. The data for sand with 25, 30 and 50 % fly ash are taken from (Regmi, 2014). The CSR required for 2.5 % and 5 % DA strain in 10 cycles are plotted with fly ash contents as shown in Figure 4-46 and Figure 4-47. The trend of results is similar to what has been discussed earlier about liquefaction defined in terms of $u = \overline{\sigma_3}$ condition.

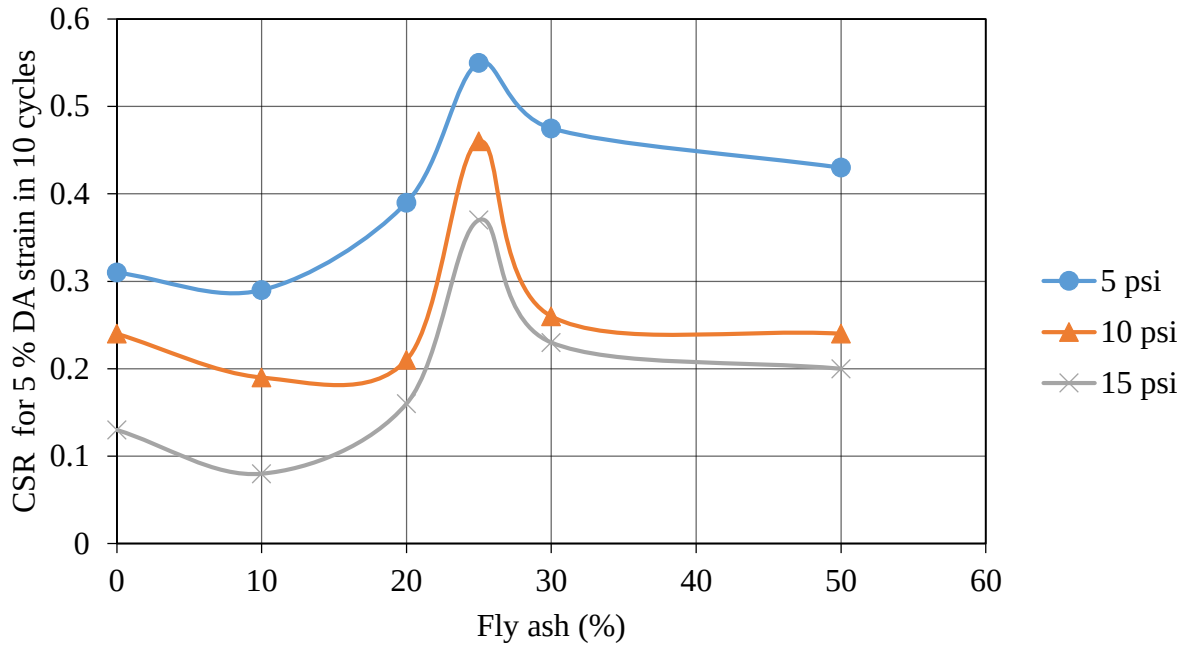

Figure 4-46 Variation in liquefaction resistance (2.5 % DA strain) of sand with fly ash contents at confining pressure of 5, 10 and 15 psi.

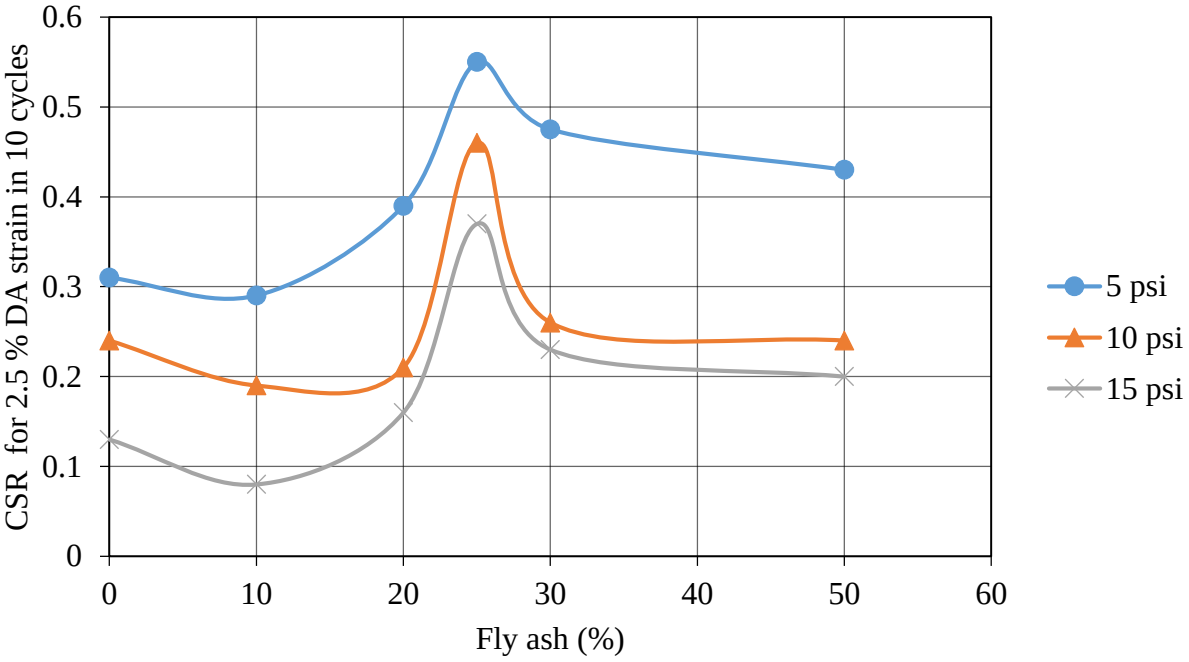

Figure 4-47 Variation in liquefaction resistance (5 % DA strain) of sand with fly ash contents at confining pressure of 5, 10 and 15 psi.

4.10 Modulus of elasticity

The same test results as used for the evaluation of initial liquefaction are also used for the determination of the modulus of elasticity. The modulus of elasticity obtained from the cyclic triaxial software is used for the analysis. The software calculates the modulus of elasticity based on double amplitude load applied and resulted double amplitude deformation during cyclic loading, according to ASTM D 3999. It calculates the modulus of elasticity for each cycle and plots the graph against axial strain.

4.10.1 Effect of confining pressure on modulus of elasticty

The effect of confining pressure on modulus of elasticity was investigated for clean sand and sand containing 10 and 20 % fly ash. The modulus of elasticity obtained from the test conducted at various CSR values for each confining pressure were combined and plotted against axial strain. It resulted three sets of curves, one for each confining pressures. Figure 4-48 to Figure 4-50 show the effects of confining pressure for sand containing various percentages of fly ash.

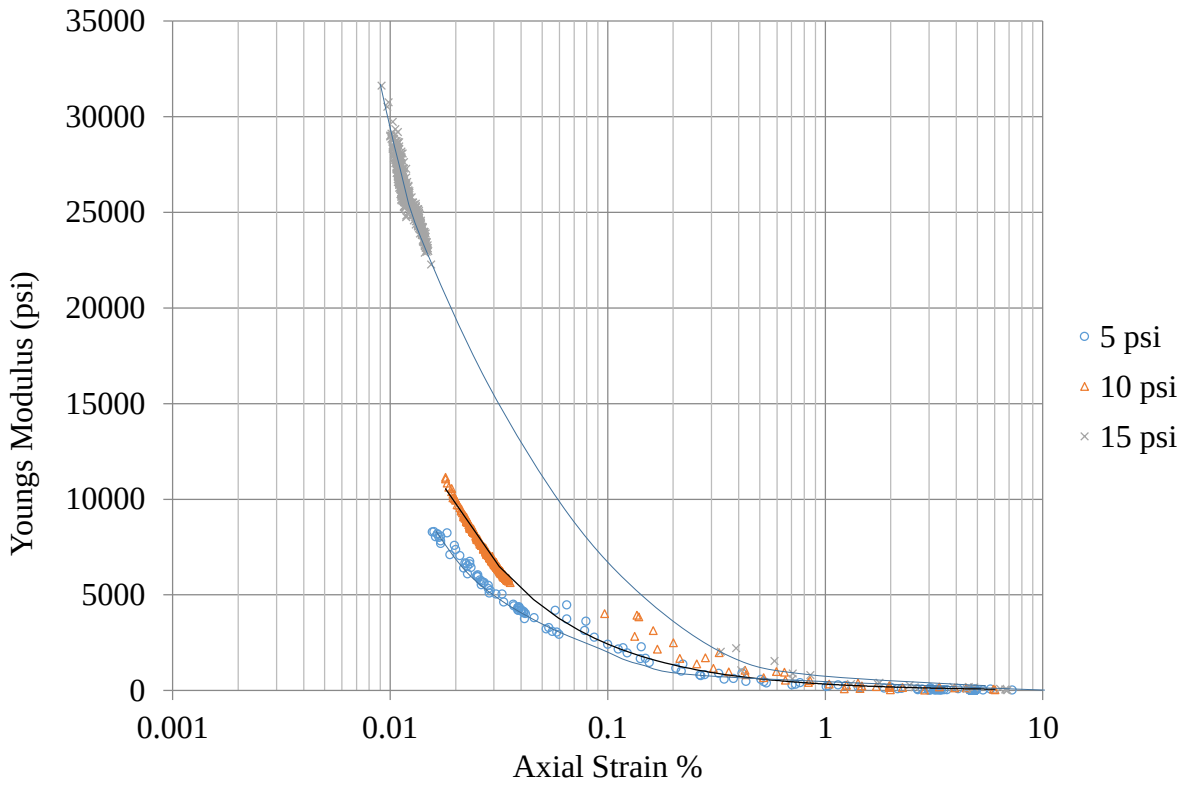

Figure 4-48 Variation of Youngs modulus of clean sand at various confining pressures.

Figure 4-48 shows the variation of modulus of elasticity of clean sand with axial strain at various confining pressures. It is clear that, the modulus of elasticity of clean sand is higher at lower strain. During cyclic loading, with a successive increase in axial strain, the modulus of elasticity decreases rapidly for all confining pressures. It is noted that, the modulus of elasticity is very small after 1 % axial strain. On the other hand, the Youngs modulus (E) is influenced by confining pressure below 1 % axial strain. It can be observed that, the Youngs modulus increases as the confining pressure increases. Further, increase in confining pressure from 10 to 15 psi resulted higher increase in Youngs modulus (E) in comparison to change in confining pressure

from 5 to 10 psi. However, at higher strain above 1 % axial strain, the modulus of elasticity is almost similar irrespective of confining pressure.

Similar plots were developed for sand containing 10 % fly ash. Figure 4-49 presents the effects of confining pressure on Youngs modulus for sand containing 10 % fly ash. Similar to clean sand, the Youngs modulus (E) is found to decrease with successive increase in axial strain. It can be noticed that, an increase in confining pressure resulted in higher Youngs modulus for the axial strain below 0.2 %. The Youngs modulus is highest at 15 psi effective confining pressure and lowest at 5 psi effective confining pressure. However, the curves for 5, 10 and 15 psi effective confining pressure tend to converge after 0.2 % axial strain.

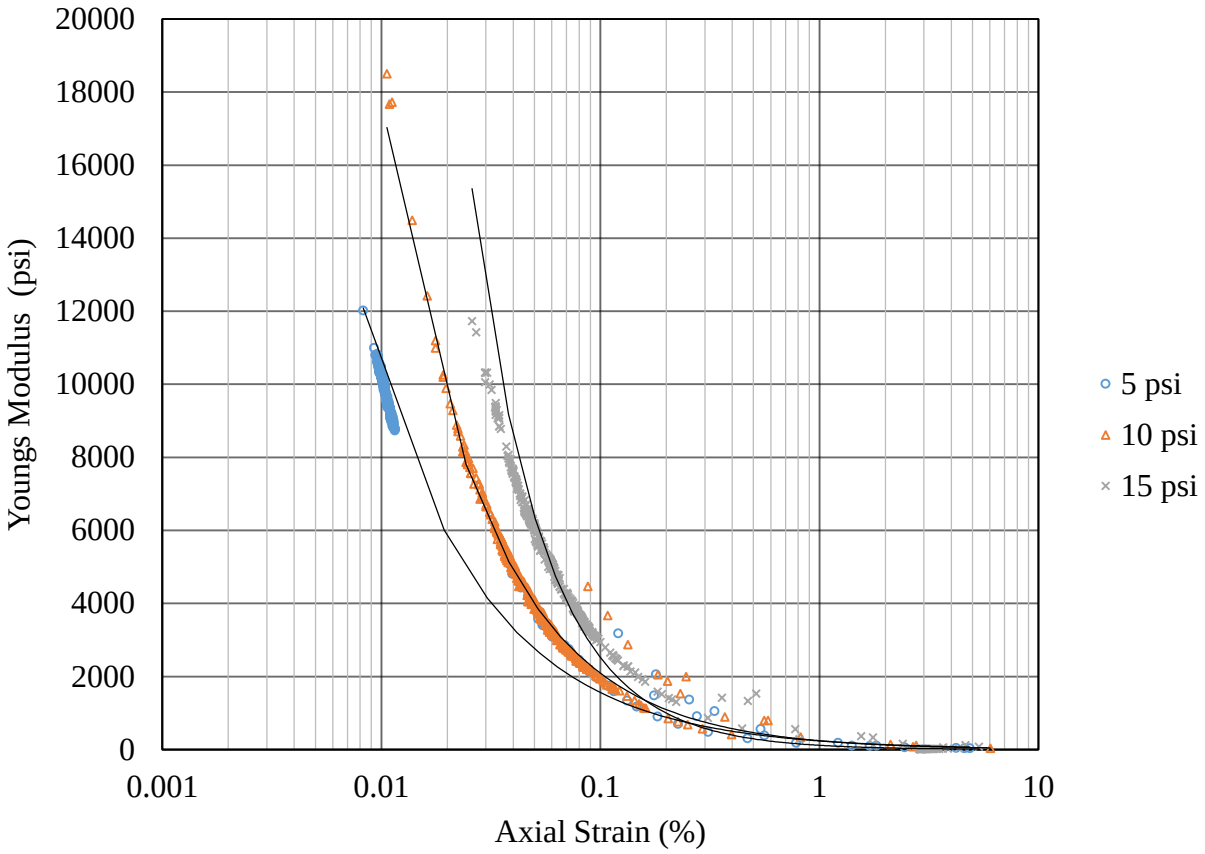

Figure 4-49 Variation of Youngs modulus of sand containing 10 % fly ash at various confining pressures.

The variation of Youngs modulus (E) for sand containing 20 % fly ash with axial strain at various confining pressures is shown in Figure 4-50. Each curve shows a continuous decrease of Youngs modulus (E) as the axial strain increases. For all confining pressures, it is negligible after 1 % axial strain. Similar to clean sand and sand containing 10 and 20 % fly ash, increase in confining pressure shifted the curve upwards at lower strain. On the other hand, for higher strain, the curve tends to converge.

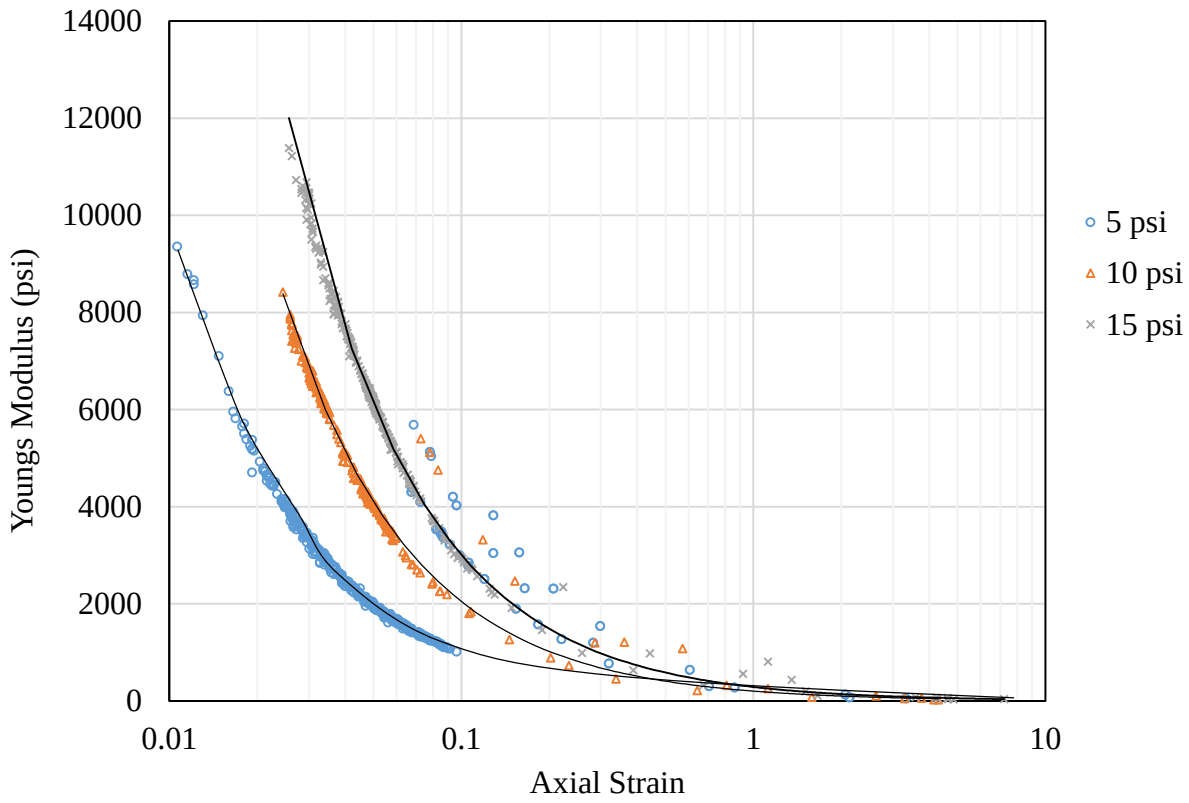

Figure 4-50 Variation of Youngs modulus of sand containing 20 % fly ash at various confining pressures.

4.10.2 Effects of fly ash addition on Youngs modulus

For the comparison of effects of addition of fly ash to sand on Youngs modulus (E) , the test results on various percentages of fly ash contents were combined for each confining pressure. Figure 4-51 to Figure 4-53 presents the comaprson of Youngs modulus (E) at 5, 10 and 15 psi effective confining pressures.

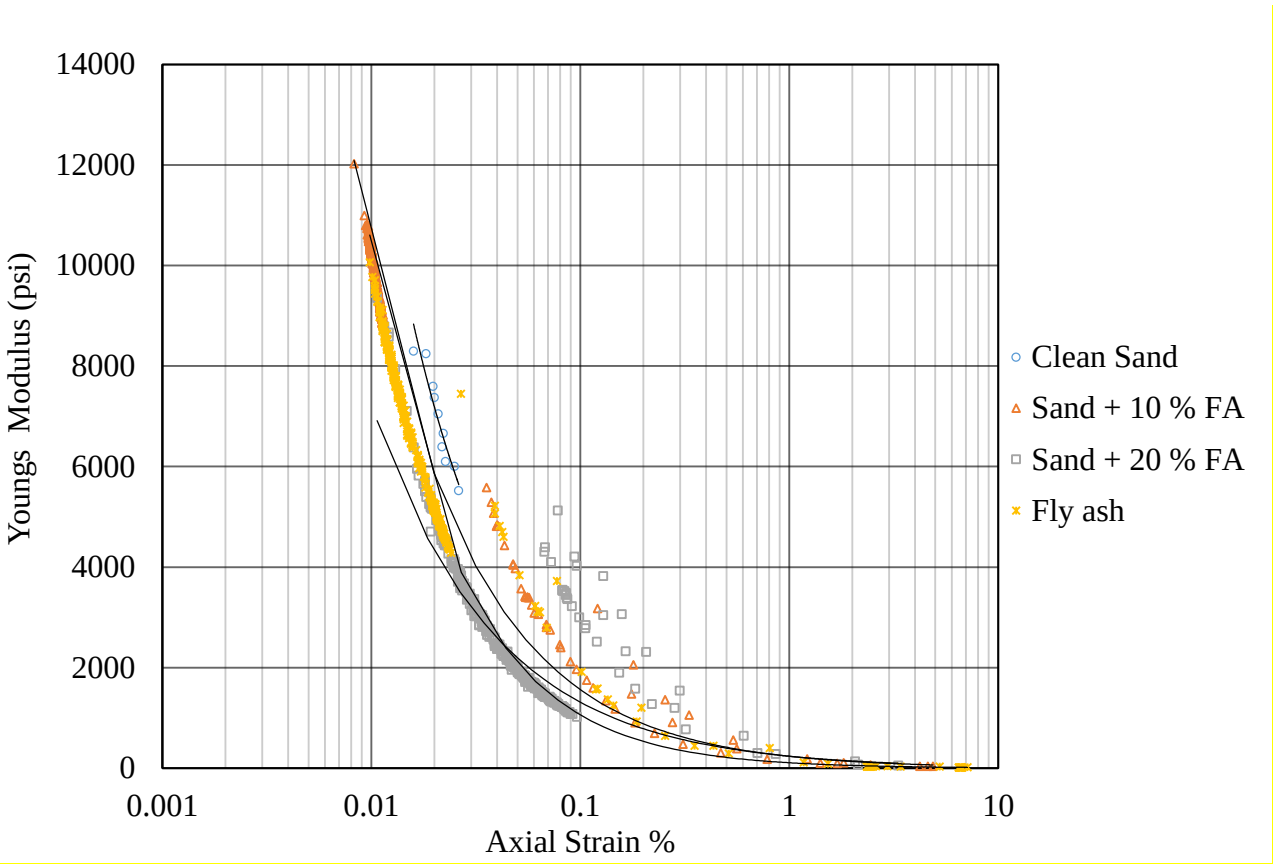

Figure 4-51 Variation of Youngs modulus with fly ash contents at 5 psi effective confining pressure.

The variation of Youngs modulus with fly ash content is shown in Figure 4-51. It presents the Youngs modulus of clean sand, sand containing 10 and 20 % fly ash and fly ash. The figure does not clearly indicate the variation of Youngs modulus with fly ash contents. The Youngs modulus of various mixtures are overlapped.

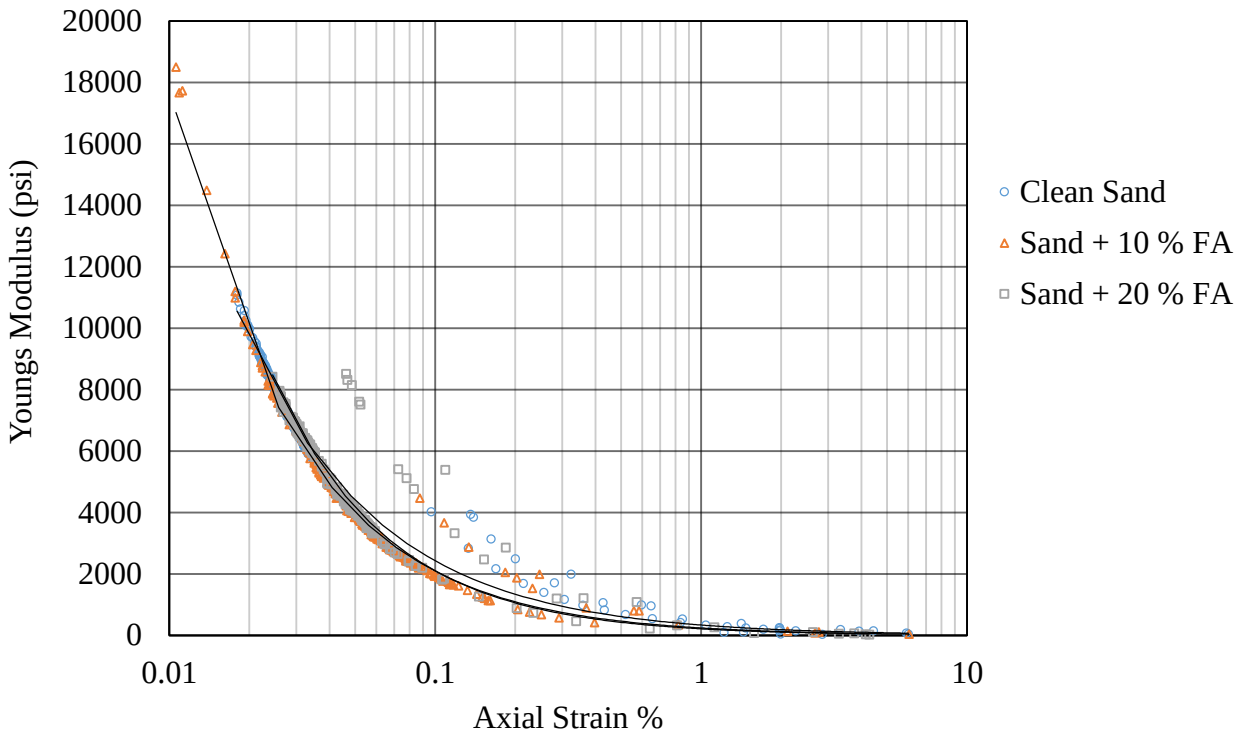

Figure 4-52 Variation of Youngs modulus with fly ash contents at 10 psi effective confining pressure.

The variation of the Youngs modulus at 10 psi effective confining pressure with various fly ash contents are plotted against axial strain as shown in Figure 4-52. It can be observed that, the Youngs modulus for clean sand, sand containing 10 and 20 % fly ash are overlapped at various axial strain. It does not show the distinct variation in Youngs modulus with variation of fly ash contents. Hence, Youngs modulus is less sensitive to fly ash contents based on results of this research.

In Figure 4-53 the effect of addition of fly ash at 15 psi effective confining pressure is examined. Similar to effective confining pressure of 5 and 10 psi, significant variation of Youngs modulus is not observed with fly ash content. The Youngs modulus of clean sand, sand containing 10 and 20 % fly ash are overlapped.

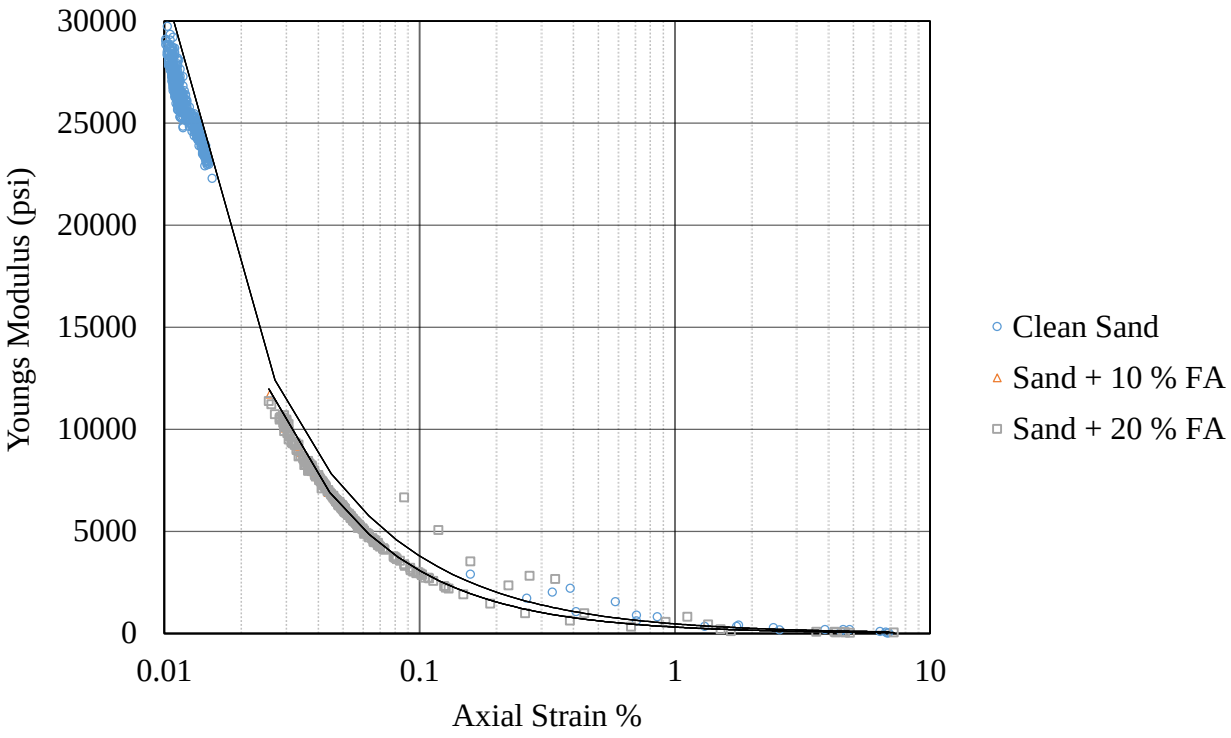

Figure 4-53 Variation of Youngs modulus with fly ash contents at 15 psi effective confining pressure.

Above results indicates that, the Youngs modulus is almost similar for all fly ash contents at various confining pressures. Hence, it can be concluded that, the Youngs modulus is less sensitive with variation of fly ash contents based on the results of this research.

4.11 Damping ratio

Similar to Youngs modulus, the results from the tests conducted at various confining pressures and CSR are utilized for the determination of damping ratio. The Cyclic Triaxial Software automatically calculates the damping ratio at each cycle. It uses the ASTM D 3999 for the calculation of damping ratio.

4.11.1 Effect of confining pressure on damping ratio

The strain developed in the samples are lower at CSR 0.1 and 0.2 and higher strains were developed at higher CSR. The combination of test results of all CSR values at a given confining pressure generates the curve of damping ratio at wide range of axial strain. Similar to the Youngs modulus (E), the damping ratio obtained at various CSR values on given confining pressure used in the tests are combined. The plotting of the damping ratio at three different confining pressure results in three sets of curves. The variation of the damping ratio are shown in Figure 4-54 to Figure 4-56.

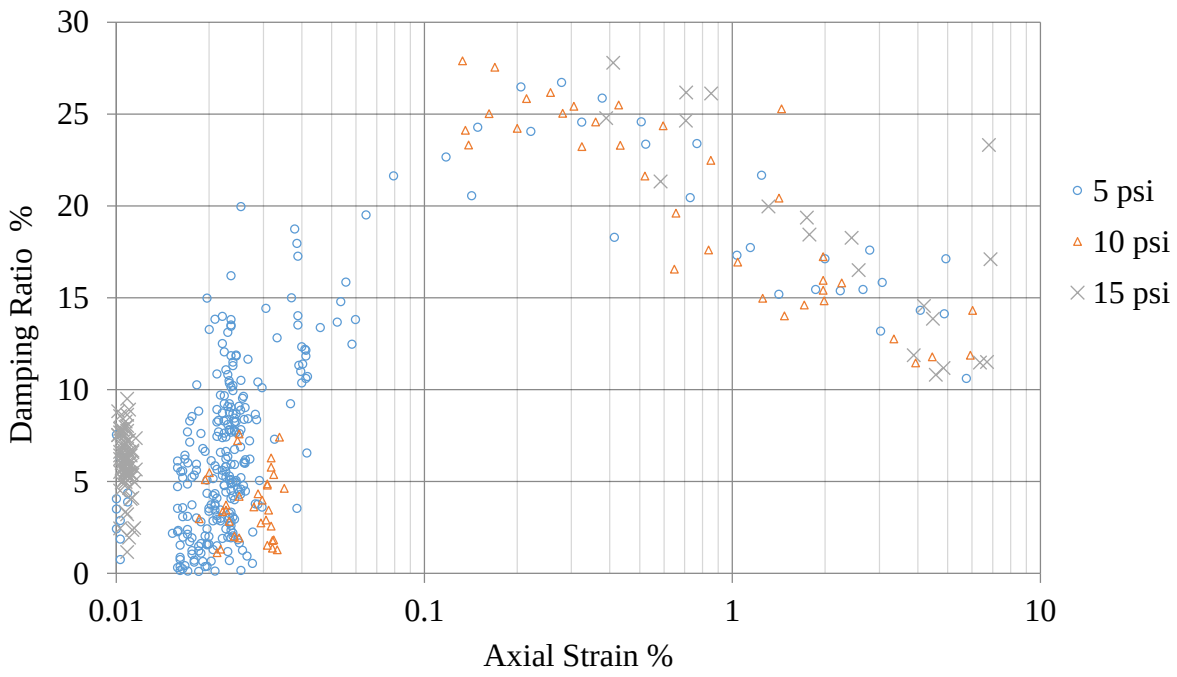

Figure 4-54 Variation of damping ratio of clean sand with axial strain at various confining pressure.

The variation of the damping ratio of clean sand with axial strain and confining pressures is shown in Figure 4-54. The graph is plotted based on the tests conducted on clean sand at 5, 10 and 15 psi confining pressures and CSR ranging from 0.1 to 0.5. Each curves shows a continuous

increase of damping ratio as the axial strain increases. After axial strain of 0.2 %, it remained constant for a certain axial strain and started to decrease slowly with increase in axial strain. However, distinct effect was not observed for the variation of confining pressure, i.e. the damping ratio at 5, 10 and 15 psi confining pressure was not much different.

The variation of damping ratio with confining pressure for sand containing 10 and 20 % fly ash is shown in Figure 4-55 and Figure 4-56. Similar to clean sand, it does not show distinct variation of damping ratio with confining pressures. For all confining pressures, the damping ratio increses with an increase in axial strain up to certain strain level. After that, it remains constant for certain axial strain range and then it decreases somewhat.

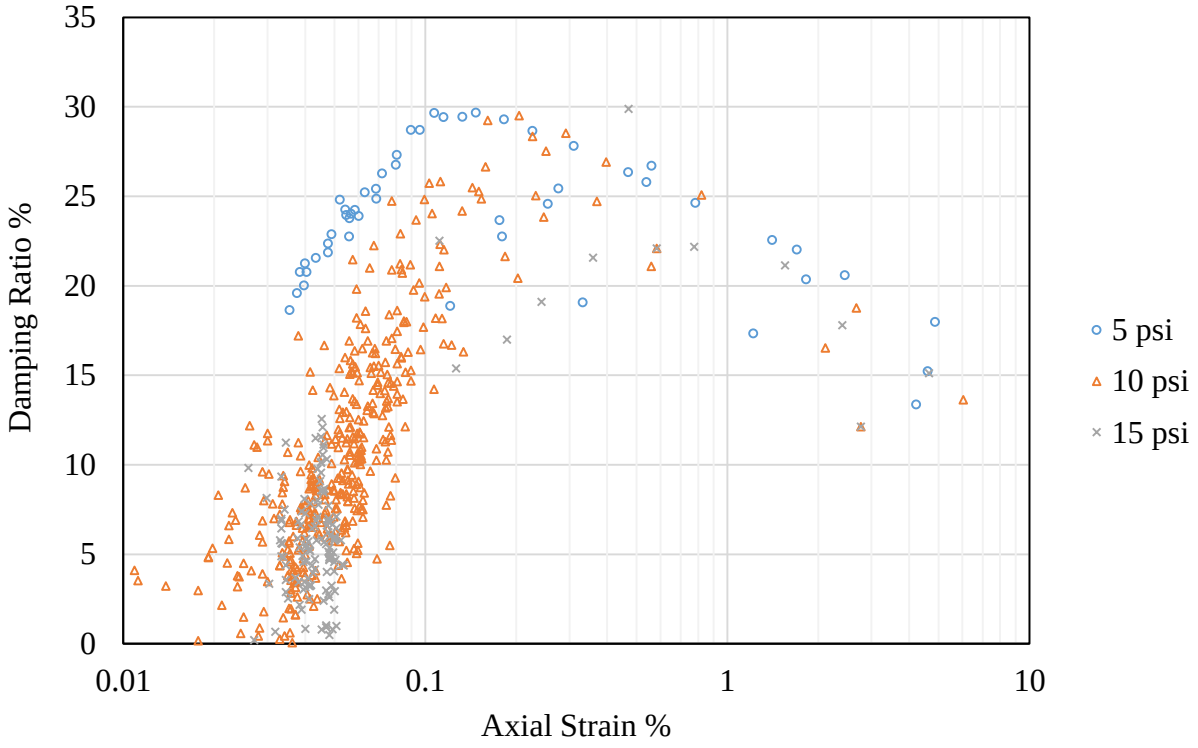

Figure 4-55 Variation of damping fratio of sand containing 10 % fly ash at various confining pressures.

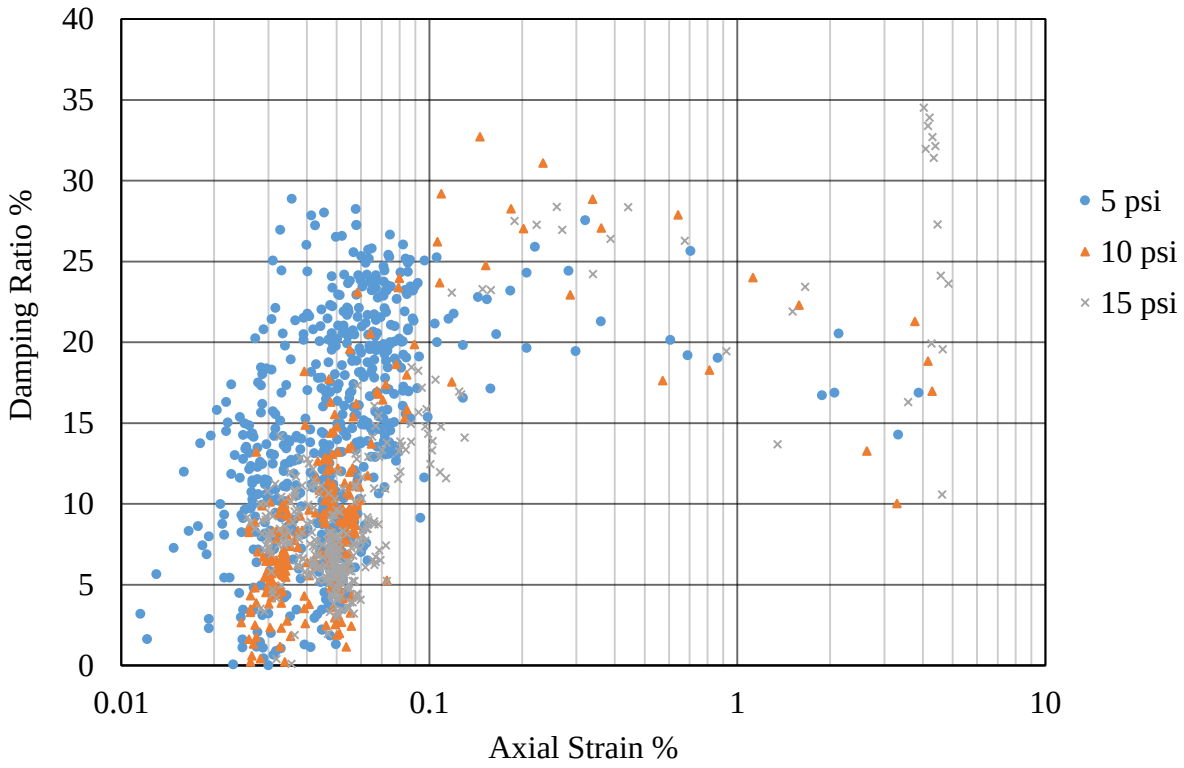

Figure 4-56 Variation of damping ratio with axial strain of sand containing 20 % fly ash at various confining pressures.

4.11.2 Effects of fly ash on damping ratio

In order to study the effects of addition of fly ash on the damping ratio of sand, the damping ratio of the different samples at certain confining pressure are plotted against the axial strain. So it is possible to compare the variation of the damping ratio with clean sand, sand containing 10 and 20 % fly ash at certain confining pressure. Three different plots are generated at the effective confining pressure 5, 10 and 15 psi as shown from Figure 4-57 to Figure 4-59. The variation of the damping ratio with clean sand, sand containing 10 and 20 % fly ash and fly ash is shown for 5 psi effective confining pressure in Figure 4-57. It can be observed that, the damping ratio of fly ash is somewhat higher at lower strain, however, it does not show a clear trend at higher strain.

Similarly, significant difference of damping ratio cannot be observed for the clean sand and sand containing 10 and 20 % fly ash for both lower strain as well as higher strain. The plots of the damping ratio at 10 and 15 psi effective confining pressure also does not show clear variation with various fly ash content. The damping ratio of clean sand, sand containing 10 and 20 % fly ash is overlapped.

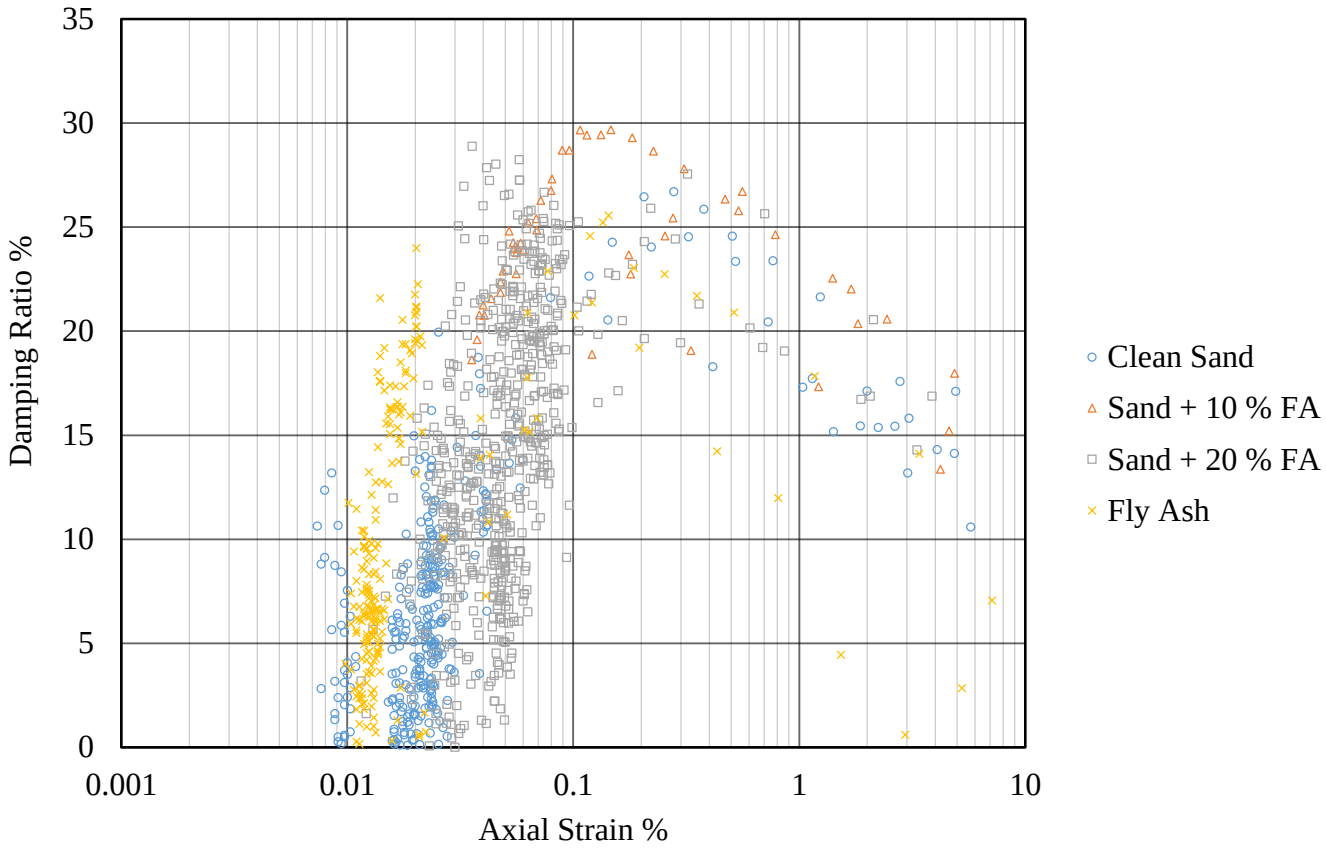

Figure 4-57 Variation of damping ratio with various fly ash contents at 5 psi effective confining pressure.

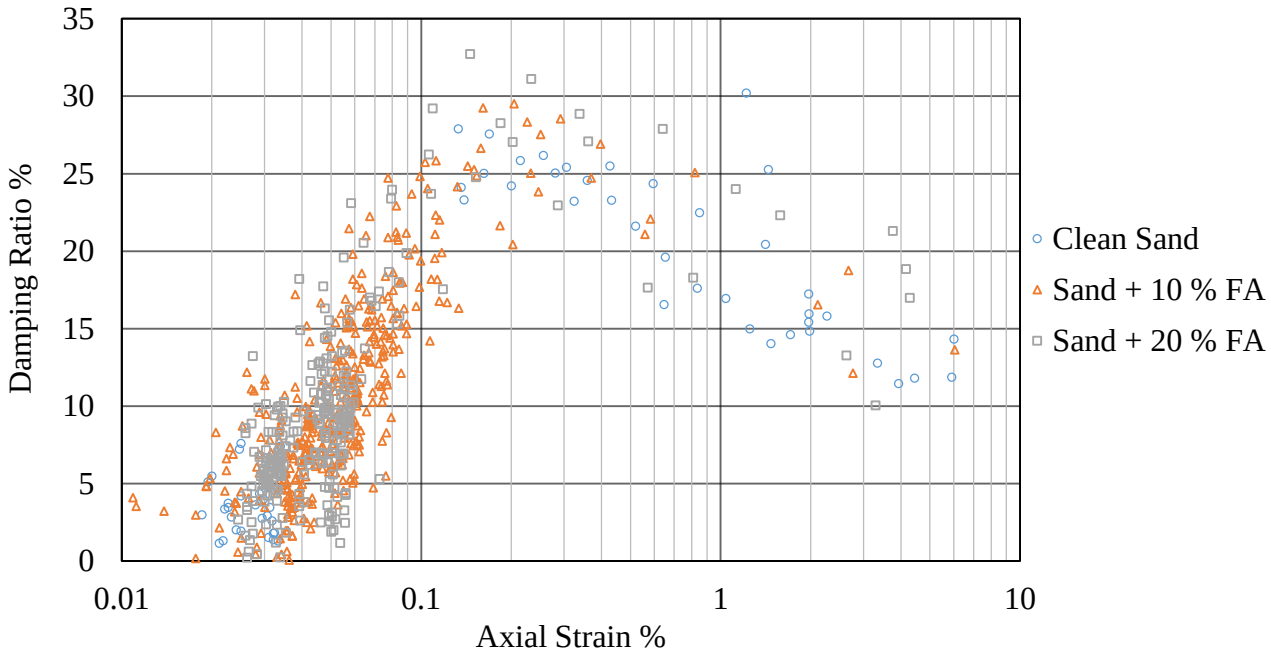

Figure 4- 58 Variation of damping ratio with various fly ash contents at 10 psi effective confining pressure.

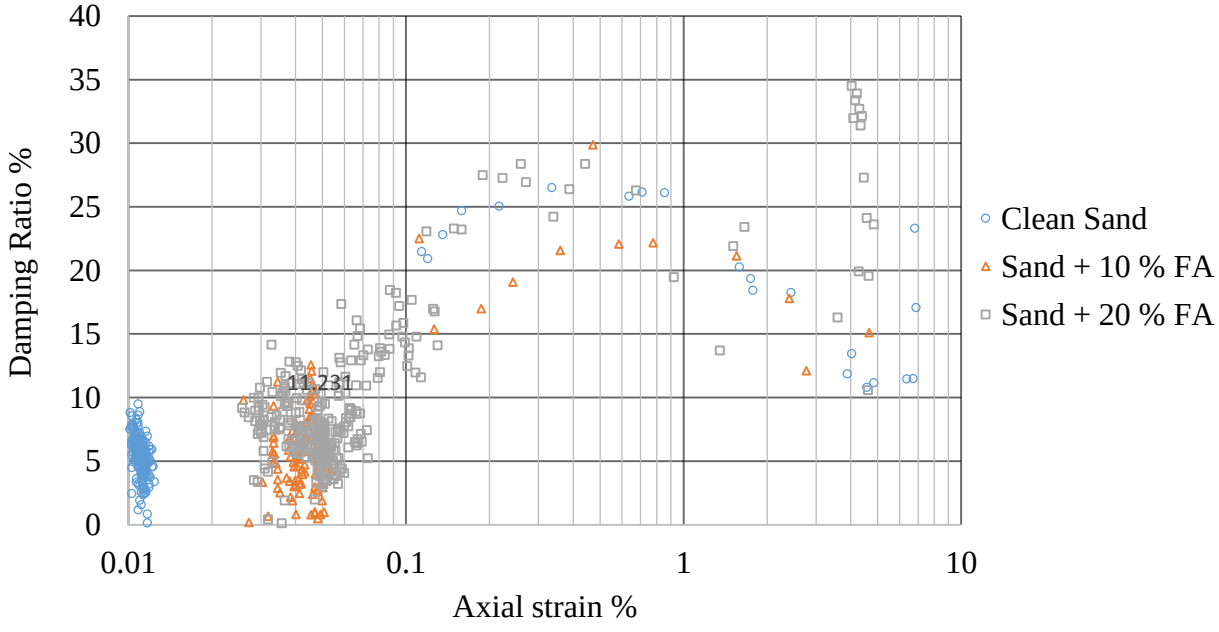

Figure 4-59 Variation of damping ratio with various fly ash contents at 15 psi effective confining pressures.

4.12 Discussion

The clean sand samples did not liquefy at lower CSR values. For example, the clean sand samples consolidated at an initial effective confining pressure of 5 psi did not liquefyat CSR= 0.1 and 0.2. On consolidating the clean sand sample with effective confining pressures of 10 and 15 psi samples did not liquefy at CSR=0.1. During the application of higher CSR, the clean sand samples liquefied in lesser number of stress cycles. For example, the clean sand sample consolidated at an initial effective confining pressure of 15 psi liquefied at 3 cycles during the application of cyclic shear stress corresponding to CSR=0.3. Similarly, the sand samples containing 10 and 20 % fly ash did not liquefy at a confining pressure of 5 psi and CSR=0.1. The sand containing 10 % fly ash did not liquefy at confining pressure of 10 psi and CSR=0.1. Distinct behavior in pore water pressure build up can be observed with the variation of fly ash contents. The pore water pressure build up starts from the beginning of the loading in case of clean sand as observed in Figure 4-1 and there is gradual increase of pore water pressure. In case of sand containing 10 % fly ash, the pore water pressure build started slighltly later and it started to increase rapidly on further application of cyclic load, which is shown in Figure 4-9. However, pore water pressure build up starts later in the case of sand containing 20 % fly ash and the sample liquefied quickly after pore water pressure developed (Figure 4-17). Although, the specimen liquefied in more cycles in comparison to clean sand and sand containing 10 % fly ash, the liquefaction is faster after the initiation of development of pore water pressure. The pore water pressure build up in case of pure fly ash sample started from the first cycle of load application. It increased continiously and liquefied in five and half cycles as shown in Figure 4-25. It can be noticed that liquefaction in pure fly ash sample is abrupt. The tests conducted at

other CSR values also show the similar behavior. Hence, it can be concluded that, at higher fly ash content, the liquefaction occurs instantly.

Distinct deformation behavior in clean sand, sand containing 10 and 20 % fly ash can be observed. For a clean sand sample as shown in Figure 4-2, the sample started to deform slowly after third cycle and gradually increased and exceeded 5 % axial strain at 12 cycles. In the case of sand sample containing 10 % fly ash, there was no deformation until third cycle as shown in Figure 4-10. After that, the sample deformed slowly in between third and fourth cycles of stress application, which can be assumed as transistion from no deformation to rapid deformation. After that, large deformation was observed. However, for a sand sample containing 20 % fly ash (Figure 4-18), the sample was not deformed till 20 cycles after that deformation was abrupt. In case of pure fly ash (Figure 4-26), the deformation started after 2.5 cycles, once it started the excessive deformation was observed. If we compare the deformation behavior of all mixture, it can be noticed that, on increasing the fly ash content the samples deforms abruptly. Similar observations were made for other CSR values. Hence, it can be concluded that, elastic deformation occurs in clean sand. However, on increasing the percentage of fly ash, the brittleness of sample increases.

For all type of samples tested, it was observed that, the cyclic shear stress required for initial liquefaction and development of 2.5 and 5 % DA strain at any number of stress cycles increases with an increase in confining pressure. Seed and Lee (1966) also observed similar effects of confining pressure and cyclic laod. Significant variation of reduction in CSR required for initial liquefaction on raising the confining pressure was observed.

As the confining pressure was increased, the CSR required to induce initial liquefaction and 2.5 , 5 % DA strain at any stress cycles was found to decrease. The number of cycles required for the

initial liquefaction at effective confining pressure of 5, 10 and 15 psi for CSR=0.3 is shown in Table 4-4. The data for CSR=0.3 is choosen because it gives more or less average for entire CSR- Number of Cycles curves. The reduction of number of cycles required for initial liquefaction on increasing confining pressure during the application of cyclic shear stress corresponding to CSR=0.3, is calculated and shown in Table 4-5. It can be seen that, the reduction in number of cycles for initial liquefaction increases with the addition of fly ash content, on increasing the confining pressure from 5 to 10 psi. In addition, the reduction of number of cycles for the initial liquefaction for samples of clean sand, sand containing 10 and 20 % fly ash are almost similar on increase in the confining pressure from 10 to 15 psi. It can be clearly observed that, the reduction in number of cycles for initial liquefaction on increasing the confining pressure from 10 to 15 psi is signifiacantly lower than that of increasing the confining pressure from 5 to 10 psi for tests at all fly ash contents used in this research. It is also noted that, the number of cycles required for initial liquefaction at higher CSR for the samples consolidated at 10 and 15 psi are almost similar.

Table 4-4: Number of cycles for intial liquefaction of clean sand, sand containing 10 and 20 % fly ash at effective confining pressures of 5, 10 and 15 psi.

Confining Pressure	Number of Cycles for initial liquefaction at CSR = 0.3		
	Clean Sand	Sand+10 % FA	Sand+20 % FA
5 psi	11.6	10.2	23.0
10 psi	7.0	3.5	5.5
15 psi	4.5	2.5	3.5

Table 4-5: Reduction of number of cycles required for intial liquefaction at CSR= 0.3 of samples of sand containing (0,10, and 20 % fly ash) on increasing confining pressure.

Increase in confining pressure	Reduction of number of cycles required for initial liquefaction at CSR = 0.3		
	Clean Sand	Sand+10 % FA	Sand+20 % FA
5 to 10 psi	40	66	76
10 to 15 psi	36	29	36

In addition, it is seen that, number of stress cycles required for initial liquefaction, development of 2.5 and 5 % DA strain in a sample consolidated at any effective confining pressure was found to decrease with an increase in cyclic load. The rate of reduction of number of cycles with an increase in CSR was also found to depend upon the fly ash contents.

Table 4-6 Reduction of number of stress cycles for the initial liquefaction of samples of sand containing (0, 10, and 20 % fly ash) on raising the CSR from 0.3 to 0.4.

Confining Pressure	Number of cycles for initial liquefaction for different samples						Reduction of number of cycles on increasing CSR from 0.3 to 0.4		
	Clean Sand		Sand+10 % FA		Sand+20 % FA		Clean Sand	Sand+10 % FA	Sand+20 % FA
	CSR= 0.3	CSR= 0.4	CSR= 0.3	CSR= 0.4	CSR= 0.3	CSR= 0.4			
5 psi	11.6	6.5	10.2	4.54	23.0	10.0	5.1	5.66	13.0
10 psi	7.0	3.5	3.5	2.2	5.5	2.5	3.5	1.3	3.0
15 psi	4.5	3.0	2.5	2.0	3.5	2.2	1.5	0.5	1.3

Table 4-6 presents the reduction of number of cycles for the initial liquefaction of sand containing (0, 10 and 20 % fly ash) on increasing the CSR from 0.3 to 0.4. It can be observed that as confining pressure increases, reduction of number of cycles with an increase in CSR decreases. For example, the reduction of number of cycles for initial liquefaction of the clean

sand sample consolidated at effective confining pressure of 5, 10 and 15 psi, on increasing CSR from 0.3 to 0.4 are 5.1, 3.5 and 1.5, respectively.

Table 4-7 Number of cycles for the development of 2.5 % DA strain at the effective confining pressures of 5, 10, and 15 psi for CSR=0.3.

Confining pressure	Number of cycles required to induce 2.5 % DA strain at CSR = 0.3		
	Clean Sand	Sand+10 % FA	Sand+20 % FA
5 psi	11	8	23
10 psi	7.5	2.75	5.5
15 psi	3.5	1.75	3.5

Table 4-8 Reduction of number of cycles required to induce 2.5 % DA strain at CSR=0.3 in samples of sand containing (0, 10, and 20 % fly ash) on increasing confining pressure.

Increase in confining pressure	Reduction of number of cycles (%) required to induce 2.5 % DA strain		
	Clean Sand	Sand+10 % FA	Sand+20 % FA
5 to 10 psi	32	66	80
10 to 15 psi	53	36	44

Table 4-9 : Number of cycles for the development of 2.5 % DA strain at the effective confining pressures of 5, 10, and 15 psi for CSR=0.3.

Confining pressure	Number of cycles required to induce 5 % DA strain at CSR=0.3		
	Clean Sand	Sand+10 % FA	Sand+20 % FA
5 psi	14	12	22.2
10 psi	8.5	3.5	4.75
15 psi	3.5	2.75	2.75

Table 4-10 Reduction of number of cycles (%) required to induce 5 % DA strain in samples of sand containing (0, 10, and 20 % fly ash) on increasing confining pressure for CSR=0.3.

Increase in confining pressure	Reduction of number of cycles (%) required to induce 5 % DA strain		
	Clean Sand	Sand+10 % FA	Sand+20 % FA
5 to 10 psi	39	71	79
10 to 15 psi	59	21	42

The number of cycles required to induce 2.5 and 5 % DA strain in samples of sand containing (0, 10 and 20 %) fly ash at CSR=0.3 on increasing the confining pressure is shown in Table 4-7 and Table 4-9, respectively. The reduction of number of cycles (%) required to induce 2.5 % and 5 % DA strain are calculated and presented in Table 4-8 and Table 4-10, respectively. As in the case of initial liquefaction, it can be seen that, reduction of number of cycles (%) required to induce 2.5 % and 5 % in samples on increasing confining pressure from 5 to 10 psi effective confining pressure increases, with an increase in fly ash contents. On the other hand, on increasing the confining pressure from 10 to 15 psi, reduction of number of cycles at CSR=0.3 decreases initially with an addition of 10 % fly ash and then increases with an addition of 20 % fly ash. For all the samples containing various fly ash contents used in this research, a reduction of number of cycles at CSR=0.3 on raising the confining pressure from 5 to 10 psi is higher than that of on increasing from 10 to 15 psi..

Fly ash was found to liquefy earlier than clean sand. The mean grain diameters (D_{50}) for sand is 0.7 mm and d_{50} for fly ash is 0.015 mm. The type F fly ash was used in this research, which does not possess cementing properties. Because of non-plastic behavior of fly ash and smaller particle size than clean sand, the fly ash possesses the lower liquefaction resistance.

For all confining pressures, liquefaction resistance was found to decrease with an addition of 10 % fly ash. According to Thevanayagam (1998), Thevanayagam et al. (2000) and Thevanayagam

(2007), the fines confine in the voids of sand particles, if fines are lesser than threshold fines content. The maximum and minimum void ratio curve as shown in Figure 4-31, at various fly ash contents indicate that, the threshold fine content lies after 20 %. Further, if the mean grain size ratio (D_{50} / d_{50}) for sand to fines is greater than 6.5, the particles can move within the voids of sand (Thevanayagam et al., 2000). If particles move within voids during cyclic loading, it may not participate in force chain and cannot transfer the forces in between the particles effectively. In our case, the mean grain size ratio (D_{50} / d_{50}) for sand to fly ash is 46.67. Therefore, the fly ash particles may be moving during cyclic loading. As a result, the liquefaction resistance of sand containing 10 % fly ash was lower clean sand.

In case of sample consolidated at effective confining pressure of 5 psi, an addition of 20 % fly ash has higher liquefaction resistance in comparison to clean sand and sand containing 10 % fly ash. As 20 % fly ash is in the range of threshold fine content, the fly ash can play effective role in force chain. It can transfer the cyclic load to the grains of sand. As a result, liquefaction resistance increased.

However, liquefaction resistance of sand containing 20 % fly ash was lower than clean sand and higher than sand containing 10 % fly ash, when it was consolidated at effective confining pressures of 10 and 15-psi. Sand containing 20 % fly ash has more fly ash to fill the voids between the sand in comparison to sand containing 10 % fly ash. The sand containing 20 % fly ash can have better participation in force chain than sand containing 10 % fly ash. Therefore, the liquefaction resistance increased at 20 % fly ash content in comparison to sand containing 10 % fly ash. The shear stress induced increases with an increase in confining pressure. Hence, for a given CSR, the shear stress applied during cyclic loading was higher at 10 and 15-psi effective confining pressure. Because of higher shear stress, the fly ash particles may move within the

voids of sand, which is the reason for the lower liquefaction resistance of sand containing 20 % fly ash in comparison to clean sand at $\overline{\sigma_3}$ = 10 and 15 psi. However, movement of particles may be lower in case of sand containing 20 % fly ash in comparison to sand containing 10 % fly ash. It is because of higher fly ash content to fill the voids. Moreover, the fly ash content is less sensitive to liquefaction resistance, when the sample was consolidated at effective confining pressure of 15 psi. It may be due to application of higher shear stress to the sample.

On combining the results of (Regmi, 2014) for 25, 30 and 50 % fly ash, it was seen that, the liquefaction resistance increases up to 25 % fly ash, after that it decreases. At 25 % fly ash, the fly ash particles fills the voids of sand and the dry density is highest at this mixture among all combination of sand-fly ash mixtures. So fly ash particles actively participate in force chain, which may be the reason of highest liquefaction resistance at 25 % fly ash content. On higher percentages of fly ash above 25 %, fly ash particles surrounds sand particles and sand particles may act as separating element. So, the liquefaction resistance sand-fly ash mixture depends upon the liquefaction resistance of fly ash. Therefore, liquefaction resistance of fly ash is lower, above 25 % fly ash liquefaction resistance decreases.

The results of this study can be compared with the published results of several other researchers. The properties of sands and fines used by various researchers are compared with this research in Table 4-11. Singh (1996) observed decreasing trends of liquefaction resistance with an increase in silt contents. The results of this research for 10 and 15 psi effective confining pressures are similar to those of Singh (1996). They have also used the effective confining pressure around 100 kPa (14.5 psi). However, drastic decrease in liquefaction resistance may be because of variation in backpressure used for saturation. The details of their findings were presented in

Chapter 2. No information was provided regarding the mean grain sizes of fines and threshold fines contents of sand-fines mixture.

Further, Sadek and Saleh (2007) also used relative density as a basis of comparison. They have used carbonaceous fines as described in Chapter 2. The liquefaction resistance increased up to threshold fine content 10 %, after that it decreased. On the other hand, in our research, the liquefaction resistance was decreased at 10 % fly ash content and after that it increased. The continuous increase in the liquefaction resistance may be because of, the particle sizes of sand and fines. They have threshold fines content of 10 % and ratio of mean grain sizes of sand to fines is 15.5, which is smaller than this research. Therefore, the chances of particles movement during cyclic loading may be less. In addition, due to lower threshold fines content, there are less voids. It indicates that, lower fines content is sufficient to provide active roles in force chain.

Table 4-11: Properties of sands and fines used in cyclic triaxial tests by various researchers.

Properties	Sadek and Saleh (2007)	Singh (1996)	This research
D_{50} (mm) for sand	0.31	0.30	0.70
d_{50} (mm) for fines	0.02	Not given	0.015
D_{50}/d_{50}	15.5	Not given	46.67
Threshold fine content	10	Not given	20-30

The variation of Youngs modulus with confining pressure is similar in all the fly ash contents. Kokusho (1980) also used the cyclic triaxial tests data for the determination of shear modulus (G). They also observed the decrease of shear modulus , with an increase in shear strain. The trends of the results of this research are also similar to those Kokusho (1980). They used special types of displacement sensor capable of measuring lower strain in the range of 10^{-6} to 10^{-3}.

However, due to the limitation of displacement transducers, strains lower than .01 could not be measured in this research. Hence, the the plots do not show the variation of Youngs modulus for the strain lower than 0.01. As the sample is consolidated at higher confining pressure, the Youngs modulus is found to increase. Similar types of behavior were observed by Kokusho (1980).

4.13 Summary

In this chapter, the results obtained from cyclic triaxial tests were analyzed and discussed. In the beginning, results on clean sand, sand containing 10 and 20 % fly ash and, fly ash were presented first. Effects of confining pressure on initial liquefaction and deformation were presented. The results showed that, liquefaction resistance decreases with an increase in confining pressure. The reduction of liquefaction resistance of the specimen with change of confining pressure from 5 to 10 psi was higher than 10 to 15 psi.

Next, the effects of the addition of fly ash in the sand on liquefaction resistance have been presented. The effects were analyzed with respect to pore water pressure generation as well as deformation. The liquefaction resistance decreased with the addition of 10 % fly ash. Further addition of 20 % fly ash decreased the liquefaction resistance for 5-psi effective confining pressure. However, for the 10 and 15-psi effective confining pressure, the addition of 20 % fly ash increases the liquefaction resistance in comparison to sand containing 10 % fly ash. Nevertheless, it was lower than that of clean sand. It was observed that, the liquefaction resistance of fly ash is lower than clean sand. The effects of fly ash on liquefaction resistance of sand at higher percentages of fly ash was also compared from (Regmi, 2014). It was observed that, liquefaction resistance increases up to 25 % of fly ash, after that it decreases.

In all the fly ash contents, the liquefaction resistance in terms of pore water generation was found to decrease with an increase in confining pressure. The effects of confining pressure on liquefaction resistance are reported by Seed and Lee (1966), Castro and Paulos (1977), Vaid et al. (1985) and Amini and Qui (2000). Seed and Lee (1966) observed that, on increasing confining pressure, the shear stress required to cause liquefaction also increases. They did not compare the results in terms of CSR. If they had compared the results in terms of CSR, the CSR required for liquefaction would decrease with increase in confining pressure. Further, Castro and Paulos (1977) reported that, liquefaction resistance decreases with the increase in confining pressure. Besides that, Vaid et al. (1985) observed substantial decrease in liquefaction resistance with an increase in confining pressure. Finally, Amini and Qui (2000) made similar observations. They observed decrease in CSR with an increase in confining pressure for the uniform and layered sands. Hence, the results obtained in this research are consistent with the reported researches in literature. Moreover, the test results indicate that, addition of fly ash increases the reduction on CSR on increasing the confining pressure from 5 to 10 psi. However, there was not a drastic change in the reduction of CSR in changing confining pressure from 10 to 15 psi. Finally, results on Youngs modulus and damping ratio were presented. Youngs modulus was found to decrease with an increase in axial strain. Effects of confining pressure on Youngs modulus was analyzed. It was observed that, Youngs modulus increased with an increase in confining pressure. After that, effects of addition of fly ash on Youngs modulus was evaluated. However, distinct variation in Youngs modulus was not observed with variation of fly ash contents. Similar to Youngs modulus, variation of damping ratio with confining pressures and fly ash contents were analyzed. However, distict variation was not observed with confining pressures as well as fly ash contents.

CHAPTER 5

CONCLUSIONS AND RECOMMENDATIONS

5.1 Conclusions

The thesis presents the results obtained from cyclic triaxial test on sand containing various percentages of fly ash used in this research. The main purpose of this study was to investigate the effects of addition of fly ash on liquefaction characteristics of sand. The conclusion obtained from this research can be separated into three main components: 1) Effects of confining pressure on liquefaction characteristics of sand-fly ash mixtures 2) Effects of fly ash contents on pore water pressure generation and deformation characteristics of sand-fly ash mixtures 3) Effects of confining pressures and fly ash contents on Youngs modulus and damping . The conclusion made are based on this research. Recommendation for future research in this area are also presented in following section.

5.1.1 Effects of confining pressure

- The test results at various confining pressures indicates that, the cyclic shear stress required for initial liquefaction of clean sand and sand-fly ash mixtures at any number of cycles increases with an increase in effective confining pressure.
- The cyclic shear stress required for the development of 2.5 % and 5 % DA strain in the clean sand and sand-fly ash mixtures at any number of cycles also increases with an increase in effective confining pressure.
- The CSR required for initial liquefaction of clean sand and sand-fly ash mixtures at any given number of cycles decreases with an increase in confining pressure.

- The CSR required for the development of 2.5 % and 5 % DA strain in clean sand and sand-fly ash mixtures at any given number of cycles decreases with an increase in confining pressure
- Further, the change in confining pressure is more sensitive to initial liquefaction in the lower range of confining pressure. The decrease of number of cycles at a given CSR required for initial liquefaction is higher on increasing the confining pressure from 5 to 10 psi in comparison to 10 to 15 psi. The clean sand, sand-fly ash mixture also shows similar behavior on deformation.
- The sensitivity of liquefaction resistance to change in confining pressure from 5 to 10 psi increases with the fly ash content. However, for a change in confining pressure from 10 to 15 psi, decrease in liquefaction resistance in terms of CSR is almost constant with fly ash content. The sand-fly ash mixtures shows similar behavior on deformation.
- At same confining pressure, liquefaction resistance decreases with an increase in CSR.

5.1.2 Effects of fly ash content on liquefaction resistance

- Addition of fly ash decreases specific gravity, and maximum and minimum void ratios up to 20 % of fly ash content used in this research.
- The fly ash used in this research has significantly lower liquefaction resistance in comparison to clean Ottawa sand.
- The liquefaction resistance of sand-fly ash mixtures depends upon the confining pressure as well as fly ash contents. For 5 psi effective confining pressure, the liquefaction resistance decreases with an addition of 10 % fly ash. It increases at 20 % fly ash. For 10 and 15 psi effective confining pressure, the liquefaction resistance decreases with an addition of 10 % fly ash and addition of 20 % fly ash, increases the liquefaction

resistance. However, it is lower than clean sand. Moreover, at 15 psi effective confining pressure, sand-fly ash mixtures having various fly ash contents liquefied in almost similar number of cycles. Hence, liquefaction resistance is less sensitive to fly ash content at higher confining pressure up to 20 % fly ash.

- The liquefaction resistance increases up to addition of 25 % fly ash, after that it decreases.
- The deformation and pore water pressure generation start earlier in sand, after that it gradually increases. On the other hand, it increases instantly in fly ash. Further addition of 10 % fly ash increases the rate of deformation and pore water pressure generation. Although the deformation and pore water pressure generation started later on addition of 20 % fly ash, the liquefaction occurs instantly. Hence, it can be concluded that, the addition of fly ash possibly increases brittleness of sample.

5.1.3 Youngs modulus and damping (Based on limited number of test and equipment limitation)

- The Youngs modulus of clean sand, sand containing 10 and 20 % fly ash decreases with an increase in axial strain. Further, with an increase in confining pressure, the Youngs modulus also increases.
- The Youngs modulus of clean sand, sand containing 10 and 20 % fly ash are almost equal.
- The damping ratio is less sensitive to confining pressures and fly ash contents.

5.2 Recommendation for future research

The following recommendations have been made in the study.

- In this research, the fly ash were added up to 20 %, which is below the threshold fine content. In order to evaluate the liquefaction behavior above threshold fine content, cyclic triaxial test can be conducted at various percentages of fly ash above 20 %.
- In the field, the soil element at any depth is not subjected equal pressure all around. The lateral pressure depends upon the lateral earth pressure coefficient. For the actual simulation of field in lab, the test can be conducted at actual lateral pressure and vertical pressure.
- The liquefaction resistance was compared at constant relative density. Further, it can be compared by preparing the sample at constant global void ratio, skeletal void ratio and dry density.
- The effect of ratio of mean grain diameter of sand to fine (D_{50}/d_{50}) can be studied. The test can be conducted using the fines having same chemical properties with different grain sizes.
- The result was analyzed for the initial liquefaction only. The post liquefaction behavior such as deformation, volumetric strain can be studied.

REFERENCES

Amini, F., and Qi, G. Z. (2000). "Liquefaction testing of stratified silty sands." *Journal of Geotechnical and Geoenvironmental Engineering*, 126(3), 208-217.

ASTM C778-13 (2003). "Standard specification for standard Sand." 1-3.

ASTM D422 (2007). "Standard test method for particle-size analysis of soils." 1-8.

ASTM D4253 (2000). "Standard test methods for maximum index density and unit weight of soils using a vibratory table." 1-14.

ASTM D3999-91 (2003). "Standard test methods for the determination of the modulus and damping properties of soils using the cyclic triaxial apparatus."1-15.

ASTM D4254 (2000). "Standard test methods for minimum index density and unit weight of soils and Calculation of Relative Density." 1-9.

ASTM D5550 - 06 (2000). "Standard test methods for specific gravity of soil solids by gas Pycnometer." 1-7.

Athanasopoulos, G., and Xenaki, V. (2008). "Liquefaction resistance of sands containing varying amounts of fines." *Geotechnical Earthquake Engineering and Soil Dynamics,* ASCE, Sacramento, California, 1-10.

Black, D. K., and Lee, K. L. (1973). "Saturating laboratory samples by back pressure." *Journal of Soil Mechanics & Foundations Div*, 99(SM1), 75-93.

Boulanger, R. W., and Idriss, I. M. (2006). "Liquefaction susceptibility criteria for silts and clays." *Journal of Geotechnical and Geoenvironmental Engineering*, 132(11), 1413-1426.

Casagrande, A. (1936). "Characteristics of cohesion less soils affecting the stability of slopes and earth fills." *Journal of Boston Society of Civil Engineers*, 23(1), 257-275.

Casagrande, A. (1938). “The shearing resistance of soils and its relation to the stability of earth dams.” *Proceedings of the Soils and Foundation Conference,* U.S. Army Corps of Engineers, Boston, Massachusetts.

Castro, G. (1975). “Liquefaction and cyclic mobility of saturated sands.” *Journal of the Geotechnical Engineering Division*, 101(6), 551-569.

Castro, G., and Paulos, S. J. (1977). “Factors affecting liquefaction and cyclic mobility.” *Journal of the Geotechnical Engineering Division*, 103(6), 501-506.

Chaney, R. C., Stevens, E., and Sheth, N. (1979). “Suggested test method for determination of degree of saturation of soil samples by B value measurement.” *Geotechnical Testing Journal*, 2(3), 158-162.

Chang, N. Y., Yeh, S. T., and Kaufman, L. P. (1982). “Liquefaction potential of clean and silty sands.” *Proceedings of the Third International Earthquake Micro zonation Conference* Seattle, USA, 1017-1032.

Cubrinovski, M., and Ishihara, K. (2002). “Maximum and minimum void ratio characteristics of sands.”*Soils and Foundations*, 42(6), 65-78.

Cubrinovski, M., and Rees, S. (2008). “Effects of fines on undrained behavior of sands.” *Geotechnical Earthquake Engineering and Soil Dynamics Congress IV*, ASCE, Sacramento, California, 1-11.

De Alba, P. A., Chan, C. K., and Seed, H. B. (1976). “Sand liquefaction in large-scale simple shear tests.” *Journal of the Geotechnical Engineering Division*, 102(9), 909-927.

De Alba, P. A., Seed, H.B., Retamal, E., and Seed R.B. (1988). “Analyses of dam failures in 1985 Chilean earthquake.” *Journal of Geotechnical Engineering*, 114(12), 1414-1434.

DeGregorio, V. B. (1990). “Loading systems, sample preparation, and liquefaction.” *Journal of Geotechnical Engineering*, 116(5), 805-821.

Dezfulian, H. (1984). “Effects of silt content on dynamic properties of sandy soils.” *Proceedings of the Eighth World Conference on Earthquake Engineering*, San Francisco, USA, 63-70.

Finn, W. D., Pickering, D. J., and Bransby, P. L. (1971). “Sand Liquefaction in Triaxial and Simple Shear Tests.” *Journal of the Soil Mechanics and Foundations Division,* 97(4), 639-659.

Geocomp Corporation (2013). “Cyclic triaxial software manual.” Geocomp Corporation.

Geokon, Inc. (2002). “Instruction Manual Model 2100 the Nold DE Aerator.” GEOKON Inc.

Holzer, T. L., Hanks, T. C., and Youd T.L. (1989). “Dynamics of liquefaction during the 1987 Superstition Hills, California, earthquake.” *Science,* 244(4900), 56-59.

Ishibashi, I., and Sherif, M. A. (1974). “Soil liquefaction by torsional simple shear device.” *Journal of the Geotechnical Engineering Division,* 100(8), 871-888.

Ishihara, K., and Li, S. I. (1972). “Liquefaction of saturated sand in triaxial torsion shear test.” *Soils and Foundation,* 12(2), 19-39.

Ishihara, K., Troncoso, J., and Takahasi, Y. (1980). “Cyclic strength characteristics of tailings materials.” *Soils and Foundation*, 20(4), 127-142.

Kishida, H. (1966). “Damage to reinforced concrete buildings in Niigata city with special reference to foundation engineering.” *Soils and Foundation,* 6(1), 71-88.

Kishida, H. (1969). “Characteristics of liquefied sands during Mino-Owari, Tohnankai and Fukui earthquakes.” *Soils and Foundation,* 9(1), 75-92.

Koester, J. P. (1994). “The influence of fines type and content on cyclic strength.” *Ground Failures under Seismic Conditions*, ASCE, New York, USA, 17-33.

Koizumi, Y. (1966). “Changes in density of sand subsoil caused by the Niigata earthquake.” *Soils and Foundation*, 6(2), 38-44.

Kokusho, T. (1980). “Cyclic triaxial test of dynamic soil properties for wide strain range.” *Soils and Foundation*, 20 (2), 45-60.

Kuerbis, R. H. (1987). “Effects of gradations and fines content on undrained response of sand.” M.S. Thesis, University of British Columbia.

Kuerbis, R., D., N., and Vaid, Y. P. (1988). “Effect of gradation and fines content on the undrained response of sand.” *Hydraulic Fill Structure*, ASCE, Colorado, U.S.A., 330-345.

Ladd, R. S. (1978). “Preparing test specimens using under compaction.” *ASTM Geotechnical Testing Journal*, 1(1),16-23.

Lade, P. V., Liggio, C. D., and Yamamuro, J. A. (1998). “Effects of non-plastic fines on minimum and maximum void ratios of sand.” *Geotechnical Testing Journal*, 21(4), 336-347.

Law, K. T., and Ling, Y. H. (1992). “Liquefaction of granular soils with non-cohesive and cohesive fines.” *The Tenth World Conference on Earthquake Engineering*, Rotterdam, Netherland, 1491-1496.

Lee, K. L., and Albasia, A. (1974). “Earthquake induced settlements in saturated sands,” *Journal of the Geotechnical Engineering Division*, 100(GT4), 387-406.

Marr, W. A., Hankour, R., and Werden, S. K. (2003). “A fully automated computer controlled resilient modulus testing system.” *ASTM Special Technical Publication*, 1437, 141-151.

Mori, K., Seed, H. B., and Chan, C. K. (1978). “Influence of sample disturbance on sand response to cyclic loading.” *Journal of the Geotechnical Engineering Division*, 104(3), 323-339.

Mohanty, M. (2014). “ Personal Communication.”

Mulilis, J. P., Seed, H. B., Chan, C. K., Mitchell, J. K., and Arulanadan, K. (1977). “Effects of

Sample Preparation on Sand Liquefaction," *Journal of the Geotechnical Engineering Division*, ASCE, 103(GT2), 91-108.

Oshaki, Y. (1966). "Niigata earthquakes, 1964 building damage and soil condition." *Soils and Foundation*, 6(2), 14-37.

Park, S., and Kim, Y. (2013). "liquefaction resistance of sands containing plastic fines with different plasticity." *Journal of Geotechnical and Geoenvironmental Engineering*, 139(5), 825-830.

Peacock, W. H., and Seed, H. B. (1968). "Sand liquefaction under cyclic loading simple shear conditions." *Journal of Soil Mechanics & Foundations Div*, 94(SM3), 689-707.

Polito, C. P., and Martin, J. R. (2001). "Effects of nonplastic fines on the liquefaction resistance of sands." *Journal of Geotechnical and Geoenvironmental Engineering*, 127(5), 408-415.

Prakash, S., and Mathur, J. N. (1965). "Liquefaction of fine sand under dynamic loads." *Symposium on Behavior of Soil under Stress*, Indian Institute of Science, Bangalore, India.

Prakash, S., and Puri, V. K. (2010). "Recent advances in liquefaction of fine grained soils." *5th International Conference on Recent Advances in Geotechnical Earthquake Engineering and Soil Dynamics San Diego, California*, 1-6.

Puri, V. K. (1984). "Liquefaction behavior and dynamic properties of loessial (silty) soils." Ph.D. Dissertation, University of Missouri Rolla.

Pyke, R. M., Chan, C. K., and Seed, H. B. (1975). "Settlement of sands under multidirectional shaking." *Journal of the Geotechnical Engineering Division*, 101(4), 379-398.

Regmi, G. (2014). "Effects of addition of large percentages of fly ash on liquefaction behavior of sand." M.S. Thesis, Southern Illinois University, Carbondale.

Sadek, S., and Saleh, M. (2007). "The effect of carbonaceous fines on the cyclic resistance of poorly graded sands." *Geotechnical and Geological Engineering*, 25(2), 257-264.

Sandoval, J. (1989). "Liquefaction and settlement characteristics of silt soils." Ph.D. Dissertation, University of Missouri Rolla, USA.

Schmidt, K. (2008). "Effects of mica content on cyclic resistance of poorly-graded sand." *Geotechnical Earthquake Engineering and Soil Dynamics IV*, ASCE, California, US, 1-8.

Seed, H. B. (1979). "Soil liquefaction and cyclic mobility evaluation for level ground during earthquakes." *Journal of the Geotechnical Engineering Division*, 105(2), 201-255.

Seed, H. B., and Idriss, I. M. (1971). "Simplified procedure for evaluating soil liquefaction potential." *Journal of the Soil Mechanics and Foundations Division*, 97(9), 1249-1273.

Seed, H. B., and Lee, K. L. (1966). "Liquefaction of saturated sands during cyclic loading." *Journal of Soil Mechanics and Foundation Division*, 92(SM6), 105-134.

Seed, H. B., and Peacock, W. H. (1971). "Test procedures for measuring soil liquefaction characteristics." *Journal of the Soil Mechanics and Foundations Division*, 97(8), 1099-1119.

Seed, H. B., Chan, C. K., and Mori, K. (1977). "Influence of seismic history on liquefaction of sands." *Journal of the Geotechnical Engineering Division*, 103(4), 257-270.

Seed, H. B., Idriss, I. M., and Arango, I. (1983). "Evaluation of liquefaction potential using field performance data." *Journal of Geotechnical Engineering*, 109(3), 458-482.

Seed, H. B., Idriss, I. M., Makdisi, F., and Benerjee, N. (1975). "Representation of irregular stress time histories by equivalent uniform stress series in liquefaction analyses." Earthquake Engineering Research Center, University of California, Berkeley, California, USA.

Seed, H. B., Lysmer, J., and Martin, P. P. (1976). "Pore-water pressure changes during soil liquefaction." *Journal of the Geotechnical Engineering Division*, 102(4), 323-346.

Seed, H. B., Tokimatsu, K., Harder, L. F., and Chung, R. M. (1985). "Influence of SPT procedures in soil liquefaction resistance evaluations." *Journal of Geotechnical Engineering*, 111(12), 1425-1445.

Singh, S. (1996). "Liquefaction characteristics of silts." *Geotechnical & Geological Engineering*, 14(1), 1-19.

Sitharam, T. G., Dash, H. K., and Jakka, R. S. (2013). "Post liquefaction undrained shear behavior of sand-silt mixtures at constant void ratio." *International Journal of Geomechanics*, 13(4), 421-429.

Tatsuoka, F., Iwasaki, T., Tokida, K., and Yasuda, S. (1980). "Standard penetration tests and soil liquefaction potential evaluation." *Soils and Foundation*, 20(4), 95-111.

Thevanayagam, S. (1998). "Effect of fines and confining stress on undrained shear strength of silty sands." *Journal of Geotechnical and Geoenvironmental Engineering*, 124(6), 479-491.

Thevanayagam, S. (2007). "Intergrain contact density indices for granular mixes- I: Framework." *Earthquake Engineering and Engineering Vibration*, 6(2), 123-134.

Thevanayagam, S., M., F., and Liang, J. (2000). "Effects of non-plastic fines on undrained cyclic strength of silty sands." *Geo Denver*, ASCE, Denver, Colorado, 77-91.

Tokimatsu, K., and Yoshimi, Y. (1981). "Field correlation of soil liquefaction with SPT and grain size." *International Conference on Recent Advances in Geotechnical Earthquake Engineering and Soil Dynamics*, University of Missouri-Rolla, 203-208.

Tuttle, M., Law, K. T., Seeber, L., & Jacob, K. (1990). "Liquefaction and ground failure induced by the 1988 Saguenay, Quebec, earthquake." *Canadian Geotechnical Journal*, *27*(5), 580-589.

Vaid, Y. P. (1994). "Liquefaction of silty soils." *Ground failures under seismic conditions*, ASCE, Atlanta, Georgia, USA, 1-16.

Vaid, Y. P., Chern, J. C., and Tumi, H. (1985). “Confining pressure, grain angularity, and liquefaction.” *Journal of Geotechnical Engineering*, 111(10), 1229-1235.

Wang, Y., and Wang, Y. (2010). “Study of effects of fines content on liquefaction properties of sand.” *Soil Dynamics and Earthquake Engineering*, ASCE, Shanghai, China, 272-277.

Xenaki, V. C., and Athanasopoulos, G. A. (2003). “Liquefaction resistance of sand-silt mixtures: an experimental investigation of the effect of fines.” *Soil Dynamics and Earthquake Engineering*, 23(3), 183-194.

Xia, H., and Hu, T. (1991). “Effects of saturation and back pressure on sand liquefaction.” *Journal of Geotechnical Engineering*, 117(9), 1347-1362.

Zhou, S. G. (1981). “Influence of fines on evaluating liquefaction of sand by SPT.” *International Conference on Recent Advances in Geotechnical Earthquake Engineering and Soil Dynamics,* University of Missouri Rolla, 167-172.

VITA

Graduate School
Southern Illinois University

Rakam Lama Tamang

rakamlama@siu.edu

Tribhuvan University, IOE, Pulchowk Campus
B.E., Civil Engineering, Dec, 2010

Thesis Title:
EFFECTS OF ADDITION OF SMALL PERCENTAGES OF FLY ASH ON LIQUEFACTION CHARACTERISTICS OF SAND

Major Professor: Dr. Vijay Puri